ВЕСТНИК

ЮЖНО-УРАЛЬСКОГО ГОСУДАРСТВЕННОГО УНИВЕРСИТЕТА

2015
Т. 7, № 3

ISSN 2076-0493 (Print)
ISSN 2412-0413 (Online)

СЕРИЯ

«ХИМИЯ»

Решением ВАК России включен в Перечень рецензируемых научных изданий

Учредитель – Федеральное государственное бюджетное образовательное учреждение высшего профессионального образования «Южно-Уральский государственный университет» (национальный исследовательский университет)

Журнал публикует рецензированные статьи по научным исследованиям, выполненным в различных отраслях химической науки: неорганическая химия, органическая химия, аналитическая химия, физическая химия и химия твёрдого тела. Приветствуется публикация статей по смежным отраслям. Редакционная коллегия поддерживает высокий уровень публикаций, строго придерживаясь политики независимой сторонней экспертизы, выполненной специалистами в соответствующей области, квалификация которых подтверждена общепризнанными наукометрическими показателями.

Основной целью журнала является пропаганда актуальных научных исследований и содействие формированию наиболее перспективных направлений.

BULLETIN
OF THE SOUTH URAL STATE UNIVERSITY
SERIES
"CHEMISTRY"

2015
Vol. 7, no. 3

ISSN 2076-0493 (Print)
ISSN 2412-0413 (Online)

Vestnik Yuzhno-Ural'skogo Gosudarstvennogo Universiteta.
Seriya "Khimiya"

South Ural State University

The journal publishes peer-reviewed papers on scientific research in various branches of chemical science: inorganic chemistry, organic chemistry, analytical chemistry, physical chemistry and solid-state chemistry. The papers in related branches are welcome. The editorial board keeps the high quality of publications, strictly adhering to the policy of independent third-party expert opinion, expressed by specialists in the corresponding branches, whose qualification is confirmed by generally recognized scientometrical indicators.

The main aim of the journal is the promotion of actual scientific research and assistance in formation of the most advanced directions.

СОДЕРЖАНИЕ

CONTENTS

Неорганическая химия

УДК 544.015.3

МОДИФИЦИРОВАНИЕ СМАЗОЧНО-ОХЛАЖДАЮЩЕЙ ЖИДКОСТИ ФУНКЦИОНАЛИЗИРОВАННЫМИ УГЛЕРОДНЫМИ НАНОТРУБКАМИ

И.А. Макарова, М.В. Бузаева, О.А. Давыдова, Е.С. Климов
Ульяновский государственный технический университет, г. Ульяновск

Проведено модифицирование смазочно-охлаждающей жидкости функционализированными многостенными углеродными нанотрубками с привитыми на поверхности карбоксильными группами и четвертичными аммониевыми солями. Модифицирование приводит к повышению устойчивости жидкости к биопоражению.

Ключевые слова: смазочно-охлаждающая жидкость, функционализация, многостенные углеродные нанотрубки, биопоражение.

Введение

Большинство современных технологических процессов обработки металлов в машиностроительных и металлургических производствах невозможно без применения смазочно-охлаждающих жидкостей (СОЖ), способствующих существенному увеличению стойкости инструмента, повышению производительности и качества обработки. СОЖ в виде водных эмульсий применяется на операциях точения, сверления, шлифования углеродистых и легированных сталей.

Основой для СОЖ служат минеральные масла различного строения. В качестве добавок используют синтетические эфиры, растительные и животные масла, эмульгаторы, спирты, бактерициды, высокомолекулярные адгезивы. В процессе использования СОЖ теряет свои технологические свойства: загрязняется инородными маслами, соединениями металлов, продуктами разложения, подвергается биопоражению [1]. Отработанные СОЖ остаются одним из главных источников загрязнения окружающей среды – концентрация нефтепродуктов в них достигает 90–100 г/дм^3.

Недостатками СОЖ являются невысокие антикоррозионные свойства в отношении черных металлов, низкие трибологические свойства. К основному недостатку следует отнести невысокую стойкость эмульсии, в результате чего при хранении и в процессе эксплуатации СОЖ расслаивается, подвергается биологическому поражению. При этом образуется огромное количество опасных нефтесодержащих отходов.

Защита смазочно-охлаждающих жидкостей от микробиологического поражения является чрезвычайно острой проблемой. Бактерии разрушают поверхностно-активные вещества, СОЖ становится непригодной для дальнейшего использования. При этом поражаются все виды СОЖ, но особенно водомасляные эмульсии.

Выходом из сложившейся ситуации может быть повышение устойчивости СОЖ введением в эмульсию углеродных нанотрубок, которые имеют большую удельную поверхность и малые размеры частиц, что позволит связать на молекулярном уровне компоненты СОЖ в устойчивую коллоидную систему.

Углеродные нанотрубки стоят в ряду наиболее перспективных наноматериалов благодаря своим уникальным свойствам, обеспечивающим возможность их применения в различных областях науки и техники [2]. В настоящее время проводятся интенсивные исследования как по изучению физико-химических свойств нанотрубок, так и по поиску областей их применения.

В связи с этим представляется перспективным получение бактерицида с улучшенными свойствами на основе функционализированных углеродных нанотрубок. Публикации, посвященные модифицированию эмульсий СОЖ наноматериалами, в настоящее время немногочисленны, хотя имеющиеся в литературе сведения позволяют считать это направление актуальным и необходимым [3].

Экспериментальная часть

Синтез углеродных нанотрубок

Синтез многостенных углеродных нанотрубок (МУНТ) проводили в токе аргона методом химического осаждения из паровой фазы с использованием металлоорганических соединений (метод MOCVD) на разработанной нами экспериментальной установке, которая включала две горизонтальные трубчатые печи (испаритель ферроцена и печь для осаждения МУНТ с изотермической зоной 200 мм) [4]. В качестве прекурсоров использовали толуол и ферроцен. Осаждение МУНТ проводили в цилиндрическом кварцевом реакторе с размещенными внутри цилиндрическими кварцевыми вкладышами.

Для всех операций с МУНТ их предварительно размельчали в механическом гомогенизаторе. При необходимости проводили ультразвуковую обработку (лабораторная установка «ИЛ 100-6/4», частота 22 кГц) в изопропиловом спирте или воде.

Функционализация МУНТ в присутствии сильных кислот

В колбу помещали 4,0 г МУНТ, приливали 200 мл смеси концентрированных серной и азотной кислот в объемном соотношении (3:1). Смесь при постоянном перемешивании нагревали при 90 °С в течение 70 мин. Полученную суспензию отфильтровывали, промывали дистиллированной водой до отсутствия в фильтрате реакции на сульфат-ионы. После высушивания масса вещества составила 2,8 г.

Прививка на поверхности МУНТ полярных групп (–OH, –C=O, –COOH) обработкой кислотами обычно проводится по максимальному накоплению карбоксильных групп на поверхности трубок.

Количество химически привитых на поверхности карбоксильных групп определяли потенциометрическим титрованием. Количество карбоксильных групп составило 4 % [5].

Функционализация МУНТ прививкой азотсодержащих групп

К 1,0 г функционализированных МУНТ (ф-МУНТ) добавляли 0,5 г триэтаноламина, смесь перетирали до получения однородной массы, добавляли 50 мл воды. Суспензию при перемешивании нагревали в течение часа при температуре не более 80 ^{o}C. После окончания реакции полученную смесь отфильтровывали, промывали водой, высушивали при 100 ^{o}C.

Для использования в качестве бактерицидной присадки 0,1–1,0 г сухого продукта диспергировали под действием ультразвука (5 мин) в 50 мл воды. Для введения в композицию СОЖ брали из расчета 5 мл суспензии на 1000 мл эмульсии СОЖ, что соответствует массовой концентрации 0,01–0,1 %.

Смазочно-охлаждающая жидкость

Для практических исследований использовали СОЖ марки «АРС-21» (г. Сызрань). Свежеприготовленная СОЖ представляет собой 3 % водную эмульсию, содержащую минеральное масло, эмульгатор, ингибитор коррозии, бактерицидную и другие присадки.

Основные характеристики СОЖ изучали согласно нормативной документации: ГОСТ 2917-76. Масла и присадки. Метод определения коррозионного воздействия на металлы; ГОСТ 9.085-78. Методы испытаний на биостойкость смазочно-охлаждающих жидкостей; ГОСТ Р 51779-2001. Жидкость смазочно-охлаждающая. Стабильность; ТУ 0258-142-057-44685-95. Масла и присадки. Методы определения pH.

Определение степени микробиологического поражения СОЖ проводили с помощью индикатора 2,3,5-трифенилтетразолия хлористого (ТТХ) по интенсивности окраски (ГОСТ 9.085-78).

В пробирки отбирали по 9 мл эмульсии, добавляли по 1мл 0,5 % раствора ТТХ, перемешивали, выдерживали в термостате при 30 °С в течение 24 ч. По наличию и интенсивности окраски определяли балл микробиологического поражения.

Физико-химические методы анализа

Топологию поверхности МУНТ изучали на сканирующем электронном микроскопе Phenom pro X с высоким разрешением.

Результаты и обсуждение

В ходе синтеза МУНТ осаждаются на цилиндрическом кварцевом вкладыше в виде макроцилиндра, поверхность которого состоит из жгутов, сформированных из длинных нитей, образованных многостенными углеродными нанотрубками (рис. 1).

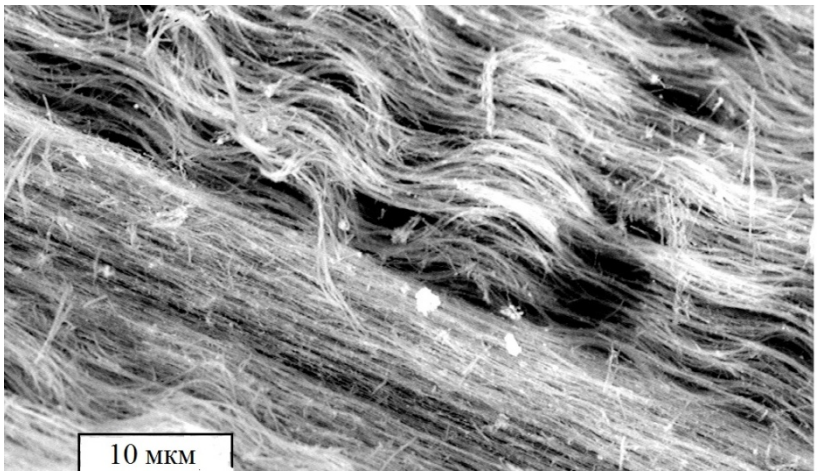

Рис. 1. СЭМ-микрофотография жгутов многостенных углеродных нанотрубок

Диаметр большей части нанотрубок 40–90 нм, длина составляет десятки нм. При ультразвуковой обработке происходит расщепление жгутов и дробление нитей на более короткие фрагменты.

Углеродные нанотрубки склонны к образованию агломератов, что затрудняет их введение в композиционные материалы. Для придания необходимых технологических свойств (совместимость с матрицей материала, образование устойчивой дисперсии) МУНТ модифицируют различными способами. Наиболее эффективным приемом является функционализация МУНТ при обработке сильными кислотами, приводящая к прививке на поверхности трубок полярных карбоксильных, карбонильных и гидроксильных групп (–COOH, –CO, –OH). В результате модифицирования образуется микродисперсная однородная поверхность с более короткими фрагментами ф-МУНТ.

Водоэмульсионная смазочно-охлаждающая жидкость «АРС-21» представляет собой сбалансированную смесь, содержащую минеральное масло, эмульгатор, ингибитор коррозии, бактерицидную и другие присадки, придающие рабочему раствору СОЖ необходимые свойства (табл. 1).

Таблица 1

Компонентный состав СОЖ марки «АРС-21»

№ п/п	Наименование компонентов «АРС-21»	Содержание в 3 % эмульсии, г/л
1	Масло индустриальное И-12	10,0
2	Кислота олеиновая	3,0
3	Карбомол	3,6
4	Триэтаноламин	3,0
5	Присадки	0,5
	Вода	Остальное до 1 л

В качестве бактерицида в состав СОЖ вводится карбомол (производное мочевины), остальные присадки – противоизносные, антикоррозионные, антипенные и другие.

Основные технологические свойства СОЖ представлены в табл. 2.

Таблица 2

Свойства 3% эмульсии СОЖ

Показатель	Эмульсия «АРС-21»
pH	7,1
Стабильность на жесткой воде (мм)	3,0
Коррозионная агрессивность	2,0 (низкая)
Биопоражение, 48 ч (баллы)	0

Для подавления роста микроорганизмов в СОЖ предложено довольно много методов – физических (ультрафиолетовое, электромагнитное и ионное облучение, термопастеризация, ультра-

звуковая обработка), химических (биоцидная обработка), механических (фильтрование, центрифугирование). Наиболее распространены химические методы.

В качестве бактерицидных добавок в композицию СОЖ дополнительно вводятся химические соединения: амиды, амины, четвертичные аммониевые соли. В этом плане представлялось перспективным функционализировать МУНТ четвертичной аммониевой солью, образованной ф-МУНТ и триэтаноламином.

Поверхность функционализированных МУНТ способна за счет карбоксильных групп химически связываться с компонентами СОЖ, в частности – с триэтаноламином (схема 1):

$$\text{МУНТ–C(O)–O}^- \text{H}^+ + :\text{N(CH}_2\text{CH}_2\text{OH)}_3 \rightarrow \quad (1)$$
$$\rightarrow \text{МУНТ–C(O)–O}^- \text{HN}^+\text{(CH}_2\text{CH}_2\text{OH)}_3$$

Реакция образования четвертичной аммониевой соли на поверхности ф-МУНТ протекает за счет неподеленной пары электронов на атоме азота и протона карбоксильной группы.

Триэтаноламин вводится в СОЖ для образования эмульгатора. Он образует с олеиновой кислотой (компонент СОЖ) так называемое «этаноламинное мыло» – поверхностно-активный эмульгатор, обеспечивающий устойчивость эмульсии на границе раздела фаз «масло – вода» (схема 2):

$$\text{C}_{17}\text{H}_{33}\text{–C(O)O}^-\text{H}^+ + :\text{N(CH}_2\text{CH}_2\text{OH)}_3 \rightarrow \quad (2)$$
$$\rightarrow \text{C}_{17}\text{H}_{33}\text{–C(O)–O}^-\text{HN}^+\text{(CH}_2\text{CH}_2\text{OH)}_3$$

Поверхность МУНТ с привитыми фрагментами триэтаноламина, входящего в состав СОЖ, должна выполнять одновременно и роль эмульгатора, и роль бактерицидного средства, поскольку четвертичные аммониевые соли являются хорошими бактерицидами. На рис. 2 представлено схематическое изображение ф-МУНТ с фрагментом четвертичной аммониевой соли, образованной триэтаноламином и карбоксильной группой (ТЭА-МУНТ).

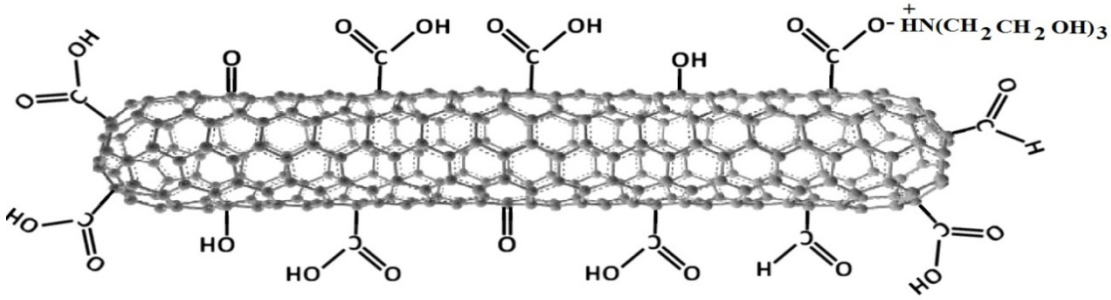

Рис. 2. Схематическое изображение ТЭА-МУНТ

Диспергирование МУНТ в СОЖ проводили при ультразвуковой обработке смеси в течение 1−5 мин в зависимости от концентрации МУНТ: 0,01; 0,05; 0,1 % (по массе).

За счет физического и химического связывания образуется устойчивая дисперсионная система с равномерным распределением углеродных нанотрубок в объеме СОЖ.

Действие бактерицидов основано на образовании кислой среды, наличие которой подавляет рост микроорганизмов. В частности, кислотность одного из эффективных бактерицидов «Софекс», pH = 3,1.

Кислотный показатель эмульсии СОЖ «АРС-21», pH = 7,1 (нейтральная среда). Суспензия функционализированных смесью кислот МУНТ имеет pH = 3,7; с привитой четвертичной аммониевой солью pH = 3,2. При введении в СОЖ этих бактерицидов кислотность среды pH = 3,0–3,3.

Нами проведено сравнение бактерицидных свойств ф-МУНТ, ТЭА-МУНТ и бактерицида «Софекс». Результаты представлены в табл. 3.

Эффективность воздействия бактерицидов на микроорганизмы уменьшается в ряду: ТЭА-МУНТ > ф-МУНТ > Софекс.

Таблица 3

Биологическое поражение СОЖ в присутствии бактерицидов. Концентрация МУНТ 0,05 % (масс.)

Бактерицид	Балл поражения					
	30 сут	60 сут	90 сут	120 сут	150 сут	180 сут
Без бактерицида	1	2	3	3	4	4
Софекс	0	0	1	1	2	3
ф-МУНТ	0	0	0	0	0	1
ТЭА-МУНТ	0	0	0	0	0	0

Биостойкость СОЖ определяется по окраске эмульсии в присутствии индикатора 2,3,5-трифенилтетразолия хлористого. Связь между биостойкостью и баллом биопоражения представлена в табл. 4.

Таблица 4

Степень биопоражения СОЖ

Характер и интенсивность окрашивания эмульсии с ТТХ	Балл	Биостойкость
Цвет эмульсии не изменился	0	Отсутствие микроорганизмов
Незначительное окрашивание в виде пятна или кольца	I	Удовлетворительная биостойкость
Ярко-красная окраска в виде пятна на дне пробирки	II	Неудовлетворительная биостойкость
Розовая окраска всей эмульсии в пробирке	III	Отсутствие биостойкости
Ярко-красная окраска всей эмульсии в пробирке	IV	Полное биопоражение

Таким образом, функционализированные МУНТ обладают высокой антимикробной активностью и значительно стабилизируют СОЖ по отношению к биопоражению.

Выводы

1. Проведена функционализация поверхности многостенных углеродных нанотрубок карбоксильными группами и четвертичными аммониевыми солями для их использования в качестве бактерицидов при модифицировании смазочно-охлаждающей жидкости.

2. Получены новые бактерицидные технические средства с высоким стабилизирующим действием по отношению к биопоражению.

Литература

1. Булыжев, Е.М. Ресурсосберегающее применение смазочно-охлаждающих жидкостей при металлообработке / Е.М. Булыжев, Л.В. Худобин. – М.: Машиностроение, 2004. – 352 с.

2. Многослойные углеродные нанотрубки и их применение / М.М. Томишко, О.В. Демичева, А.М. Алексеев и др. // Рос. хим. журн. (Журн. Рос. хим. о-ва им. Д.И. Менделеева). – 2008. – Т. LII. – № 5. – С. 39–43.

3. Пат. 2417253 Российская Федерация. Синтетическая смазочно-охлаждающая жидкость с углеродными нанотрубками / А.А. Фомин, В.А. Мышкин. – № 2009143638/04; заявл. 26.11.09; опубл. 27.04.2011, Бюл. № 12. – 6 с.

4. Некоторые аспекты синтеза многостенных углеродных нанотрубок химическим осаждением из паровой фазы и характеристики полученного материала / Е.С. Климов, М.В. Бузаева, О.А. Давыдова и др. // Журнал прикладной химии. – 2014. – Т. 87. – № 8. – С. 1128–1132.

5. Изменение поверхности и некоторых технологических свойств углеродных нанотрубок при их модифицировании / Е.С. Климов, М.В. Бузаева, О.А. Давыдова и др. // Башкирский химический журнал. – 2014. – Т. 21. – № 3. – С. 109–113.

Макарова Ирина Алексеевна – аспирант кафедры химии, Ульяновский государственный технический университет. 432027, г. Ульяновск, ул. Северный Венец, 32. E-mail: gorlovskaya.irin@bk.ru.

Бузаева Мария Владимировна – доктор химических наук, профессор кафедры химии, Ульяновский государственный технический университет. 432027, г. Ульяновск, ул. Северный Венец, 32. E-mail: m.buzaeva@mail.ru.

Давыдова Ольга Александровна – доктор химических наук, профессор кафедры химии, Ульяновский государственный технический университет. 432027, г.Ульяновск, ул. Северный Венец, 32. E-mail: olga1103@inbox.ru.

Климов Евгений Семенович – доктор химических наук, профессор, заведующий кафедрой химии, Ульяновский государственный технический университет. 432027, г. Ульяновск, ул. Северный Венец, 32. E-mail: eugen1947@mail.ru.

Поступила в редакцию 10 мая 2015 г.

THE MODIFICATION OF LUBRICATING COOLANTS BY FUNCTIONALIZED CARBON NANOTUBES

I.A. Makarova, Ulyanovsk State Technical University, Ulyanovsk, Russian Federation, gorlovskaya.irin@bk.ru
M.V. Buzaeva, Ulyanovsk State Technical University, Ulyanovsk, Russian Federation, m.buzaeva@mail.ru
O.A. Davydova, Ulyanovsk State Technical University, Ulyanovsk, Russian Federation, olga1103@inbox.ru
E.S. Klimov, Ulyanovsk State Technical University, Ulyanovsk, Russian Federation, eugen1947@mail.ru

A modification of lubricating coolants by functionalized multi-walled carbon nanotubes grafted on the surface carboxyl groups and quaternary ammonium salts is condacted. The modification leads to increased stability to biodegradation fluid.

Keywords: lubricating coolant, functionalization, multi-walled carbon nanotubes, biodegradation.

References

1. Bulyzhev E.M., Hudobin L.V. *Resursosberegayushchee primenenie smazochno-okhlazhdayushchikh zhidkostey pri metalloobrabotke* [Resourse-saving Use Coolant-cutting Fluids in Metal-working]. Moscow, Mashinostroenie Publ., 2004. 352 p.

2. Tomishko M.M., Demicheva O.V., Alekseev A.M., Tomishko A.G., Klinova L.L., Fetisova O.E. [Multilayer Carbon Nanotubes and Their Applications]. *Rossiyskiy khimicheskiy zhurnal* [Russian Journal of General Chemistry], 2008, vol. LII, no. 5, pp. 39– 43. (in Russ.)

3. Fomin A.A., Myshkin V.A. *Sinteticheskaya smazochno-okhlazhdayushchaya zhidkost' s uglerodnymi nanotrubkami* [Synthetic Lubricant Coolant with Carbon Nanotubes]. Patent RF, no 2417253, 2011.

4. Klimov E.S., Buzaeva M.V., Davydova O.A., Makarova I.A., Svetuhin V.V., Kozlov D.V., Pchelinceva E.S., Bunakov N.A. [Some Aspects of Multi-walled Carbon Nanotube Synthesis by Chemical Cooling from Vapour Phase and the Characteristics of Obtained Material]. *Russian Journal of Applied Chemistry,* 2014, vol. 87, no. 8, pp. 1128–1132. (in Russ.)

5. Klimov E.S., Davydova O.A., Buzaeva M.V., Makarova I.A., Bunakov N.A., Panov A.A., Pynenkov A.A. [Change of Surface and Some Technological Properties of Carbon Nanotubes at Their Modification]. *Baskirskii khimicheskii zhurnal* [Bashkir chemical journal], 2014, vol. 21, no. 3, pp. 109–113. (in Russ.)

Received 10 May 2015

ОБРАЗЕЦ ЦИТИРОВАНИЯ

Модифицирование смазочно-охлаждающей жидкости функционализированными углеродными нанотрубками / И.А. Макарова, М.В. Бузаева, О.А. Давыдова, Е.С. Климов // Вестник ЮУрГУ. Серия «Химия». – 2015. – Т. 7, № 3. – С. 5–10.

FOR CITATION

Makarova I.A., Buzaeva M.V., Davydova O.A., Klimov E.S. The Modification of Lubricating Coolants by Functionalized Carbon Nanotubes. *Bulletin of the South Ural State University. Ser. Chemistry.* 2015, vol. 7, no. 3, pp. 5–10.

Органическая химия

RESEARCH OF 2-THIOURACIL DERIVATIVES BY X-RAY METHOD

T.V. Frolova, *South Ural State University, Chelyabinsk, Russian Federation, chemitash@gmail.com*
D.G. Kim, *South Ural State University, Chelyabinsk, Russian Federation, kim_dg48@mail.ru*
V.V. Sharutin, *South Ural State University, Chelyabinsk, Russian Federation, vvsharutin@rambler.ru*
K.Yu. Osheko, *South Ural State University, Chelyabinsk, Russian Federation, osheko_kseniya@mail.ru*

2-Propargylthio-6-methyl-5-ethyl-4(3*H*)-pyrimidinone has been synthesized by alkylation of S-sodium salt of 6-methyl-5-ethyl-2-thiouracil with propargyl bromide. It has been found by X-ray method that S-derivatives of 2-thiouracil are in the tautomeric form with the proton at the nitrogen atom N^3. The substitute at the sulfur atom is within the plane of pyrimidine ring at the angle 59–84°. The 2-alkylthio-4(3*H*)-pyrimidinones molecules are combined in dimers with formation of two intermolecular hydrogen bonds.

Keywords: 2-prenylthio-6-trifluoromethyl-4(3H)-pyrimidinone, cis-2-(3-chloroallyl)thio-6-trifluoromethyl-4(3H)-pyrimidinone, 2-allylthio-6-methyl-4(3H)-pyrimidinone, 2-propargylthio-6-methyl-5-ethyl-4(3H)-pyrimidinone, alkylation, propargyl bromide, tautomerism, molecular structure, X-ray analysis.

Introduction

It is known that alkylation of 6-methyl-2-thiouracil and 6-trifluoromethyl-2-thiouracil occurs at the sulfur atom [1]. At the same time information about alkylation of 6-methyl-5-ethyl-2-thiouracil by propargyl bromide has not been discussed in literature. The aim of the present study is the synthesis of 2-propargylthio-6-methyl-5-ethyl-4(3*H*)-pyrimidinone and the investigation of its structure and other 2-thiouracil S-derivatives by X-ray analysis.

Experimental

Synthesis of 2-propargylthio-6-methyl-5-ethyl-4(3*H*)-pyrimidinone (1)

Propargyl bromide (0.9 mL, 0.001 mol) and NaOH (0.04 g, 0.001 mol) were added to the S-sodium salt of 6-methyl-5-ethyl-2-thiouracil solution (0.912 g, 0.001 mol) in 20 mL of water. The reaction mixture was stirred with a magnetic stirrer for 2 h. Mixture was neutralized by the addition of acetic acid, the obtained precipitate was filtered off, washed with water, dried and recrystallized from hexane. The product yield: 0.154 g (55%), T_m=162°C, R_f=0.55(ethyl acetate:hexane 1:3). Crystals for X-ray analysis were obtained from the isooctane–acetone (3:1) solution.

Compounds **2–4** were obtained by the interaction between S-sodium salt of 6-methyl- and 6-trifluoromethyl-2-thiouracil with allyl bromide, prenyl chloride and 1,3-dichloropropene by the method [2].

The X-ray analysis of the crystals of compounds **1–4** was performed on the automatic four-circle Bruker D8 Quest diffractometer (Mo K_α-radiation, λ = 0.71073 Å, graphite monochromator).

The data collection and editing, as well as the refinement of unit cell parameters and the absorption accounting were carried out using SMART and SAINT *Plus* program packages [3]. All calculations for the structure determination and refinement were carried out using the SHELXTL/PC [4] program packages. The structures of compounds **1–4** were determined by the direct method and refined by least-squares method calculations in anisotropic approximation for non-hydrogen atoms. Selected crystallographic data and structure refinement results are given in Table 1.

The full tables of atomic coordinates, bond lengths, and bond angles were deposited with the Cambridge Crystallographic Data Centre (№ 998573, 1061098, 1061104, 1028131; deposit@ccdc.cam.ac.uk; http://www.ccdc.cam.ac.uk).

Table 1

Crystallographic data and the experimental and structure refinement parameters for compounds 1–4

Parameter	Value			
	1	**2**	**3**	**4**
Empirical formula	$C_{10}H_{12}N_2OS$	$C_8H_{10}N_2OSH_{10}$	$C_{10}H_{11}N_2SF_3O$	$C_8H_6N_2OSClF_3$
Formula weight	208.28	182.24	264.27	270.66
T, K	273.15	273.15	295.0(2)	295.0(2)
Crystal system	Monoclinic	Triclinic	Monoclinic	Monoclinic
Space group	$P2_1/c$	P-1	$P2_1/n$	$P2_1/n$
a, Å	9.8551(18)	4.6742(2)	12.675(17)	12.080(11)
b, Å	21.875(3)	9.5013(4)	7.156(9)	7.43(2)
c, Å	4.8936(8)	11.4968(5)	13.644(17)	12.650(16)
α, deg	90.00	113.905(2)	90.00	90.00
β, deg	93.569(4)	99.243(2)	95.10(6)	91.56(9)
γ, deg	90.00	92.850(2)	90.00	90.00
V, Å^3	1052.9(3)	456.98(3)	1233(3)	1134(4)
Z	4	2	4	4
ρ(calcd.), g/cm^3	1.314	1.324	1.424	1.585
μ, mm^{-1}	0.276	0.307	0.286	0.540
F(000)	440.0	192.0	544.0	544.0
Crystal size, mm	0.24 × 0.09 × 0.025	0.53 × 0.25 × 0.13	0.61 × 0.2 × 0.12	0.6 × 0.27 × 0.25
θ Range of data collection, deg	6.96 to 52.78°	7.32 to 52.84°	4.6 to 57.04°	4.6 to 42.9°
Range of refraction indices	−12 ≤ h ≤ 12, −27 ≤ k ≤ 27, −6 ≤ l ≤ 6	−5 ≤ h ≤ 5, −11 ≤ k ≤ 11, −14 ≤ l ≤ 14	−8 ≤ h ≤ 16, −9 ≤ k ≤ 9, −18 ≤ l ≤ 18	−12 ≤ h ≤ 12, −7 ≤ k ≤ 7, −9 ≤ l ≤ 13
Measured reflections	14398	10518	11916	3767
Independent reflections	2138	1868	3107	1248
R_{int}	0.1804	0.0233	0.0362	0.0328
GOOF	0.996	0.984	1.017	1.088
R factors for $F^2 > 2\sigma(F^2)$	R_1 = 0.0613, wR_2 = 0.1025	R_1 = 0.0347, wR_2 = 0.1123	R_1 = 0.0764, wR_2 = 0.2049	R_1 = 0.0726, wR_2 = 0.2012
R factors for all reflections	R_1 = 0.1481, wR_2 = 0.1283	R_1 = 0.0458, wR_2 = 0.1233	R_1 = 0.1189, wR_2 = 0.2376	R_1 = 0.0987, wR_2 = 0.2425
Residual electron density (min/max), *e*/Å^3	0.22/−0.21	0.21/−0.20	0.93/−0.24	0.72/−0.25

Results and Discussion

We are the first to find that alkylation of S-sodium salt of 6-methyl-5-ethyl-2-thiouracil by propargyl bromide is carried out with the synthesis of 2-propargylthio-6-methyl-5-ethyl-4(3*H*)-pyrimidinone (**1**).

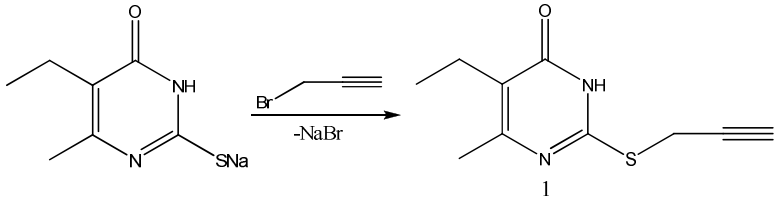

1

2-Allylthio-6-methyl-4(3*H*)-pyrimidinone (**2**), 2-prenylthio-6-trifluoromethyl-4(3*H*)-pyrimidinone (**3**) and *cis*-2-(3-chloroallyl)thio-6-trifluoromethyl-4(3*H*)-pyrimidinone (**4**) are synthesized by the method [2]. Note that alkylation of 6-trifluoromethyl-2-thiouracil by 1,3-dichloropropene is carried out

with the formation of mixture of *cis*- and *trans*-isomers. The monocrystal of *cis*-isomer has been isolated mechanically after recrystallization from hexane.

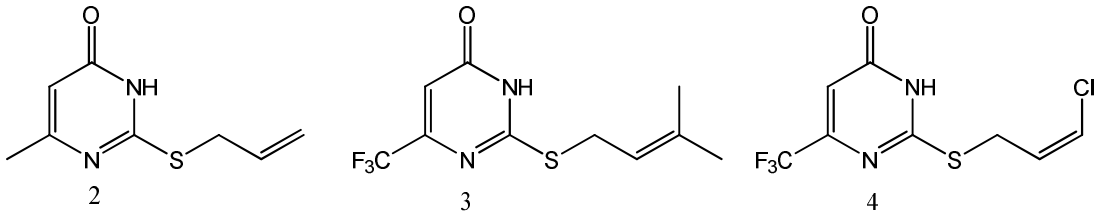

It has been found by X-ray method that derivatives at the sulfur atom in sulfides 1–4 (Fig. 1–4) are almost in the perpendicular plane to pyrimidine ring at the angle 72–84°. Exception is chloroallylsulfide **4**, in which the chloroallyl fragment is at the angle that equals 59° for pyrimidine ring.

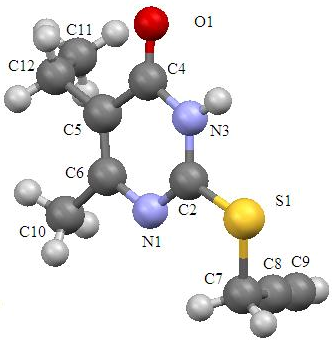

Fig. 1. The structure of compound 1

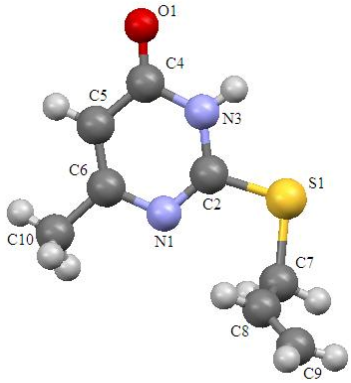

Fig. 2. The structure of compound 2

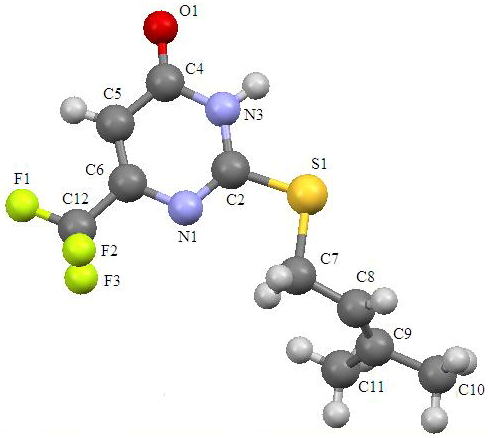

Fig. 3. The structure of compound 3

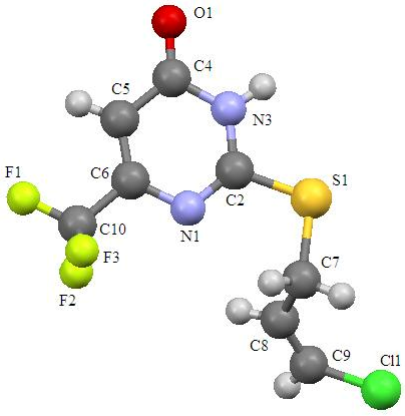

Fig. 4. The structure of compound 4

Sulfides **1–4** have standard geometry. Particularly there is noticeable asymmetry of the C–S bond lengths, which is the result of heterocycle effect (C(2)–S(1)= 1.727–1.759 Å, C(7)–S(1)= 1.802–1.822 Å). The bond lengths of heterocycles in all analyzed compounds are in the range 1.299–1.384 Å. Exception is the bond length C(5)–C(4) 1.420–1.442 Å. It is the result of the influence of the electron acceptor oxygen atom at C(4).

Three tautomeric forms for sulfides **1–4** can be presented:

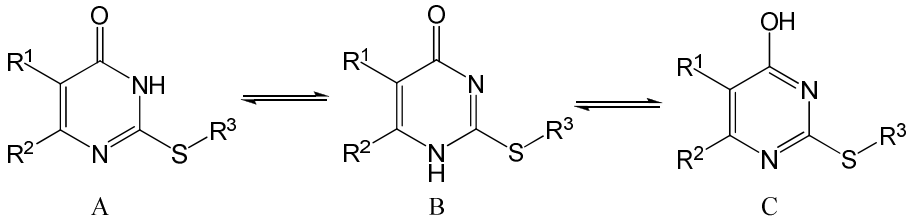

Table 2

Selected bond lengths in the structures of compounds 1–4

Bond length, Å	Compound			
	1	2	3	4
C4–O1	1.242(3)	1.238(2)	1.224(4)	1.229(8)
C2–S1	1.750(3)	1.759(2)	1.741(4)	1.759(7)
C7–S1	1.811(3)	1.807(2)	1.822(5)	1.818(9)
C2–N3	1.353(4)	1.353(2)	1.353(4)	1.347(9)
C6–N1	1.380(4)	1.379(2)	1.364(4)	1.379(9)
C4–N3	1.377(4)	1.381(2)	1.384(4)	1.397(8)
C2–N1	1.292(4)	1.300(2)	1.295(4)	1.313(9)
C5–C6	1.357(4)	1.358(2)	1.347(5)	1.356(10)
C4–C5	1.441(4)	1.421(2)	1.420(5)	1.442(10)

The C–O bond length of sulfides **1–4** corresponds to the carbonyl group (1.224–1.242 Å) which is absent in tautomeric form C. The C(2)–N(1) bond length in compounds **1–4** is 1.299–1.313 Å. It is the result of double bond C=N formation in sulfides, which opposes structure B. Thus, compounds **1–4** are in tautomeric form A. It corresponds to the various quantum-chemical calculations and analysis of vibrational spectra in the works [5, 6].

The molecules of sulfides **1–4** are combined in dimers due to formation of hydrogen bonds, these dimers are oriented in the following way: the oxygen atom of the first molecule is bonded with the NH group of the second molecule, and the NH group of the first molecule is bonded with the oxygen atom of the second molecule (Fig. 5). The length of hydrogen bonds in compounds **2** and **4** is 1.889 and 1.896 Å. This length in compounds **1** and **3** is equal to 1.921 and 1.923 Å. The dimers are almost in the same plane, and the deviation is not more than 1–2°. The dimers of sulfides **1–4** are packed in parallel planes due to short contacts (Fig. 6).

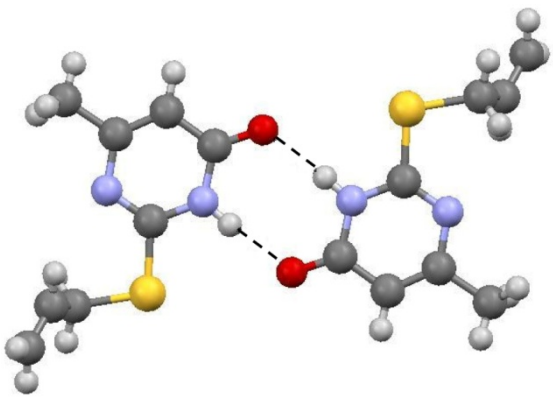

Fig. 5. The structure of compound 2 dimer

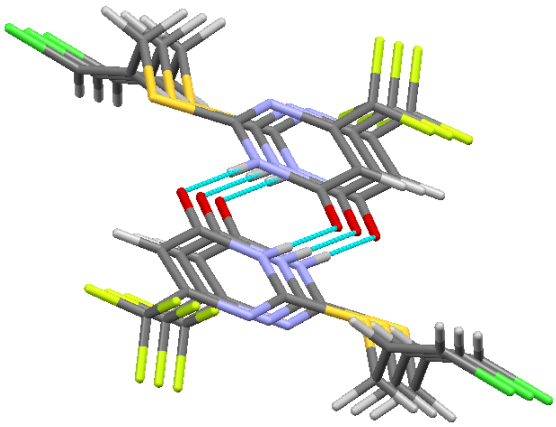

Fig. 6. The packing of molecules in crystal 4

The oxygen of one molecule and the proton of the prenyl fragment methyl group of another molecule form this contact in prenyl sulfide **3** (Fig. 7). The oxygen of one molecule and the proton at the β-carbon atom in the allyl fragment of another molecule form this contact in chloroallyl sulfide **4** (Fig. 8).

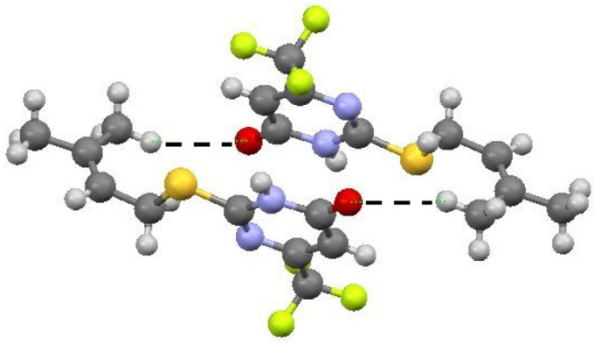

Fig. 7. The packing of molecules in crystal 3

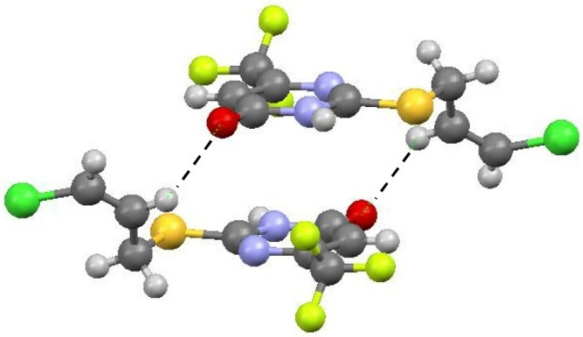

Fig. 8. The packing of molecules in crystal 4

Dimers in propargyl sulfide **1** and allyl sulfide **2** are packed through short contacts between carbonyl carbon atoms O=C … C=O. These lengths are 3.309 and 3.398 Å, respectively (Fig. 9, 10).

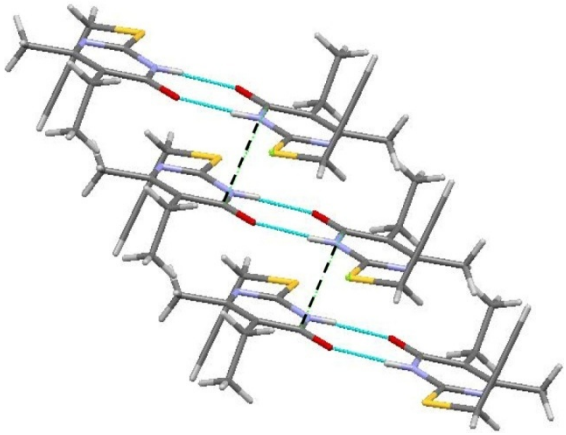

Fig. 9. The short contact in compound 1

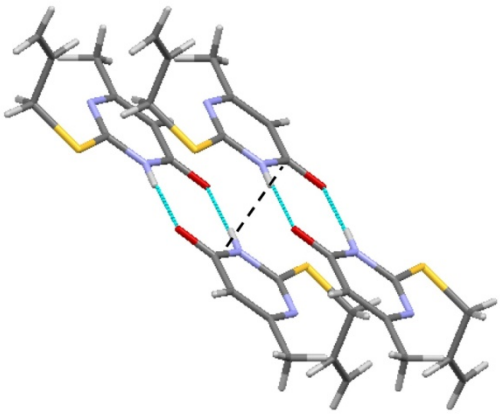

Fig. 10. The short contact in compound 2

In contrast to sulfides **3** and **4**, compounds **1** and **2** have short contacts between sulfur atoms, 3.321 and 3.409 Å, respectively (Fig. 11). It makes the packing of dimers by stacks possible (Fig. 12).

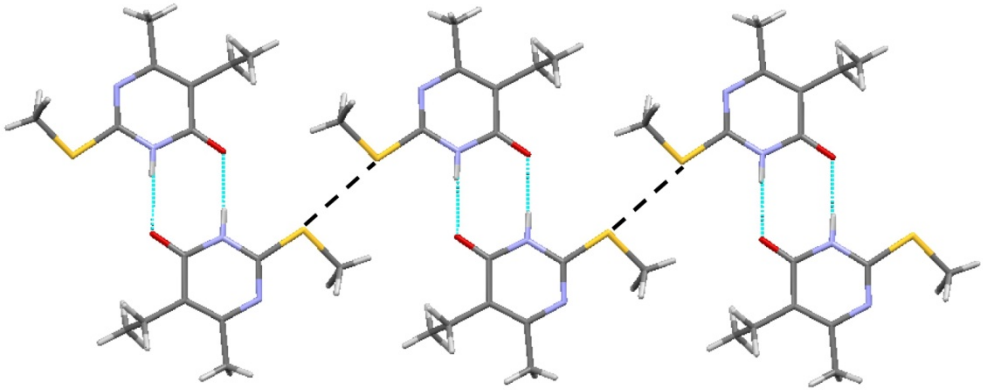

Fig. 11. The short contact in compound 1

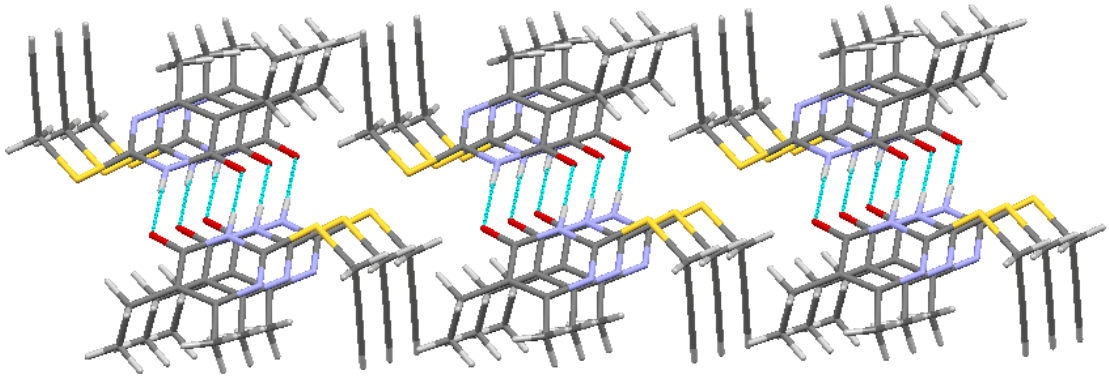

Fig. 12. The packing of molecules in crystal compound 2

In spite of the differences, the packing of compounds **2–4** is similar; it is presented on figures 13 and 14. Only in the case of allyl sulfide **1** the packing has two perpendicular directions (Fig. 13), while there is only one direction in compounds **3** and **4** (Fig. 14).

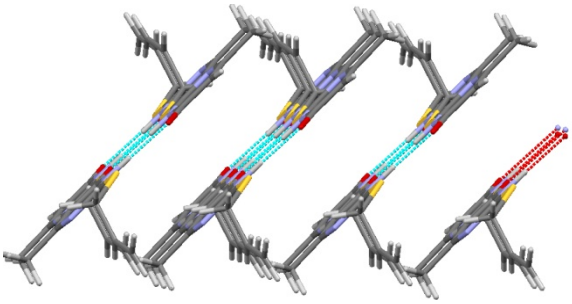

Fig. 13. The packing of molecules in crystal 2

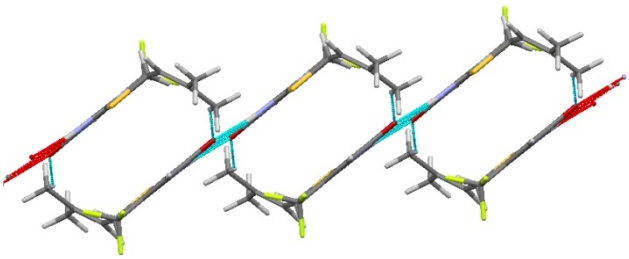

Fig. 14. The packing of molecules in crystal 3

In contrast with crystals **2–4**, the stack packing of dimers in the crystal of propargyl sulfide **1** is in perpendicular plane (Fig. 15).

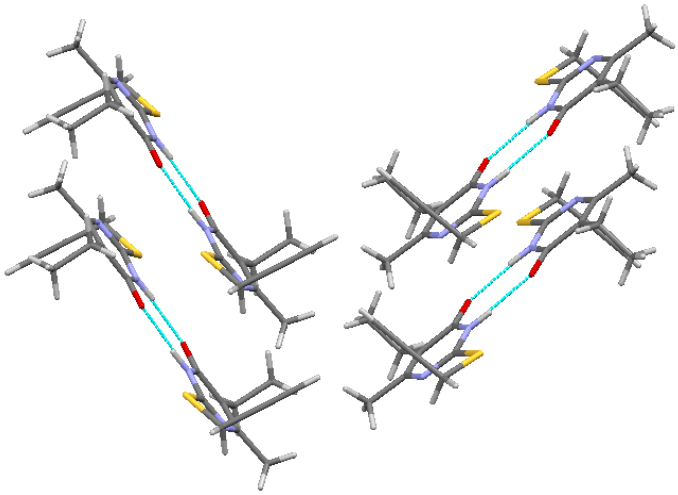

Fig. 15. The packing of molecules in crystal 1

Conclusion

We have found that S-sodium salt of 6-methyl-5-ethyl-2-thiouracil reacts with propargyl bromide to produce 2-propargylthio-6-methyl-5-ethyl-4(3*H*)-pyrimidinone. By X-ray method it has been found that S-derivatives of 2-thiouracil are in the tautomeric form with the proton at the nitrogen atom N^3. The substitute group at the sulfur atom is placed at the angle 59–84° with the plane of pyrimidine ring. The 2-alkylthio-4(3*H*)-pyrimidinone molecules are combined in dimers with formation of two intermolecular hydrogen bonds.

References

1. Slivka N.Yu., Gevaza Yu.I., Staninets V.I. Halocyclization of Substituted 2-(Alkenylthio)-pyrimidin-6-ones. Chemistry of Heterocyclic Compounds, 2004, no. 5, pp. 776–783. doi: 10.1023/B:COHC.0000037323.22839.9f

2. Frolova T.V., Kim D.G., Slepukhin P.A. [The Synthesis and Analysis of S-allyl-2-thiouracile Derivatives]. *Bulletin of South Ural State University. Ser. Chemistry,* 2010, no. 11, iss. 3, pp. 9–15. (in Russ.)

3. Bruker (2000) SMART. Bruker Molecular Analysis Research Tool, Versions 5.625 Bruker AXS, Madison, Wisconsin, USA.

4. Bruker (2000) SAINTPlus Data Reduction and Correction Program Versions 6.02a, Bruker AXS, Madison, Wisconsin, USA.

5. Ten G.N., Burova T.G., Baranov V.I. [Determination of the Tautomeric Structures of Uracil Thiosubstituted Derivatives by IR and RRS Spectroscopy]. *Journal of Structural Chemistry*, 2007, vol. 48, no. 3, pp. 447–455. doi: 10.1007/s10947-007-0067-z.

6. Ten G.N., Nechaev V.V., Shcherbakov R.S., Baranov V.I. Calculation and Analysis of the Structure and Vibrational Spectra of Uracil Tautomers. *Journal of Structural Chemistry*, 2010, vol. 51, no. 1, pp. 32–39. doi: 10.1007/s10947-010-0005-3.

Received 10 May 2015

УДК 547.854.83+548.312.5

ИССЛЕДОВАНИЕ МЕТОДОМ РЕНТГЕНОСТРУКТУРНОГО АНАЛИЗА ПРОИЗВОДНЫХ 2-ТИОУРАЦИЛА

Т.В. Фролова, Д.Г. Ким, В.В. Шарутин, К.Ю. Ошеко
Южно-Уральский государственный университет, г. Челябинск

Алкилированием S-натриевой соли 6-метил-5-этил-2-тиоурацила бромистым пропаргилом синтезирован 2-пропаргилтио-6-метил-5-этил-4(3*H*)-пиримидинон. Методом рентгеноструктурного анализа установлено, что S-производные 2-тиоурацилов находятся в таутомерной форме с протоном у атома азота N^3, а заместитель при атоме серы находится под углом 59–84° к плоскости пиримидинового кольца. Молекулы 2-алкилтио-4(3*H*)-пиримидинонов объединены в димеры, в которых образуются две межмолекулярные водородные связи.

Ключевые слова: 2-пренилтио-6-трифторметил-4(3H)-пиримидинон, цис-2-(3-хлораллил)тио-6-трифторметил-4(3H)-пиримидинон, 2-аллилтио-6-метил-4(3H)-пиримидинон, 2-пропаргилтио-6-метил-5-этил-4(3H)-пиримидинон. алкилирование, пропаргилбромид, таутомерия, молекулярные структуры, рентгеноструктурный анализ.

Литература

1. Сливка, Н.Ю. Галогенциклизация замещенных 2-(алкенилтио)-пиримидин-6-онов / Н.Ю. Сливка, Ю.И. Геваза, В.И. Станинец // Химия гетероциклических соединений. – 2004. – № 5. – С. 776–783.

2. Фролова, Т.В. Синтез и исследование S-аллильных производных 2-тиоурацилов / Т.В. Фролова, Д.Г. Ким, П.А. Слепухин // Вестник ЮУрГУ. Серия «Химия». – 2010. – Вып. 3. – №. 11. – С. 9–15.

3. Bruker (2000) SMART. Bruker Molecular Analysis Research Tool, Versions 5.625 Bruker AXS, Madison, Wisconsin, USA.

4. Bruker (2000) SAINTPlus Data Reduction and Correction Program Versions 6.02a, Bruker AXS, Madison, Wisconsin, USA.

5. Тен, Г.Н. Определение таутомерных структур тиозамещенных урацила методом ИК и РКР спектроскопии / Г.Н. Тен, Т.Г. Бурова, В.И. Баранов // Журнал структурной химии. – 2007. – Т. 48. – № 3. – С. 492–500.

6. Расчет и анализ структуры и колебательных спектров таутомера урацила / Г.Н. Тен, В.В. Нечаев, Р.С. Щербаков, В.И. Баранов // Журнал структурной химии. – 2010. – Т. 51. – № 1. – С. 38–45.

Фролова Татьяна Владимировна – старший преподаватель, кафедра органической химии, Южно-Уральский государственный университет. 454080, г. Челябинск, пр. им. В.И. Ленина, 76. E-mail: chemitash@gmail.com

Ким Дмитрий Гымнанович – доктор химических наук, профессор, кафедра органической химии, Южно-Уральский государственный университет. 454080, г. Челябинск, пр. им. В.И. Ленина, 76. E-mail: kim_dg48@mail.ru

Шарутин Владимир Викторович – доктор химических наук, профессор, химическмй факультет, Южно-Уральский государственный университет. 454080, г. Челябинск, пр. им. В.И. Ленина, 76. E-mail: vvsharutin@rambler.ru

Ошеко Ксения Юрьевна – студентка химического факультета, Южно-Уральский государственный университет. 454080, г. Челябинск, пр. им. В.И. Ленина, 76. E-mail: osheko_kseniya@mail.ru

Поступила в редакцию 10 мая 2015 г.

ОБРАЗЕЦ ЦИТИРОВАНИЯ

Study on reaction of 2-allylthiobenzimidazole with bromine / T.V. Frolova, D.G. Kim, V.V. Sharutin, K.Yu. Osheko // Вестник ЮУрГУ. Серия «Химия». – 2015. – Т. 7, № 3. – С. 11–18.

FOR CITATION

Frolova T.V., Kim D.G., Sharutin V.V., Osheko K.Yu. Study on Reaction of 2-allylthiobenzimidazole with Bromine. *Bulletin of the South Ural State University. Ser. Chemistry.* 2015, vol. 7, no. 3, pp. 11–18.

STUDY ON REACTION OF 2-ALLYLTHIOBENZIMIDAZOLE WITH BROMINE

E.S. Il'inykh, *South Ural State University, Chelyabinsk, Russian Federation, elena.ilinykh@mail.ru*
D.G. Kim, *South Ural State University, Chelyabinsk, Russian Federation, kim_dg48@mail.ru*

It has been found by ^{1}H NMR method that bromination of 2-allylthio-benzimidazole proceeds to give the bromocyclization products (benzimidazo-[2,1-b]thiazolium and benzimidazo[2,1-b][1,3]thiazinium bromides) and two isomeric products of bromine addition to the double bond of allyl moiety.

Keywords: 2-mercaptobenzimidazole, 2-allylthiobenzimidazole, bromocyclization, bromonium and thiiranium ions, ^{1}H NMR spectroscopy.

Introduction

The chemistry of benzimidazole and particularly 2-mercaptobenzimidazole and its derivatives has received considerable attention because of their synthetic and biological importance. Natural compounds (e.g. vitamin B_{12}) and various medicines (e.g. dibazole, omeprazole, mebendazole, afobazole, *etc.*) contain benzimidazole moiety in their structure. 2-Mercaptobenzimidazole is widely used in industrial application as a stabilizer and an antioxidant in rubber [1, 2], an adsorbent for some metals [3–5] and a corrosion inhibitor [6]. Besides, many kinds of biological activities have been reported for various N,S-derivatives of 2-mercaptobenzimidazole [7].

The chemistry of fused heterocyclic systems obtained from benzimidazole, as well as synthetic paths to thiazolo[3,2-*a*]benzimidazoles and their chemical properties, has been described in the reviews [8, 9]. However, literature data on electrophilic heterocyclization of S-allyl derivatives of 2-mercaptobenzimidazole (**1**) and 5-ethoxy-2-mercaptobenzimidazole by the treatment with iodine and bromine are limited [10–13]. In the present paper we study the interaction of 2-allylthiobenzimidazole (**2**) with bromine and show unexpected results that are different from earlier data [11].

As demonstrated previously by Korotkikh *et al* [11], the reaction between 2-allylthiobenzimidazole **2** and bromine in acetic acid leads to bromine addition to the double bond and formation of 2-(2,3-dibromopropyl)thiobenzimidazole hydrobromide (**3**) precipitated from the reaction mixture. However, the authors do not explain the origin of HBr in the reaction. The treatment of hydrobromide **3** with mild alkaline agents produces 2-(2,3-dibromopropyl)thiobenzimidazole (**3a**), which undergo cyclization into 3-bromo-2,3,4,10-tetrahydrobenzimidazo[2,1-*b*][1,3]thiazinium bromide (**4**) and isomeric 2*H*-benzimidazo[2,1-*b*][1,3]thiazine (**5**) and 4*H*-benzimidazo[2,1-*b*][1,3]thiazine (**6**) at room temperature in acetone or acetonitrile solution or in the melt (Scheme 1). The mixture of thiazines **5** and **6** is also obtained by refluxing bromide **4** in methanol solution of alkali.

We have earlier reported iodo- and bromocyclization of 3-allylthio-1,2,4-triazoles [14–16]. Notably, bromination of 3-allylthio-1,2,4-triazole and 2-allylthiobenzthiazole with the structure similar to that of compound **2** leads to predominant annelation of thiazole ring. In order to make these issues clear, we have attempted to study the reaction between 2-allylthio-benzimidazole **2** and bromine in more detail.

Experimental

^{1}H NMR spectra were recorded for DMSO-d_6 or $CDCl_3$ solutions of compounds on a Bruker DRX-400 instrument (400 MHz) using Me_4Si as the internal standard.

2-Allylthiobenzimidazole (2). To the solution of 2-mercaptobenzimidazole **1** (0.300 g, 2 mmol) in DMF (5 mL) a solution of KOH (0.112 g, 2 mmol) in water (2 mL) and 3-bromopropene (0.18 mL, 2 mmol) were added. After 24 h, the reaction mixture was poured into water (50 mL) and the produced white precipitate was filtered off, washed with water and dried. The precipitate was recrystallized from the hexane–chloroform mixture (1:1) to give compound **2** as a white solid. Yield 0.266 g (70 %), mp 137 °C.

Bromination of 2-allylthiobenzimidazole (2). To a solution of 2-allylthiobenzimidazole **2** (0.190 g, 1 mmol) in acetic acid (3 mL) at 0–5 °C a solution of bromine (0.05 mL, 1 mmol) in acetic

acid (3 mL) was added dropwise. The produced white precipitate was filtered off and washed with acetone. Yield 0.300 g (the mixture of compounds **3**, **4**, **7** and **8**). The solvent was removed from the filtrate; the residue was treated with acetone, after removing acetone a white solid was obtained. Yield 0.103 g (the mixture of compounds **3–8**).

Results and Discussion

Initial 2-allylthiobenzimidazole **2** was synthesized by the reaction of 2-mercapto-benzimidazole **1** with 3-bromopropene in the DMF–KOH medium (Scheme 1).

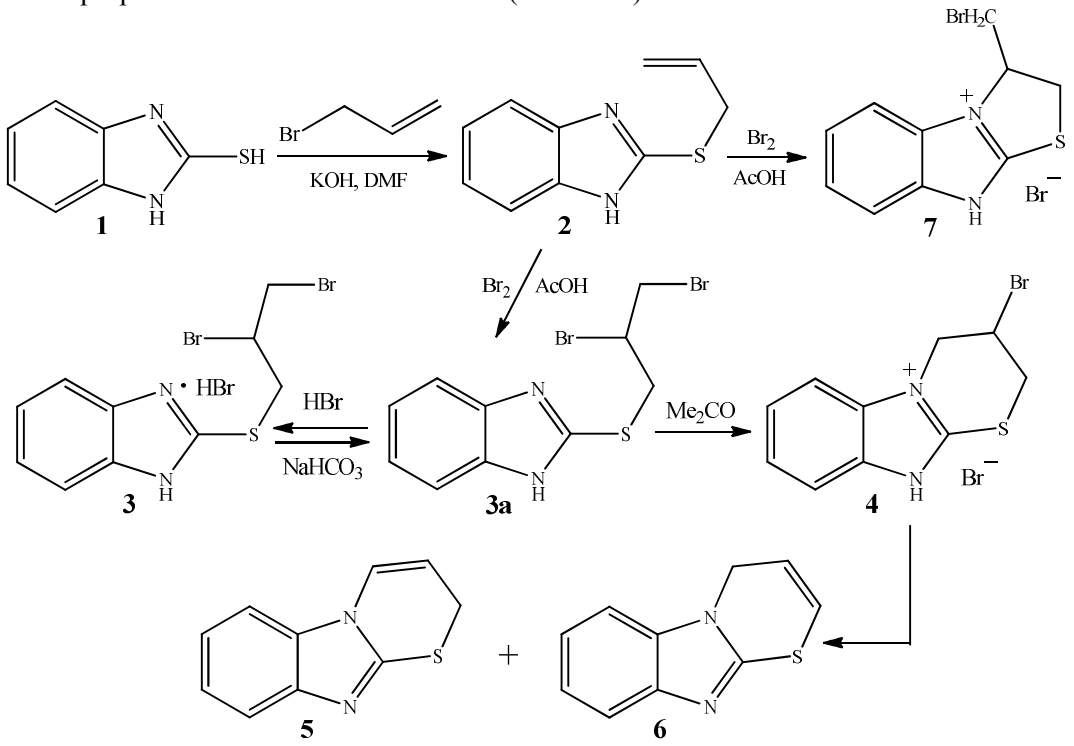

Scheme 1. Synthesis and bromination of 2-allylthiobenzimidazole (2)

We have studied the interaction of allyl sulfide **2** with bromine in acetic acid at the allylsulfide **2**:bromine ratio of 1:1.5 under conditions similar to those in [11]. Study of the precipitated product by ^{1}H NMR method have made it possible to reveal not only hydrobromide **3**, but also benzimidazothiazinium bromide **4** and the second bromocyclization product, 3-bromomethyl-2,3-dihydro-9*H*-benzimidazo-[2,1-*b*]thiazolium bromide (**7**) resulting from the thiazole ring annelation. From ^{1}H NMR data, the ratio of compounds **3**, **4** and **7** is ~ 1.0 : 0.3 : 0.1. There is a logical question, why only hydrobromide **3** is revealed by the authors of paper [11]. In our opinion, this is due to the fact that ^{1}H NMR studies were carried out by us on a Bruker instrument (400 MHz), whereas the authors of [11] used a Gemini 200 instrument (200 MHz).

Apparently, bromide **4** was produced *via* intramolecular nucleophilic substitution of adduct **3a**.

The adduct of bromine as hydrobromide **3** was likely formed due to a partial cleavage of HBr from bromides **4** and **7** as a result of their interaction with 2-(2,3-dibromopropyl)thiobenzimidazole **3a**. Thus, bromides **4** and **7** were converted into bases which remained in the solution. This fact may also explain a high prevalence of hydrobromide **3** in the mixture of obtained salts **3**, **4** and **7**.

Notably, a thorough analysis of the ^{1}H NMR spectra recorded for the resulting mixture has allowed us to identify not only abovementioned compounds **3**, **4** and **7**, but also the adduct of bromine different from compound **3**, namely, 2-[2-bromo-1-(bromomethyl)ethyl]thiobenzimidazole hydrobromide (**8**) (HBr was cleaved from bromides **4** and **7**). It could be produced *via* intermediate formation of bromonium ion (**I**) that was able to undergo intramolecular rearrangement into thiiranium ion (**II**), which was then easily converted into the adduct of bromine of symmetrical structure **8** (Scheme 2). The intramolecular rearrangement of bromonium ion into thiiranium ion has first been studied in the bromination of methylallyl sulfide [17]. In addition, this rearrangement has also been revealed by us during the study of bromination of 3-allylthio-1,2,4-triazoles [16].

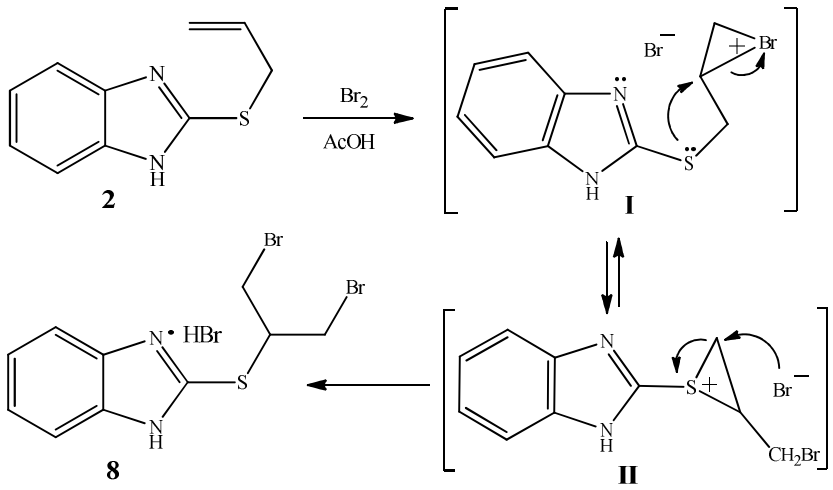

Scheme 2. The mechanism of formation of 2-[2-bromo-1-(bromomethyl)ethyl]thiobenzimidazole hydrobromide (8)

^{1}H NMR spectral data of the synthesized compounds are shown in the table.

Table

^{1}H NMR spectral data of the synthesized compounds

Compound	^{1}H NMR spectra, δ, ppm (*J*, Hz)
2	4.04 (2H, d, ^3J = 6.8, –SCH_2–); 5.07 (1H, m, =CH_2); 5.25 (1H, m, =CH_2); 6.03 (1H, m, –C<u>H</u>=); 7.11 (2H, m, H_{arom}); 7.46 (2H, m, H_{arom})
3	4.05 (2H, m, –SCH_2–); 4.10 (2H, m, –CH_2Br); 4.86 (1H, m, –C<u>H</u>Br–); 7.50 (2H, m, H_{arom}); 7.73 (2H, m, H_{arom})
4	3.98 (1H, m, –SC<u>H_A</u>H_B–); 4.02 (1H, m,–SCH_A<u>H_B</u>–); 4.61 (1H, m, –NC<u>H_M</u>H_N–); 4.73 (1H, m,–NCH_M<u>H_N</u>–); 5.08 (1H, m, –C<u>H_X</u>Br–); 7.42 (2H, m, H_{arom}); 7.78 (2H, m, H_{arom})
7	4.05 (1H, m, –C<u>H_A</u>H_BBr); 4.10 (1H, m, –CH_A<u>H_B</u>Br); 4.13 (1H, m, –SC<u>H_M</u>H_N–); 4.56 (1H, m, –SCH_M<u>H_N</u>–); 5.19 (1H, m, –$^+$NC<u>H_X</u>–); 7.44 (2H, m, H_{arom}); 7.76 (2H, m, H_{arom})
8	3.94 (2H, dd, ^2J = 11.0, ^3J = 6.6, -CH_2Br); 3.98 (2H, dd, ^2J = 11.0, ^3J = 6.6, -CH_2Br); 4.63 (1H, m, -SC<u>H</u><); 7.52 (2H, m, H_{arom}); 7.73 (2H, m, H_{arom})

A set of proton signals of both bromocyclization products, bromides **4** and **7**, contained signals for aromatic protons shifted downfield and multiplet for the –C<u>H_X</u>Br– proton (*δ* 5.08 ppm) and the -$^+$NC<u>H_X</u>– proton (*δ* 5.19 ppm), respectively, as well as the characteristic proton signals for such ABMNX spin systems.

In the ^{1}H NMR spectrum of compound **8** the –SC<u>H</u>< proton was revealed as multiplet at *δ* 4.63 ppm. Two-proton doublets of doublets of four –$(CH_2Br)_2$ protons having a double integral intensity appeared at *δ* 3.94 and 3.98 ppm.

The filtrate obtained after separation of the mixture of products **3**, **4**, **7**, and **8** has been also studied (such study was not carried out by the authors of paper [11]). After evaporation of acetic acid we managed to obtain a crystalline precipitate which was the mixture of compounds **3**, **4**, **7**, and **8,** as well as 2*H*-thiazine **5** and 4*H*-thiazine **6** (from ^{1}H NMR data). Formation of thiazines **5** and **6** as by-products of this reaction has also been reported previously [11]. ^{1}H NMR spectral data produced by us for the mentioned compounds are identical to the published ones [11].

Bromination of compound **2** has also been studied by us in the ^{1}H NMR experiment. To its solution in $CDCl_3$ a solution of an equimolar amount of bromine in $CDCl_3$ was added, and after 1 hour ^{1}H NMR spectrum of the reaction mixture was recorded. Compound **2** reacted with bromine at once as the spectrum recorded did not contain characteristic signals for the alkenyl protons. From ^{1}H NMR data, bromine adducts **3** and **8** at the ratio of ~ 1:3 predominated in the studied reaction mixture. These results

indicate that the bromocyclization products **4** and **7** were probably formed directly from intermediate bromine adducts **3** and **8**.

To summarize, allyl sulfide **2** reacted with bromine to give the mixture of adducts **3a** and **8**, as well as bromide **7** formed from adduct **8**. Compound **3a** was partially converted to bromide **4**, and partly it reacted with bromide **7** to give hydrobromide **3** *via* cleavage of HBr from bromide **7**. Thiazines **5** and **6** were formed in minor amounts by the reaction between adduct **3a** or **8** and bromide **4** followed by the removal of two HBr molecules.

Conlusions

It has been found that the interaction of 2-allylthiobenzimidazole **2** with bromine in acetic acid proceeds to give not a single product as reported in [11] but the mixture of two bromocyclization products, 3-bromo-2,3,4,10-tetrahydrobenzimidazo[2,1-*b*][1,3]thiazinium and 3-bromomethyl-2,3-dihydro-9*H*-benzimidazo[2,1-*b*]thiazolium bromides, and two products of bromine addition to the double bond of allyl moiety with symmetrical and asymmetrical structure. It has been found by ^{1}H NMR experiment that at the initial stage of bromination of 2-allylthiobenzimidazole bromine adducts are formed, and then they are partially converted into the bromocyclization products.

This work was supported by the program «U.M.N.I.K. 1-14-11» of the Fund for Assistance to Small Innovative Enterprises in the scientific and technical sphere.

References

1. Zhong B., Jia Z., Luo Y., Guo B. Jia D. Preparation of Halloysite Nanotubes Supported 2-Mercaptobenzimidazole and Its Application in Natural Rubber. *Compos. Part A.*, 2015, vol. 73, pp. 63–71. doi: 10.1016/j.compositesa.2015.03.007.

2. Zhong B., Shi Q., Jia Z., Luo Y., Chen Y., Jia D. Preparation of Silica-supported 2-Mercaptobenzimidazole and Its Antioxidative Behavior in Styrene-Butadiene Rubber. *Polym. Degrad. Stab.*, 2014, vol. 110, pp. 260–267. doi: 10.1016/j.polymdegradstab.2014.09.008.

3. Moreira J.C., Luiz C.P., Yoshitaka G. Adsorption of Cu(II), Zn(II), Cd(II), Hg(II) and Pb(II), from Aqueous Solutions on a 2-Mercaptobenzimidazole – Modified Silicagel. *Mikrochim. Acta II*, 1990, vol. 102, pp. 107–115. doi: 10.1007/BF01244293.

4. Pourreza N., Ghanemi K. Determination of Mercury in Water and Fish Samples by Cold Vapor Atomic Adsorption Spectrometry after Solid Phase Extraction on Agar Modified with 2-Mercaptobenzimidazole. *J. Hazard. Mater.*, 2009, vol. 161, no. 2–3, pp. 982–987. doi: 10.1016/ j.jhazmat.2008.04.043.

5. Pourreza N., Rastegarzadeh S., Larki A. Nano-TiO_2 Modified with 2-Mercaptobenzimidazole as an Efficient Adsorbent for Removal of Ag(I) from Aqueous Solutions. *J. Ind. Eng. Chem.*, 2014, vol. 20, no. 1, pp. 127–132. doi: 10.1016/j.jiec.2013.04.016.

6. Izquierdo J., Santana J.J., González S., Souto R.M. Scunning Microelectrochemical Characterization of the Anti-corrosion Performance of Inhibitor Films Formed by 2-Mercaptobenzimidazole on Copper. *Prog. Org. Coat.*, 2012, vol. 74, no. 3, pp. 526–533. doi: 10.1016/j.porgcoat.2012.01.019.

7. Seredenin S.B., Blendov J.A., Saveliev V.L., Mozhaeva T.Y. *2-Mercaptobenzimidazole Derivatives Possessing Pharmacological Activity*. US Patent 6376666, 2002.

8. Al-Rashood K.A., Abdel-Aziz H.A. Thiazolo[3,2-*a*]Benzimidazoles: Synthetic Strategies, Chemical Transformations and Biological Activities (Review). *Molecules*, 2010, vol. 15, no. 6, pp. 3775–3815. doi: 10.3390/molecules15063775.

9. Dawood K.M., Elwan N.M., Abdel-Wahab B.F. Recent Advances on the Synthesis of Azoles, Azines and Azepines Fused to Benzimidazole. *ARKIVOC*, 2011, (i), pp. 111-195.

10. Kim D.G., Avdin V.V., Gavrilova L.V. Interaction of 2-Alkenylthiobenzimidazoles with Iodine. *Chem. Heterocycl. Compd.*, 1997, vol. 33, no. 8, pp. 986–988. doi: 10.1007/BF02253175.

11. Korotkikh N.I., Raenko G.F., Shvaika O.P. Heterocyclization of 2-Allylthiobenzimidazoles into Derivatives of Benzimidazo[2,1-*b*]-1,3-Thiazines. *Chem. Heterocycl. Compd.*, 1995, vol. 31, no. 3, pp. 359–363. doi: 10.1007/BF01373558.

12. Korotkikh N.I., Aslanov A.F., Raenko G.F., Shvaika O.P. [Halocyclization and Recyclization Reactions: Synthesis of Thiirane, Thiethane and Selenatane Derivatives of Azolones]. *Zh. Organ. Khimii*, 1999, vol. 35, iss. 5, pp. 752–761. (in Russ.)

13. Slivka N.Yu., Gevaza Yu.I., Staninets V.I., Turov A.V. [Chemo- and Regioselectivity in the Halocyclization Reactions of Substituted 2-Alkenylthiobenzimidazoles]. *Ukr. Khim. Zhurn*., 2003, vol. 69, no. 9-10, pp. 104–110. (in Russ.)

14. Il'inykh E.S., Kim D.G. Iodocyclization of S-Allyl Derivatives of 3-Mercapto-4-Methyl-1,2,4-Triazole. *Chem. Heterocycl. Compd*., 2011, vol. 47, no. 5, pp. 636–638. doi: 10.1007/s10593-011-0809-x.

15. Il'inykh E.S., Kim D.G., Kodess M.I., Matochkina E.G., Slepukhin P.A. Synthesis of Novel Fluorine- and Iodine-containing [1,2,4]Triazolo[3,4-*b*][1,3]thiazines Based 3-(Alkenylthio)-5-(Trifluoromethyl)-4*H*-1,2,4-Triazole-3-Thiols. *J. Fluorine Chem.*, 2013, vol. 149, pp. 24–29. doi: 10.1016/j.jfluchem.2013.01.025.

16. Il'inykh E.S. *Geterotsiklizatsiya alkenil'nykh i propargil'nykh proizvodnykh 1,2,4-triazol-3-tionov*. Avtoref. kand. dis. [Heterocyclization of Alkenyl and Propargyl Derivatives of 1,2,4-Triazole-3-Thiones. Abstract of cand. diss.]. Yekaterinburg, 2013. 24 p.

17. Bland J.M., Stammer C.H. An Intramolecular Bromonium to Thiiranium Ion Rearrangement. *J. Org. Chem*., 1983, vol. 48, no. 23, pp. 4393–4394. doi: 10.1021/jo00171a049.

Received 1 June 2015

УДК 547.781

ИССЛЕДОВАНИЕ РЕАКЦИИ 2-АЛЛИЛТИОБЕНЗИМИДАЗОЛА С БРОМОМ

Е.С. Ильиных, Д.Г. Ким
Южно-Уральский государственный университет, г. Челябинск

Методом ЯМР ^{1}H установлено, что бромирование 2-аллилтиобенз-имидазола сопровождается образованием продуктов бромциклизации (бромиды бензимидазо[2,1-*b*]тиазолия и бензимидазо[2,1-*b*][1,3]тиазиния) и двух изомерных друг другу продуктов присоединения брома по двойной связи аллильного фрагмента.

Ключевые слова: 2-меркаптобензимидазол, 2-аллилтиобензимидазол, бромциклизация, бромониевый ион, тиираниевый ион, спектроскопия ЯМР ^{1}H.

Литература

1. Preparation of Halloysite Nanotubes Supported 2-Mercaptobenzimidazole and Its Application in Natural Rubber / B. Zhong, Z. Jia, Y. Luo et al. // Compos. Part A. – 2015. – Vol. 73. – P. 63–71. doi: 10.1016/j.compositesa.2015.03.007.

2. Preparation of Silica-supported 2-Mercaptobenzimidazole and Its Antioxidative Behavior in Styrene-butadiene Rubber / B. Zhong, Q. Shi, Z. Jia et al. // Polym. Degrad. Stab. – 2014. – Vol. 110. – P. 260–267. doi: 10.1016/j.polymdegradstab.2014.09.008.

3. Moreira, J.C. Adsorption of Cu(II), Zn(II), Cd(II), Hg(II) and Pb(II), from Aqueous Solutions on a 2-Mercaptobenzimidazole – Modified Silicagel / J.C. Moreira, C.P. Luiz, G. Yoshitaka // Mikrochim. Acta II. – 1990. – Vol. 102. – P. 107–115. doi: 10.1007/BF01244293.

4. Pourreza, N. Determination of Mercury in Water and Fish Samples by Cold Vapor Atomic Adsorption Spectrometry after Solid Phase Extraction on Agar Modified with 2-Mercaptobenzimidazole / N. Pourreza, K. Ghanemi // J. Hazard. Mater. – 2009. – Vol. 161. – No. 2–3. – P. 982–987. doi: 10.1016/j.jhazmat.2008.04.043.

5. Pourreza, N. Nano-TiO_2 Modified with 2-Mercaptobenzimidazole as an Efficient Adsorbent for Removal of Ag(I) from Aqueous Solutions / N. Pourreza, S. Rastegarzadeh, A. Larki // J. Ind. Eng. Chem. – 2014. – Vol. 20. – No. 1. – P. 127–132. doi: 10.1016/j.jiec.2013.04.016.

6. Scunning Microelectrochemical Characterization of the Anti-corrosion Performance of Inhibitor Films Formed by 2-Mercaptobenzimidazole on Copper / J. Izquierdo, J.J. Santana, S. González et al. // Prog. Org. Coat. – 2012. – Vol. 74. – No. 3. – P. 526–533. doi: 10.1016/j.porgcoat.2012.01.019.

7. 2-Mercaptobenzimidazole Derivatives Possessing Pharmacological Activity / S.B. Seredenin, J.A. Blendov, V.L. Saveliev et al. // US Patent 6376666, 2002.

8. Al-Rashood, K.A. Thiazolo[3,2-*a*]benzimidazoles: Synthetic Strategies, Chemical Transformations and Biological Activities (Review) / K.A. Al-Rashood, H.A. Abdel-Aziz // Molecules. – 2010. – Vol. 15. – No. 6. – P. 3775–3815. doi: 10.3390/molecules15063775.

9. Dawood, K.M. Recent Advances on the Synthesis of Azoles, Azines and Azepines Fused to Benzimidazole / K.M. Dawood, N.M. Elwan, B.F. Abdel-Wahab // ARKIVOC. – 2011. – (i). – P. 111-195.

10. Ким, Д.Г. Реакция 2-алкенилтиобензимидазолов с иодом / Д.Г. Ким, В.В. Авдин, Л.В. Гаврилова // Химия гетероцикл. соед. – 1997. – № 8. – С. 1130–1132.

11. Коротких, Н.И. Гетероциклизация 2-аллилтиобензимидазолов в производные бензимидазо[2,1-*b*]-1,3-тиазинов / Н.И. Коротких, Г.Ф. Раенко, О.П. Швайка // Химия гетероцикл. соед. – 1995. – № 3. – С. 410–415.

12. Реакции галогенциклизации и рециклизации: синтез тиирановых, тиетановых и селенетановых производных азолонов / Н.И. Коротких, А.Ф. Асланов, Г.Ф. Раенко и др. // Ж. орган. химии. – 1999. – Т. 35, Вып. 5. – С. 752–761.

13. Хемо- и региоселективность в реакциях галогенциклизации замещенных 2-алкенилтиобензимидазолов / Н.Ю. Сливка, Ю.И. Геваза, В.И. Станинец и др. // Укр. хим. журн. – 2003. – Т. 69, № 9–10. – С. 104–110.

14. Ильиных, Е.С. Иодциклизация of S-аллильных производных 3-меркапто-4-метил-1,2,4-триазола / Е.С. Ильиных, Д.Г. Ким // Химия гетероцикл. соединений. – 2011. – № 5. – С. 766–769.

15. Synthesis of Novel Fluorine- and Iodine-containing [1,2,4]Triazolo[3,4-*b*][1,3]thiazines Based 3-(Alkenylthio)-5-(Trifluoromethyl)-4*H*-1,2,4-Triazole-3-Thiols / E.S. Il'inykh, D.G. Kim, M.I. Kodess et al. // J. Fluorine Chem. – 2013. – Vol. 149. – P. 24–29. doi: 10.1016/j.jfluchem.2013.01.025.

16. Ильиных, Е.С. Гетероциклизация алкенильных и пропаргильных производных 1,2,4-триазол-3-тионов: автореф. дис. … канд. хим. наук / Е.С. Ильиных. – Екатеринбург, 2013. – 24 с.

17. Bland, J.M. An Intramolecular Bromonium to Thiiranium Ion Rearrangement / J.M. Bland, C.H. Stammer // J. Org. Chem. – 1983. – Vol. 48. – No. 23. – P. 4393–4394. doi: 10.1021/jo00171a049.

Ильиных Елена Сергеевна – кандидат химических наук, доцент, кафедра органической химии, Южно-Уральский государственный университет. 454080, г. Челябинск, пр. им. В.И. Ленина, 76. E-mail: elena.ilinykh@mail.ru

Ким Дмитрий Гымнанович – доктор химических наук, профессор, кафедра органической химии, Южно-Уральский государственный университет. 454080, г. Челябинск, пр. им. В.И. Ленина, 76. E-mail: kim_dg48@mail.ru

Поступила в редакцию 1 июня 2015 г.

ОБРАЗЕЦ ЦИТИРОВАНИЯ

Il'inykh, E.S. Study on reaction of 2-allylthiobenzimidazole with bromine / E.S. Il'inykh, D.G. Kim // Вестник ЮУрГУ. Серия «Химия». – 2015. – Т. 7, № 3. – С. 19–24.

FOR CITATION

Il'inykh E.S., Kim D.G. Study on Reaction of 2-allylthiobenzimidazole with Bromine. *Bulletin of the South Ural State University. Ser. Chemistry.* 2015, vol. 7, no. 3, pp. 19–24.

Физическая химия

VARIATIONS OF STRUCTURE MODELING METHODS AND RAMAN SPECTRAL CHARACTERISTICS FOR THE IODINE CRYSTAL

I.D. Yushina, *South Ural State University, Chelyabinsk, Russian Federation, idu-xda@mail.ru*
L.M. Bulatova, *South Ural State University, Chelyabinsk, Russian Federation, luciyabulat@yandex.ru*
S.E. Nasibullina, *South Ural State University, Chelyabinsk, Russian Federation, svetlaya.n.e@ yandex.ru*
E.V. Bartashevich, *South Ural State University, Chelyabinsk, Russian Federation, kbartash@yandex.ru*

On the example of the iodine crystal structure we have selected the optimal basis sets, allowing reproduction of interatomic distances and Raman spectral characteristics by 3D periodic Kohn-Sham calculations. Advantages of two approaches, taking into account the relativistic effect, have been compared: Effective Core Pseudopotentials and the Gaussian type basis set, constructed on the basis of the Douglas-Kroll-Hess approach. It has been shown that the latter approach not only correctly reproduce the experimentally observed geometric parameters of the iodine interactions and characteristics of Raman spectra, but also it reveals the electron density accumulation and depletion in the area of outermost valence shell of an iodine atom. That is directly illustrated by the Laplacian of electron density function.

Keywords: iodine crystal structure, halogen bond, Quantum Topological Analysis of Electron Density, relativistic effect, Raman scattering spectroscopy.

Introduction

Structure-forming non-covalent interactions of halogens Hal…Hal in crystals and solid states in many ways determine thermodynamic, thermophysical, spectral and other properties [1, 2]. It is known that because of anisotropy of electrostatic potential on the Van der Waals surfaces of a molecule, the halogen atom, bound in the molecule, can form two types of non-covalent interactions [3, 4]. The Type I interactions are purely Van der Waals interactions in their nature; they are characterized by random positioning of two covalent bonds of halogens, belonging to different molecules. The Type II interactions are strongly directed. They are noted for mutual orientation of molecules, in which two covalent bonds of halogens are situated at the right angle to each other. In this case the area of electron density accumulation in one halogen atom is directed to the area of electron density depletion in the other atom. This area of electron density depletion is always formed on the extension of the covalent bond of a halogen atom; it is called σ-hole [5]. In this area the nucleus is shielded by valence electrons to a lesser degree, and the area of generally positive values of electrostatic potential is formed [6, 7]. This type of non-covalent interactions is called halogen bonds [8, 9].

Halogen bond properties can be successfully studied from the perspective of QTAIMC – Quantum Theory of Atoms in Molecules and Crystals [10], because this theory is aimed at searching for binding interactions, including those which occur among non-covalent ones. Such interactions are characterized by bond paths: two lines, each point of which is different from other neighboring points of space by larger values of electron density. These lines connect atomic nuclei, which are separated by the general interatomic surface, where through the vector gradient of electron density equals zero. The QTAIMC approach includes the topological analysis of electron density $\rho(\mathbf{r})$, obtained by quantum-chemical calculations, or within precise X-ray diffraction experiment. In its turn the topological analysis allows us to identify critical points of electron density. The electron density and its properties in the bond critical points are important characteristic values describing chemical bond properties in molecules and crystals.

Halogen bonds in a chlorine crystal were first described from the perspective of electron density distribution properties, obtained through high-resolution X-ray diffraction experiment [11]. The paper

presents the visual presentation of mutually consistent orientation of the exhaustion area on to the area of electron accumulation with the Laplacian of electron density $\nabla^2\rho(\mathbf{r})$. The Laplacian of electron density characterizes three-dimensional curvature of its dropping with increase of distance from the atom nucleus. Depending on the ratio of radial positive curvature of electron density and the curvature in the orthogonal directions, the Laplacian will alternate in signs. Alternating minimums and maximums of $\nabla^2\rho(\mathbf{r})$ correspond to areas of accumulation $\nabla^2\rho(\mathbf{r})<0$ and depletion $\nabla^2\rho(\mathbf{r})>0$ of the electron density around the nucleus, so they show atom electron shells. However, ranges of the Laplacian negative values, which should correspond to outermost electron shells, do not appear at atomic numbers $Z > 29$, as it is specified in the paper [12]. That is why, as a rule, other functions of electron density, for instance, one-electron potential, are used for the Br and I compounds for the sake of outermost electron shells localization [9, 13].

Another important feature at reproduction of some experimentally observed properties of halogens with high atomic numbers, such as I or At, is the importance of relativistic effect, this is particularly manifested when analyzing properties, connected with outermost electron shells [14, 15]. Together with structural information, obtained from the electron density distribution analysis in the iodine crystal, the special attention shall be paid to its vibrational properties. The most informative method in studying I–I covalent bonds in crystals and solids is Raman spectroscopy [16, 17]. A great number of works deal with the theoretical frequency rates, obtained for structures of isolated polyiodide anions or cation-anions systems [18, 19]. However, this approach does not allow us to take into consideration the influence of crystal environment, effects of intermolecular interactions in solids, that makes it difficult to compare with the experimental spectral data. Such differences can be partly due to significant disturbance of isolated structure geometry of a molecular complex or a cluster in comparison with the crystal structure. The dynamic approach to crystal lattice with consideration of atomic vibrations around equilibrium positions allows us to explain physicochemical crystal properties, connected with thermal effects, phase transitions, conduction properties. Theoretical calculations allow us to deduce vibrational spectra, to forecast crystal structure stability and to obtain thermodynamic properties, such as heat of formation and sublimation, entropy, and others [20].

The purpose of this paper is to select basis sets, allowing to provide the accurate modeling of covalent and halogen bonds and their characteristics in the iodine crystal, as well as to calculate wavenumbers for vibrations, that are active in Raman spectra. The method should provide data, suitable for the topological analysis of electron density in conditions of periodic quantum-chemical calculations, and should reproduce experimental data as accurately as possible. For this purpose several of basis sets for the iodine atom available in literature have been tested in this paper, and possibilities and advantages of the two approaches to relativistic effect consideration have been compared. These two approaches are: usage of Effective Core Pseudopotentials and the Gaussian-type basis set, constructed according to Douglas-Kroll-Hess approach [21, 22]. We make the comparison of calculated geometric characteristics of the iodine crystal structure and of electron density properties, calculated for covalent and halogen bonds, with the data obtained on the basis of the high resolution X-ray diffraction experiment [23]. Theoretical vibrational characteristics are compared to the experimental polarized Raman spectra for the single crystal of iodine [24].

Calculations

As a part of the study the periodic calculations of the wave function in the iodine crystal were made using the program CRYSTAL14, by the Kohn-Sham method (B3LYP) and various basis sets, shown in Table 1. Two groups of basis sets were tested. One group included Stuttgart fully-relativistic energy-consistent pseudopotentials ECP-mdf28 and ECP-mdf46 including 28 and 46 core electrons, respectively [25]. The pseudopotential ECP-mdf28 could be attributed to the group of potentials with the small core, and ECP-mdf46 had the member of the group with the large core. When using the pseudopotential ECP-mdf46 only outer-shell electrons $5s^2$ и $5p^5$ were included into the valence part. The valence part in both cases was described by the three-time split basis sets of the VTZ type. The other group was represented by the DZVP basis set, including 14 shells [26] and its analogue $DZVP^{mod}$ including 11 shells [27]. In the $DZVP^{mod}$ basis set the *sp*-type hybrid shells were used to describe internal electron levels, so that up to 8 electrons that could be situated existed in that shell. Accounting of relativistic effect was implemented with the help of the DZPDKH basis set in terms of the Douglas-Kroll-Hess ap-

proach [21, 22]. The basis set was obtained through optimization of standard Gaussian function coefficients [28, 29], approximating equations, obtained from the electronic part of Dirac Hamiltonian [30].

Iodine crystal structure optimization was made for all atoms of the irreducible cell part with fixed cell parameters. Allowed atom coordinate variations were only those, which did not cause changes in the crystal symmetry. The Hessian matrix was calculated for the found optimal atom configuration at the Γ point in the center of the Brillouin zone. Vibration frequencies were calculated at the Γ point in the harmonic approximation. On the basis of the obtained data the total Raman intensities were calculated for the single crystal of iodine.

Results and Discussion

Mutual arrangement of molecules with halogen bonds in the iodine crystal and with the interatomic distances, stated in the paper [23], is shown in Fig. 1. It has been found that in the case of using fully-relativistic core pseudopotentials ECP-mdf28 and the valence part, described by the VTZ basis set, such geometric characteristics, as the covalent and halogen bond lengths, are reproduced most accurately: $\Delta R_{I\text{-}I} = 0.04$ Å, $\Delta R_{I\ldots I} = -0.03$ Å, where $\Delta R = R^{\text{calculated}} - R^{\text{experimental}}$. According to the data, represented in Table 1, other basis sets also show satisfactory results when localizing equilibrium geometry in the crystal. In all considered cases the positive values of $\Delta R_{I\text{-}I}$ have been observed, besides, the I…I halogen bond lengths have been underestimated in most of the cases.

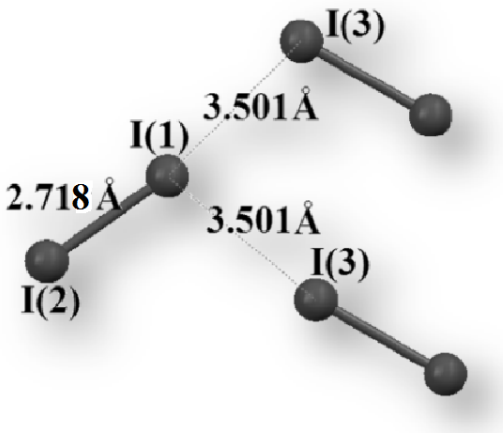

Fig. 1. Mutual arrangement of molecules with halogen bonds in the iodine crystal

Table 1

Distances (Å), the values of the electron density in the bond critical point (a.u.) in the crystal structure of iodine, optimized in different basis sets

Basis set	I(1)–I(2) Covalent bond		I(1)…I(3) Halogen bond		I(1)…I(1) Van der Waals interactions	
	$R^{\text{calculation}}$	$\rho(\mathbf{r}_b)$	$R^{\text{calculation}}$	$\rho(\mathbf{r}_b)$	$R^{\text{calculation}}$	$\rho(\mathbf{r}_b)$
ECP-mdf46 VTZ	2.876	0.045	3.709	0.011	-	-
ECP-mdf28 VTZ	2.755	0.059	3.474	0.018	3.977	0.008
$DZVP^{\text{mod}}$	2.791	0.062	3.473	0.018	3.940	0.009
DZVP	2.802	0.061	3.467	0.019	3.939	0.009
DZPDKH	2.812	0.060	3.414	0.022	4.060	0.007
Experimental [23]	R^{exp} =2.718 $\rho(\mathbf{r}_b)^{\text{exp}}$ =0.050		R^{exp} =3.501 $\rho(\mathbf{r}_b)^{\text{exp}}$ =0.015		R^{exp} =3.980 $\rho(\mathbf{r}_b)^{\text{exp}}$ =0.009	

The results of the theoretical topological analysis of electron density have been compared to the data from the paper [23]. There the adjusted values of electron density restored on the basis of the extended multipole modeling Hansen and Coppens approach [31] have been analyzed for I-I covalent bonds and the strongest I…I noncovalent interactions. The application of basis sets with core pseudopo-

tentials leads to underestimation (ECP-mdf46 VTZ) and overestimation (ECP-mdf28 VTZ) of electron density in the I-I covalent bond critical points. The DZPDKH basis set provides a significantly underestimated halogen bond length and, consequently, an overestimated electron density in the halogen bond critical points $\Delta\rho(\mathbf{r}_b) = 0.007$ atomic units. However, the observed range of $\Delta\rho(\mathbf{r}_b)$ values both for covalent and halogen bonds may be considered to be reasonable.

The following characteristic features have been observed while analyzing the Laplacian of electron density distribution in the crystal plane, containing halogen bonds between diiodine molecules. When using the DZVP basis sets with core pseudopotentials, the covalent bond area and the space between neighbouring molecules are described in the similar way. In both cases the covalent bond areas have similar level of observed details. However, the Laplacian of electron density in Fig. 2a,b does not show the electron density accumulation in the outermost electron shell area of iodine. This fact evidences low informative value of the $\nabla^2\rho(\mathbf{r})$ function when describing iodine ability to form halogen bonds. On the contrary, the outline map of the electron density Laplacian, obtained through the DZPDKH basis set and indicated in Figure 2c demonstrates the electron density accumulation in the iodine atom equatorial area and exhaustion formed on the continuation of the covalent bond. Consequently, the DZPDKH basis set appears to be the only one of the studied sets, which demonstrates the principle of halogen bond formation: orientation of the area of electron density accumulation of one atom up on the area of electron density exhaustion of the other. Figure 2c shows the I-I covalent bond area in greater details (contour lines of 0.002, 0.004 and 0.008 atomic units) and it also has the contour line of 0.002 atomic units in the halogen bond area unlike Fig. 2a and 2b.

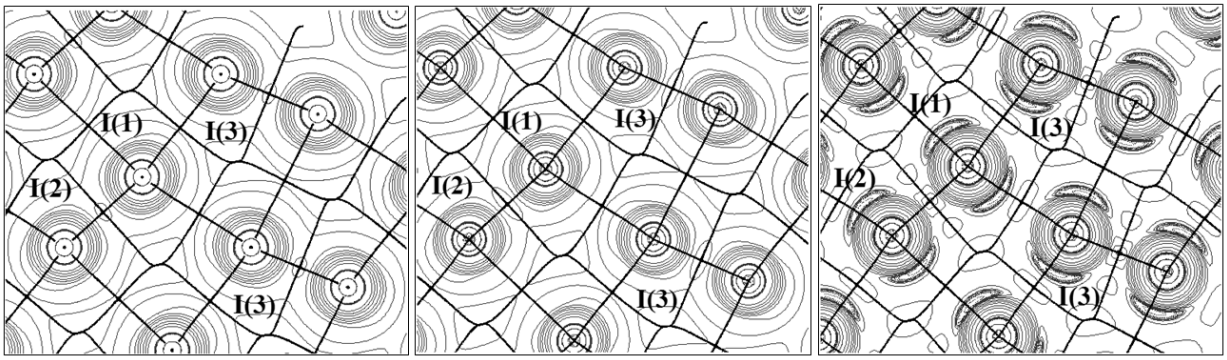

a) b) c)

Fig. 2. The contour lines of the Laplacian of the electron density, accompanied by bond paths in iodine crystal in a variety of basis sets: in fully-relativistic pseudopotential basis set type ECP-28mdf VTZ (a), in the DZVP basis set (b) and DZPDKH (c)

According to the data of experimental polarized spectra [24], two lines are observed for the iodine crystal. These lines correspond to the in-phase and out-of-phase valence symmetrical vibrations. In the first case, the change of lengths of neighboring molecules is in coordination, while in the second case, it is out of phase: the stretch of the covalent bond in one molecule corresponds to the contraction in the neighboring molecule. Symmetry of obtained in-phase A_g and out-of-phase B_{2g} vibrations corresponds to the experimental data from the polarized spectra [24] (Table 2).

Table 2

The wavenumbers of valence vibrations in the crystal of iodine calculated using a variety of basis sets

Basis set	υ (A_g) I–I, cm^{-1}	υ (B_{2g}) I–I, cm^{-1}
ECP-mdf46 VTZ	166.5	177.5
ECP-mdf28 VTZ	196.5	202.2
$DZVP^{mod}$	178.6	187.4
DZVP	180.7	188.5
DZPDKH	180.5	188.8
Experimental [25]	180	189

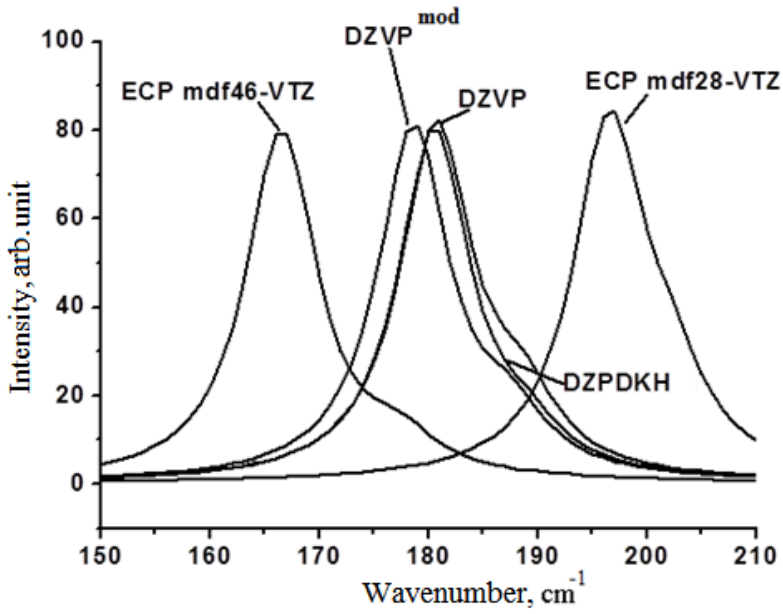

Fig. 3. Calculated unpolarized Raman spectra of iodine crystal optimized in various basis sets

On the basis of obtained theoretical wavenumbers for stretching vibrations in the iodine crystal it is possible to select a group of preferable basis sets, reproducing the data of experimental polarized spectra within the error of 2 cm^{-1}. They are $DZVP^{mod}$, DZVP and DZPDKH. The application of the core pseudopotential with a big core ECP-mdf46 leads to substantial decrease of obtained wavenumbers, and application of the pseudopotential with a small core ECP-mdf28 leads to underestimation, where deviations from the experimental value in these cases are comparable.

Display of the calculated integrated Raman spectra (Fig. 3) allows us to visually assess the ratio of in-phase and out-of-phase vibrations and overlapping of the lines, corresponding to them. Maximum resolution of lines is attained through the use of the basis set ECP-mdf46 VTZ, the difference between stretching peaks equals 13 cm^{-1}. The greatest overlapping of lines is observed in the basis set ECP-mdf28 VTZ, where the difference between stretching peaks equals 6 cm^{-1}. Basis sets of the DZVP group demonstrate roughly the same difference between wavenumbers of in-phase and out-of-phase vibrations; however, in case of the DZPDKH basis the out-of-phase vibration is characterized by relatively lower intensity.

Conclusion

As can be seen from the above, basis sets with fully-relativistic core pseudopotentials slightly underestimate electron density in the critical point of the covalent bond. However, lack of overlapping in grade lines in the area linking to the core makes it vulnerable to apply basis sets with core pseudopotentials in the electron density topological analysis tasks.

Calculated wavenumbers of iodine vibrations in the crystal, which have been obtained when analyzing the basis sets, show that the application of core pseudopotentials ECP-mdf46 and ECP-mdf28 leads to significant deviations from experimentally observed values. Other basis sets reproduce experimentally observed wavenumbers within the accuracy up to ±2 cm^{-1}, only underestimating the difference between in-phase and out-of-phase vibrations a little.

The Laplacian of electron density, obtained with the use of the DZPDKH basis set, demonstrates accumulation of electron density in the area of the outermost valence shell of iodine atoms. That is why the DZPDKH basis set, where the relativistic effect on the basis of the Douglas-Kroll-Hess approach is taken into consideration, is the most suitable for modeling and analyzing electron density topological properties in crystals of iodine containing compounds with halogen bonds.

The work was supported by the Russian Ministry for Education and Science GZ729, and was carried out on a supercomputer "TORNADO" SUSU.

References

1. Kupper F.C., Feiters M.C., Olofsson B., Kaiho T., Yanagida S., Zimmermann M.B., Carpenter L.J., Luther G.W., Lu Z., Jonsson M., Kloo L. [Commemorating Two Centuries of Iodine Research: An Interdisciplinary Overview of Current Research]. *Angew. Chem., Int. Ed.*, 2011, vol. 50, pp. 11598–11620.

2. Svensson P. H., Kloo L. [A Vibrational Spectroscopic, Structural and Quantum Chemical Study of the Triiodide Ion]. *Journal of the Chemical Society, Dalton Trans*, 2000, pp. 2449–2455.

3. Sakurai T., Sundaralingam M., Jeffrey G.A. [A Nuclear Quadrupole Resonance and X-ray Study of the Crystal Structure of 2,5-dichloroaniline]. *Acta Crystallogr*., 1963, vol. 16, pp. 354–363.

4. Desiraju G.R. [Crystal Engineering: the Design of Organic Solids]. *J. Appl. Cryst.*, 1991, vol. 16, pp. 265.

5. Politzer P., Murray J.S., Clark T. [Halogen Bonding: an Electrostatically-driven Highly Directional Noncovalent Interaction]. *Phys. Chem. Chem. Phys.*, 2010, vol. 12, pp. 7748–7757.

6. Politzer P., Riley K.E., Bulat F.A., Murray J.S. [Perspectives on Halogen Bonding and Other σ-hole Interactions: Lex Parsimoniae (Occam's Razor)]. *Comput. Theor. Chem.*, 2012, pp. 2–8.

7. Clark T., Hennemann M., Murray J.S., Politzer P. [Halogen Bonding: the σ-Hole]. *J. Mol. Model.*, 2007, vol. 13, pp. 291–296.

8. Desiraju G.R. Ho P.S., Kloo L., Legon A.C., Marquardt R., Metrangolo P., Politzer A. P., Resnati G., Rissanen K. [Definition of the Halogen Bond (IUPAC Recommendations 2013)]. *Pure Appl. Chem.*, 2013, vol. 85, pp. 1711–1713.

9. Bartashevich E.V., Yushina I.D., Stash A.I., Tsirelson V.G. [Halogen Bonding and Other Iodine Interactions in Crystals of Dihydrothiazolo(Oxazino)Quinolinium Oligoiodides from the Electron-Density Viewpoint]. *Cryst Growth Des.*, 2014, vol. 14, pp. 5674–5684.

10. R.F.W. Bader, Atoms in Molecules. A Quantum Theory, Oxford University Press, New York, 1990, 532 p.

11. Tsirelson V.G., Zou P.F., Tang T.H., Bader R. [Topological Definition of Crystal Structure: Determination of the Bonded Interactions in Solid Molecular Chlorine]. *Acta Crystallogr.*, 1995, vol. 51, pp. 143–153.

12. Kohout M., Savin A., Preuss H. [Contribution to the Electron Distribution Analysis. I. Shell Structure of Atoms. *J. Chem. Phys*., 1991, vol. 95, pp. 1928–1929.

13. Hunter G. [Conditional Probability Amplitudes in Wave Mechanics]. *Int. J. Quant. Chem.,* 1975, vol. 9, pp. 237–238.

14. Silvi B., Savin A., Causà M. [Classification of Chemical B based on Topological Analysis of Electron Localization Functions]. *Nature*, 1994, vol. 371, pp. 683–686.

15. Pilmé J., Renault E., Ayed T., Montavon G., Galland N. J. [Introducing the ELF Topological Analysis in the Field of Quasirelativistic Quantum Calculations]. *Chem. Theor. Comput.*, 2012, vol. 8, pp. 2985–2990.

16. Svensson P. H., Kloo L. [Synthesis, Structure, and Bonding in Polyiodide and Metal Iodide-Iodine Systems]. *Chemical Reviews*, 2003, vol. 103, pp. 1649–1684.

17. Deplano P., Ferraro J. R., Mercuri M. L., Trogu E. F. Structural and Raman Spectroscopic Studies as Complementary Tools in Elucidating the Nature of the Bonding in Polyiodides and in Donor-I2 Adducts. Coordination Chemistry Reviews, 1999, vol. 188, pp. 71–95.

18. Al-Hashimi N. A., Hussein Y. H. A. [Ab Initio Study on the Formation of Triiodide CT Complex from the Reaction of Iodine with 2,3-Diaminopyridine]. *Spectrochimica Acta Part A*, 2010, vol. 75, pp. 198–202.

19. Otsuka M., Mori H., Kikuchi H., Takano K. [Density Functional Theory Calculations of Iodine Cluster Anions: Structures, Chemical Bonding Nature, and Vibrational Spectra]. *Computational and Theoretical Chemistry*, 2011, vol. 973, pp. 69–75.

20. Matta C.F., Boyd R.J. [The Quantum Theory of Atoms in Molecules. From Solid State to DNA and Drug Design]. *Wiley-VCH Verlag GmbH & Co. KGaA*, 2007, pp. 527.

21. Douglas M., Kroll N.M. [Quantum Electrodynamical Corrections to Fine-structure of Gelium]. *Ann Phys*, 1974, vol. 82, pp. 89–155.

22. Hess B.A. [Relativistic Electronic-structure Calculations Employing a Two-component No-pair Formalism with External-field Projection Operators]. *Phys. Rev.*, 1986, vol. 33, pp. 3742–3748.

23. Bertolotti F., Tsirelson V. G. Shishkina A. V., Forni A., Gervasio G., Stash A. I. [The Intermolecular Bonding Features in Solid Iodine]. *Crystal Growth & Design*, 2014, pp. 1–20.

24. Congeduti A., Nardone M., Postorino P. [Polarized Raman Spectra of a Single Crystal of Iodine]. *Chemical Physics*, 2000, vol. 256, pp. 117–123.

25. Peterson K.A. et al. [On the Spectroscopic and Thermochemical Properties of ClO, BrO, IO, and Their Anions]. *J. Phys. Chem*, 2006. vol. 110, pp. 13877–13878.

26. Godbout N., Salahub D. R. et al. [Optimization of Gaussian-type Basis Sets for Local Spin Density Functional Calculations. Part I. Boron Through Neon, Optimization Technique and Validation]. *Can. J. Chem*, 1992, vol. 70, pp. 560–562.

27. http://www.tcm.phy.cam.ac.uk/~mdt26/basis_sets/I_basis.txt

28. Jorge F.E., Canal Neto A., Camiletti G.G., Machado S.F. [Contracted Gaussian Basis Sets for Douglas-Kroll-Hess Calculations: Estimating Scalar Relativistic Effects of Some Atomic and Molecular Properties]. *J. Chem. Phys.*, 2009, vol. 130, pp. 064108.

29. Barros C.L., Jorge F.E., Canal Neto A., Campos M. [Gaussian Basis Set of Double Zeta Quality for Atoms Rb Through Xe: Application in Non-relativistic and Relativistic Calculations of Atomic and Molecular Properties]. *Mol. Phys.*, 2010, vol. 108, pp. 1965–1972.

30. Reiher M. [Relativistic Douglas–Kroll–Hess theory]. *Wiley Interdisciplinary Reviews: Computational Molecular Science*, 2012, vol. 2, pp. 139–149.

31. Hansen N.K., Coppens P. [Testing Aspherical Atom Refinements on Small-molecule Data Sets]. *Acta Cryst*, 1978, vol. 34, pp. 909–921.

Received 23 May 2015

УДК 541.2, 544.18

ВАРИАЦИИ МЕТОДОВ МОДЕЛИРОВАНИЯ ЭЛЕКТРОННЫХ И СПЕКТРАЛЬНЫХ СВОЙСТВ В КРИСТАЛЛИЧЕСКОЙ СТРУКТУРЕ ЙОДА

И.Д. Юшина, Л.М. Булатова, С.Э. Насибуллина, Е.В. Барташевич
Южно-Уральский государственный университет, г. Челябинск

На примере кристаллической структуры йода произведен подбор оптимальных базисных наборов, позволяющих в условиях периодических расчетов воспроизводить межъядерные расстояния, распределение электронной плотности и спектральные свойства йодсодержащих молекулярных кристаллов. Сопоставлены преимущества двух подходов к учету эффектов релятивизма: эффективные остовные псевдопотенциалы и базисный набор гауссового типа, конструируемый на основе методологии Дугласа-Кролла-Гесса. Показано, что последний позволяет корректно воспроизвести не только экспериментально наблюдаемые геометрические параметры кристалла йода и характеристические колебания в спектрах комбинационного рассеяния, но и накопление электронной плотности в области внешней валентной оболочки атома йода, что наглядно иллюстрирует функция лапласиана электронной плотности.

Ключевые слова: кристаллическая структура йода, галогенные связи, топологический анализ электронной плотности, релятивистский эффект, спектроскопия комбинационного рассеяния.

Юшина Ирина Дмитриевна – аспирант, кафедра экологии и природопользования, Южно-Уральский государственный университет. 454080, г. Челябинск, пр. им. В.И. Ленина, 76. E-mail: idu-xda@mail.ru

Булатова Люция Марсельевна – студентка химического факультета, Южно-Уральский государственный университет. 454080, г. Челябинск, пр. им. В.И. Ленина, 76. E-mail: luciyabulat@yandex.ru

Насибуллина Светлана Эдуардовна – студентка химического факультета, Южно-Уральский государственный университет. 454080, г. Челябинск, пр. им. В.И. Ленина, 76. E-mail: svetlaya.n.e@yandex.ru

Барташевич Екатерина Владимировна – кандидат химических наук, доцент, кафедра органической химии, Южно-Уральский государственный университет. 454080, г. Челябинск, пр. им. В.И. Ленина, 76. E-mail: kbartash@yandex.ru

Поступила в редакцию 23 мая 2015 г.

ОБРАЗЕЦ ЦИТИРОВАНИЯ

Variations of structure modeling methods and raman spectral characteristics for the iodine crystal / I.D. Yushina, L.M. Bulatova, S.E. Nasibullina, E.V. Bartashevich // Вестник ЮУрГУ. Серия «Химия». – 2015. – Т. 7, № 3. – С. 25–32.

FOR CITATION

Yushina I.D., Bulatova L.M., Nasibullina S.E., Bartashevich E.V. Variations of Structure Modeling Methods and Raman Spectral Characteristics for the Iodine Crystal. *Bulletin of the South Ural State University. Ser. Chemistry.* 2015, vol. 7, no. 3, pp. 25–32.

UV-VISIBLE SPECTRA OF PEROXOTITANATE COMPLEXES

Yu.V. Matveychuk, *South Ural State University, Chelyabinsk, Russian Federation, diff@inbox.ru*
I.V. Krivtsov, *South Ural State University, Chelyabinsk, Russian Federation, zapasoul@gmail.com*
M.V. Ilkaeva, *South Ural State University, Chelyabinsk, Russian Federation, mylegenda@gmail.com*
V.V. Avdin, *South Ural State University, Chelyabinsk, Russian Federation, avdin@susu.ru*

Comparative analysis of calculated (subject to solvent influence in PCM model) and experimental UV-visible spectra of peroxotitanate complexes in solutions at various conditions of occurrence. It has been shown that the change of complex composition, dependent on the solution pH value, leads to the change of characteristic absorption bands of UV-visible spectra in the wavelength range exceeding 320 nm. The tendency of the absorption bands in solution spectra to shift is correlated to the change of calculated spectra in accordance with the monomer complex unit. It has been suggested that the color of the complex solution in weakly acidic and neutral media is related to appearance of hydroperoxy-bonds between titanium atoms.

Keywords: peroxotitanate complexes, electronic absorption spectra, PCM, TD–DFT.

Introduction

At present the syntheses of catalytic materials on the basis of green technology have acquired a special significance and popularity in terms of ecological compatibility and possibility of controlling the synthesis process. Oxides of titanium, magnesium, zirconium, silicon are widely used as such materials, both individually and in mixed compositions.

Previously titanium alkoxides were used as handy precursors (initial substances) for the synthesis of titania-based catalysts. As they are toxic, nowadays the attention of researchers is directed at study and development of appropriate synthesis techniques with the use of other precursors: titanium citrate, oxalate and peroxide complexes [1]. The state of titanium peroxide complexes in aqueous solutions has been studied experimentally in considerable detail in papers [2–4], but their precise composition is unknown so far, as it strongly depends on the synthesis conditions, primarily on the solution pH and the ratio "hydrogen peroxide – titanium". At that the understanding of the state and structure of peroxide complexes in precursor solution is important in order to control the following synthesis of titania catalysts. Modern quantum-chemical computational methods can play the supportive role for it, especially *ab initio* methods.

The most widespread use for calculation of the structure and characteristics of both organic and inorganic complexes belongs to Kohn-Sham method (DFT), which provides adequate description of the states of ions, complexes, crystals that correlates to experimental data. Numerous extensions of the method – use of various functionals, atomic basis sets, inclusion of environment for investigated structures – have enabled the description of various classes, states and properties of any elements, including heavy ones (in [5], as an example) and their compounds. Investigation of theoretical electronic spectra with by application of calculation of energy characteristics within the bounds of TD-DFT method [6, 7] is widely used in global practice in an effort of detailed interpretation of observed experimental data. Recently the similar calculations have been carried out in order to determine the state of many oxide materials and their precursors, including titania-based catalysts. Thus, in papers [8–10] calculation methods (DFT) have been used for determination of the properties of peroxide complexes emerging at H_2O_2 application to the surface of titanium and titanium silicate catalysts. Likewise, much information has been extracted concerning occurrence of active centers and their properties, transition complexes at interaction of catalysts with ethylene, ammonia and other compounds, the direction of possible catalyzed reactions. Calculated data concerning the structure of titania doped with nitrogen [11–12] and iron [13] have been given, the laws of changing width of forbidden band have been theoretically explained, as well as the UV-visible spectra at various conditions of synthesis and further material processing.

All abovementioned studies pursue the processes on the completely formed phase interface, at that the theoretical investigation of the state and the properties of titania precursors, which greatly influence the formation of the spatial structure of the solid phase, has been practically ignored.

In order to account for the influence of medium (solvent) on the studied substances the clarifying models are invoked, within which various types of solvate-solvent interaction are considered: dipole-dipole, dipole-induction, dispersion and so on. One of such models (COSMO, [14]) was previously used to investigate the interaction of some titanium tungstate complexes with hydrogen peroxide and the properties of the obtained peroxy compounds. The results were in good agreement with the experimental properties, they had certain prognostic ability in relation to their oxidizing properties. In recent decade the precise numerical polarized continuum model (PCM) has been developed [15, 16]. Within the model a solvent is considered as an isotropic medium characterized by some physical constants, at that the specific interactions are not taken into account in an explicit form. A molecule of a solute is placed in a cavity which forms in this continuous medium. All its atoms are surrounded by spheres with Van der Waals radius. In order to construct the smooth surface necessary for the method convergence, secondary surrounding of minor radius spheres is carried out, with the following triangulation in order to form the surface elements. By means of several iterations the surface charge field of the formed cavity and the free energy of a molecule in a solvent are estimated. The popularity of PCM is explained by speedy calculations of electron states in the environment of the solvent molecules, which is but little less compared to calculations for gas phase. At that the theoretical results and tendencies of changing compound spectra, obtained with the use of this model, most adequately correlate to the dependencies of experimental spectra of the synthesized compounds in solutions and explain their characteristic features. PCM in the simplified version (IEF-PCM) has been used for calculation of the interaction of terminal titanium oxide groups with the aqueous solution of hydrogen peroxide [8], which has been of great help in determination of arrangement of the solvent molecules as ligands in the peroxycomplex structure: by way of hydrogen bonding intermediates are formed with predominantly five-membered cycles. Likewise, the prognosis of the complex catalytic properties with respect to epoxidation reaction has been defined more accurately.

At interaction of titanium compounds with hydrogen peroxide the formation of several possible complex types can occur. Thus, in [2–3] it is noted that the reaction of titanium tetrachloride with hydrogen peroxide in acidic medium produces complexes with one peroxy group of the series $[Ti(O_2)(OH)_x]^{(2-x)+}$ (**I**). We can suggest that during the synthesis of titania peroxide precursors the formation of both the similar complexes and the complexes with peroxy and hydroperoxy group of the series $[Ti(O_2)(OOH)(OH)_x]^{(1-x)+}$ (**II**) takes place – at the great excess (10-100-fold) of hydrogen peroxide. Besides, it is noted in [2–3] that complexes of the series (**I**) are especially inclined to dimerization, as well as to further condensation and addition of new monomeric units. Therefore it is important for us to consider the behavior of such structures surrounded by the molecules of water in the role of a solvent, as immediate precursors during controlled formation of hydrated titania precipitate, which has not been studied previously. Investigation of other complexes of $[Ti(O_2)(OOH)_2]$ type or of the series $[Ti(OOH)_y(OH)_x]^{(4-x-y)+}$ (**III**) is not of interest, as their existence in aqueous solution is not confirmed by the previously published data. Formation of several OOH groups, bonded to titanium, is carried out on the completely formed phase interface: for example, in paper [8] titanium complexes of the series (**III**) have been studied as the active centers on the surface of titanium silicate catalyst. The existence of the complexes with two and three peroxy groups, fully considered in [17], is also of low probability in the conditions described below, for the reason that their formation demands very great excess (by the factor of hundreds) of hydrogen peroxide compared to titanium. On the other hand, the directions of their further oligomerization are analogous to the reaction directions of the series (**I**) complexes.

In its turn, electronic spectroscopy is one of the most accessible and dependable investigation methods of solution compositions. Therefore we aimed chiefly at the following: to establish the existence of the absorption bands in the UV-visible spectra of peroxotitanate complex solutions, related to definite chemical composition and forms, or to explain the absence of such bands within the studied range, considering the possible change of complex composition in a solution with changing pH value. This we plan to carry out by means of comparing the UV-visible spectra of solutions to the electronic absorption spectra of optimized complex forms obtained by way of quantum chemical calculation, taking into account aqueous environment in PCM. We suggest that the consideration of predominating types of bonding for

titanium atoms in the calculated complez forms from several monomeric units will give an opportunity to prognosticate the reaction direction of further oligomerization at specific conditions, as well as formation of specific forms of hydrated titania precipitate. The necessary information of occurrence of such forms in a solution we can get from its UV-visible spectrum.

Experimental

In order to obtain peroxotitanate complexes $TiOSO_4 \cdot nH_2O$ (Aldrich) was used. Titanium oxysulfate was dissolved in distilled water at 50 °C, then it was diluted to obtain 50 mL of 0.05 M solution, and hydrolized by 3 M sodium hydroxide. Addition of NaOH was stopped when pH of the reaction mixture reached 5.0. The resulting titanium hydroxide precipitate was centrifuged at 7000 rpm and washed by distilled water until the negative reaction for sulfate. Then titanium hydroxide was dissolved in 10 mL 30 % hydrogen peroxide, and the formed peroxy complex was diluted by distilled water up to 50 mL. The pH value of the obtained solution varied in the range 2.0...2.3, which was the consequence of peroxytitanic acid decomposition. Mole ratio "hydrogen peroxide – titanium" was 35:1. In order to slow down the hydrogen peroxide decomposition process the solution was placed in an ice bath. The UV-visible spectra of solutions were registered with the use of Shimadzu UV-2700 spectrophotometer.

Computational

The present study investigates the electronic spectra of several complexes of the series (**I**) and the neutral complex of the series (**II**), formed at the reaction of hydrogen peroxide with titanium hydroxide precipitate in neutral, acidic and weakly basic media (at pH < 9). The complexes have been modeled, beginning from the corresponding monomer, by means of consecutive addition of single-type monomers to each other one by one and to the calculated complex of two monomer units. Monomer units of the complexes are presented in Fig. 1. In the first stage optimization of structure geometry has been carried out through the necessary number of steps until the stationary point with the greatest energy gradient value (not exceeding 0.0001 Hartree/Bohr) has been reached. Frequency analysis of the obtained Hessian for all the structures has shown the absence of imaginary frequencies.

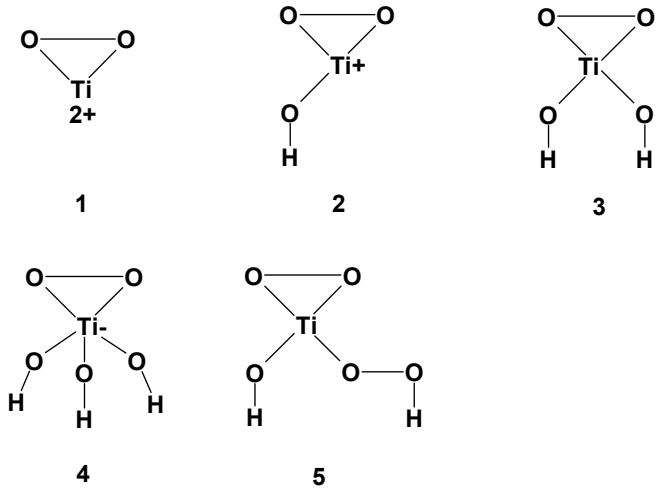

Fig. 1. Monomer units for calculation of spectra of the peroxotitanate complexes

Functionals PBE0 [18] and B3LYP [19, 20] and basis sets: polarized all-electron 6-31G** [21, 22] and pseudopotential LANL2DZ [23] are most often used in the present time, they are the most universal for determination of molecule characteristics of oxides for the elements of periods I–IV. For example, the calculations in [11, 13] and [8, 12], respectively, were carried out with the use of those parameters. At that the combined basis sets were used: the second of the abovementioned for titanium atoms, the first of them for atoms of the remaining elements. Geometry optimization of the studied complexes was carried out by Kohn-Sham method (DFT) with the use of the functional B3LYP on the basis of the basis set 6-31G** for all elements. Influence of water solvent was accounted for by the use of D-PCM model in the basic version with the following parameters: the same coefficient for all parts of the cavity, with-

out calculation of cavitation, repulsion and dispersion energies, at standard temperature 298 K. Van der Waals radii were taken from [24].

In the second stage the energy characteristics of the complex ground state were calculated, with further calculation of excited states and electronic spectra, also accounting for the influence of water solvent. Electronic spectra of the optimized structures were obtained by TD-DFT method. Such a calculation was carried out for 10–40 excited states with the necessary number of iterations and the energy convergence criterion for each state (not exceeding 0.00003 Hartree/Bohr), so that to encompass the spectrum range with the lower bound 220...240 nm. The whole calculation of the optimized structure and energy characteristics was carried out with the program package Firefly 8.0.1 [25].

Results and Discussion

We have considered the electronic spectra of the calculated structures of peroxotitanate complexes of the series **I** $\{[Ti(O_2)(OH)_x]^{(2-x)+}\}_n$ and the neutral complex $[Ti(O_2)(OOH)(OH)]_n$ from the series **II** (in both cases n=1...3). Depending on the acidity the number of OH-groups in the monomer units of the complexes increases with increasing pH. Such an increase of x is related to deprotonation of water molecules, surrounding the complexes [2], and to coordination of hydroxyl groups on titanium atoms. Reasoning from this, the complexes of the series (**I**), where x=0, 1, 2 and 3 (Fig. 1), have been used as the monomer units for the calculation.

In order to estimate the thermodynamic probability of complex formation from various amounts of different monomer units and the possibility of their existence in aqueous solution the energy of monomer units addition to complexes has been estimated (Table 1) on the basis of calculated amounts of free energy in the solvent. It is necessary to note that bond formation between monomers is more probable for neutral monomers **3** and **5**, at that titanium atoms are bonded by oxy- and hydroxy bonds, while monomer units **5** in the complex are bridged through oxygen of hydroperoxy group.

Table 1

Energy of monomer units addition to complexes, kJ/mol

Monomer unit / Number of units in the complex	**1**	**2**	**3**	**4**	**5**
One	**229.27**	**14.98**	**–158.15**	**–62.65**	**–157.08**
Two	**465.98**	**–13.00**	**–144.99**	**–86.71**	**–52.99**

Existence of bonded complexes from ionic monomers **2** and **4** is less probable, the monomer units are bonded only by hydrogen bonds. Ions **1** exist in solution solely in the form of hydrated monomers, therefore the electronic spectrum is obtained only for the monomer unit. Likewise, in the context of the sloping potential energy surface for the complex consisting of three monomer units **4** in the used method we can calculate only transition states with one imaginary vibration frequency. The specified data pertain to one of such states with the minimal energy.

For all optimized complex structures the energy values for electron transitions between the ground state and the excited state have been calculated, and the corresponding electronic line spectra in the range from 220–240 nm to absorption with the minimal transition energy (λ_{max}) have been obtained. The calculated spectra of complexes with monomer units from **1** to **5** are shown in Fig. 2–4 (line spectrum is approximated by Lorentz function).

Experimental spectra of the synthesized peroxotitanate complexes (for titanium concentrations 0.05 M; 0.005 M; 0.0005 M) are shown in Fig. 5.

Analyzing the obtained results, first of all we should note that the range of wavelength lower than 300 nm is not informative both for indication of existence of this or that series of complexes in solution and for monitoring oligomerization process and subsequent formation of precipitation phase during hydrolysis of complexes. Our experimental data and previously accomplished studies [2, 26] have shown that in this range the intensive absorption band is observed at all conditions (besides strongly acidic media), at that the band is continuous, smooth, and lacking maxima. Clearly defined absorption maximum within this range (245 nm) appears only for the anatase phase of hydrated titania, that is, after complete hydrolysis of peroxotitanate complex. The calculation of electronic spectra also supports (Fig. 2–4)

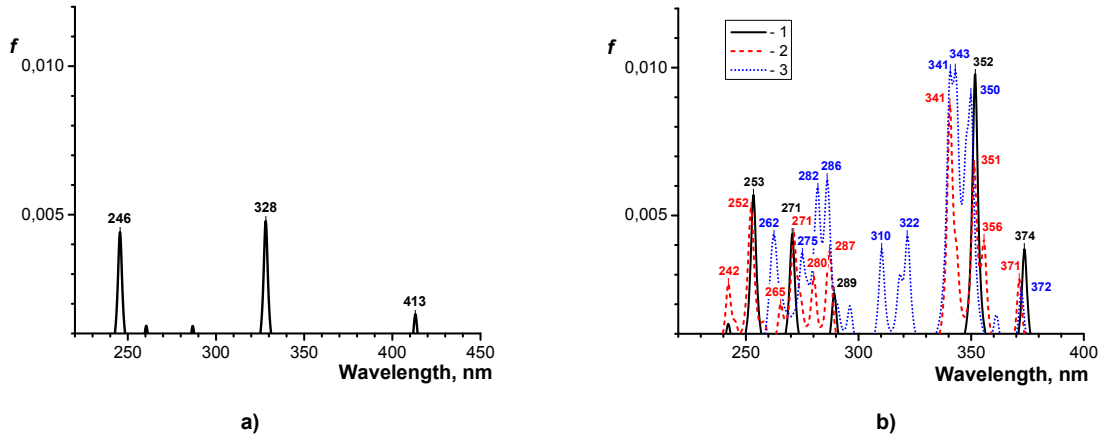

a) b)

Fig. 2. Calculated spectra: a) spectrum of the complex with monomer unit 1; b) spectrum of the complexes with monomer unit 2. Numbers in line designations correspond to the number of monomer units in the complex

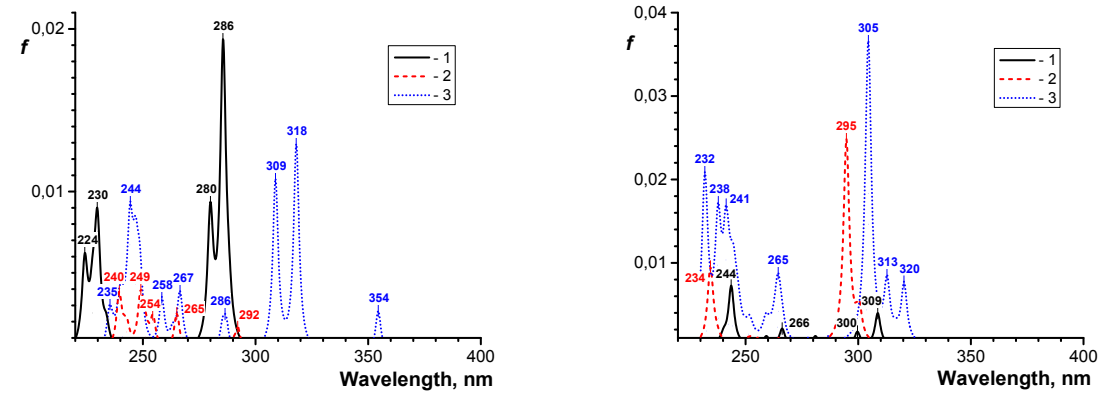

a) b)

Fig. 3. Calculated spectra: a) spectrum of the complexes with monomer unit 3; b) spectrum of the complexes with monomer unit 4. Numbers in line designations correspond to the number of monomer units in the complex

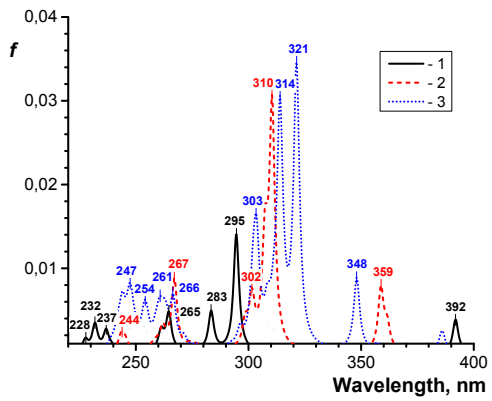

Fig. 4. Calculated spectra of the complexes with monomer unit 5. Numbers in line designations correspond to the number of monomer units in the complex

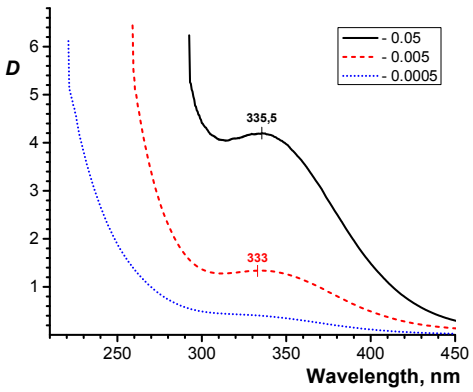

Fig. 5. Spectra of solutions of peroxotitanate complexes at pH 2.3. Titanium molar concentration of solutions is shown in line designations

the fact that within the range 240...300 nm the absorption bands with comparable oscillator strengths are situated near enough to each other, which leads to appearance of continuous absorption band with allowance made for band broadening and equilibrium of complexes with different monomer units in the solution.

At the values pH < 1 such a band is observed in the range lower than 240 nm. Therefore for strongly acidic medium (where the complex exists mostly in the form of monomer **1**) it is possible to establish the correspondence between the calculated absorption bands and the experimentally observed ones [26] in a wider range. Thus, two-fold increase of absorbance from 330 to 300 nm corresponds to the calculated band 328 nm, and the right edge of the absorption band for wavelengths lower than 250 nm corresponds to the calculated band 246 nm.

Study of absorption in the range of wavelengths exceeding 300 nm seems important for investigation of the state in the solution of various peroxotitanate forms and their subsequent oligomerization. Experimentally it has been found that light absorption significantly decreases compared to the range of wavelengths lower than 300 nm, but at that the bands with clearly defined maxima changing their position subject to acidity are observed.

For strongly acidic media it has been shown that the complex spectra contain wide absorption bands with maxima at 397 nm [26] and 412 nm [2] and a smooth slope of absorbance up to wavelength 500 nm/ Such spectra determine reddish orange color of the solution. This absorption band corresponds to the calculated line of the monomer **1** spectrum at 413 nm. The spatial parts of the monomer **1** molecular orbitals (MO), which determine excited states of the molecule due to electron transitions between them, are presented in Fig. 6a. Besides, there also is the correspondence of these transitions to the absorption bands in the spectrum with SAP coefficients. SAP squared determine the contribution of each transition into the excited state. It has been found that both abovementioned absorption bands (413 and 328 nm, charge transfer bands) are induced by electron transitions from occupied atomic orbitals (AO) of peroxy group oxygen atoms p_x to vacant AO of titanium atoms D_{xz} and D_{xy}, which (in various combinations) mostly form vacant MO L+1 and L+2 of $(TiOO)^{2+}$ cation. Increasing intensity and widening absorption band of the solution compared to calculated data can be due to a number of causes influencing the electronic state of a complex: more complicated and multivariate type of ion hydration compared to the interactions studied within the bounds of PCM; significant cavitation energy; significant ionic strength of a solution, etc.

Gradual disappearance of the absorption band near 400 nm with increasing pH to 2 is related to transition of the complex from monomer **1** to complexes with monomer units **2** and **3**. At that the maximum smoothly shifts from 412 nm at pH=1 to values 330...340 nm ([2] and Fig. 5) at pH=2.5. The smoothness of the shift points at equilibrium in the solution of monomer forms $(TiOO)^{2+} \leftrightarrow (TiOO)(OH)^{+}$, which shifts to the right with increasing pH. In the range pH 2.5...3.0 the absorption maximum is near 335 nm, and absorbance smoothly decreases up to ~450 nm. So the solution has yellowish orange color. The calculated spectra of complexes with monomer unit **2** reasonably explain the absorption curve of the solution, when the absorption envelope lines are constructed. The most intensive bands are in the ranges 335...360 nm, as well as 370...380 nm (Fig. 2b), while in the range 400...500 nm a few weak absorption bands are present with oscillator strength not exceeding 0.0004 (not shown in the figure). Pictorial representation of MO, the transitions between which determine the solution spectrum, are shown in Fig. 6–7. As the calculations show, the most intensive absorption bands are determined by electron transitions, similar to those mentioned above, namely, the charge transfer transitions. In the case

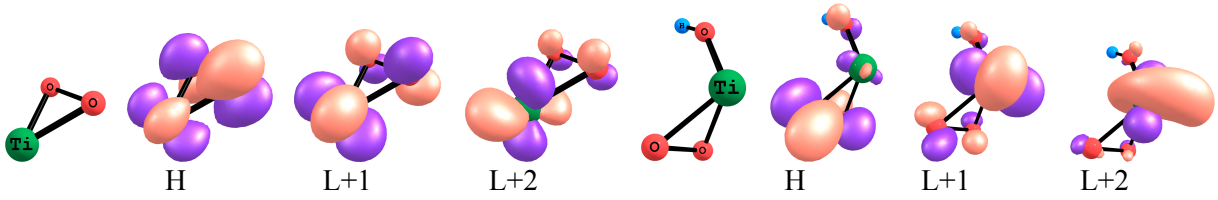

Fig. 6. Pictorial representation: a) MO for monomer unit 1. Absorption bands and the corresponding electron transitions: 413 nm: H→L+2 (*–0.98*); 328 nm: H→L+1 (*0.95*); b) MO for monomer unit 2. Absorption bands and the corresponding electron transitions: 374 nm: H→L+2 (*0.98*); 352 nm: H→L+1 (*–0.94*)

of complexes with monomer unit **2** the upper occupied MO are similar to those of $(TiOO)^+$ ion, they are formed from the combination of AO p_x, p_y, p_z of peroxy group oxygen atoms, whereas the lower vacant MO are formed from the combination of the abovementioned vacant AO of titanium atoms D_{xz} and D_{xy}, as well as the vacant AO of titanium D_x^2, D_y^2, D_z^2, and deeper AO of titanium. Calculation-proved increase of oscillator strength for absorption bands in the range near 350 nm for the complexes with monomer unit **2** compared to the band 413 nm for monomer **1** is also consistent with the experimental data [2].

Going from the cationic peroxotitanate complexes to neutral and anionic ones with monomer units **3** and **4**, which means increasing pH of the solution to neutral and weakly basic values, we observe absorption only in the range of wavelengths lower than 320 nm (Fig. 3). The calculated data have also shown that the absorption bands with lower transition energy, if any, are due to the existence in the complex structure of the fragment bonded to others with one bridging bond through the hydroperoxy group oxygen (example in Fig. 8). Therefore one of the appearance causes for such absorption bands in UV-visible spectrum of peroxotitanate complexes at specific conditions (ratio "hydrogen peroxide – titanium" is small and pH > 6) can be the formation of hydroperoxy bonds between titanium atoms in a complex. Formation of one or two hydroxy bonds between monomer units of a complex does not lead to changing spectrum in the range of wavelengths greater than 300 nm. Change of the solution color to maize yellow at changing pH to the abovementioned value, noted by us (and also in [26]), does not contradict the calculated data, though it demands more thorough investigation.

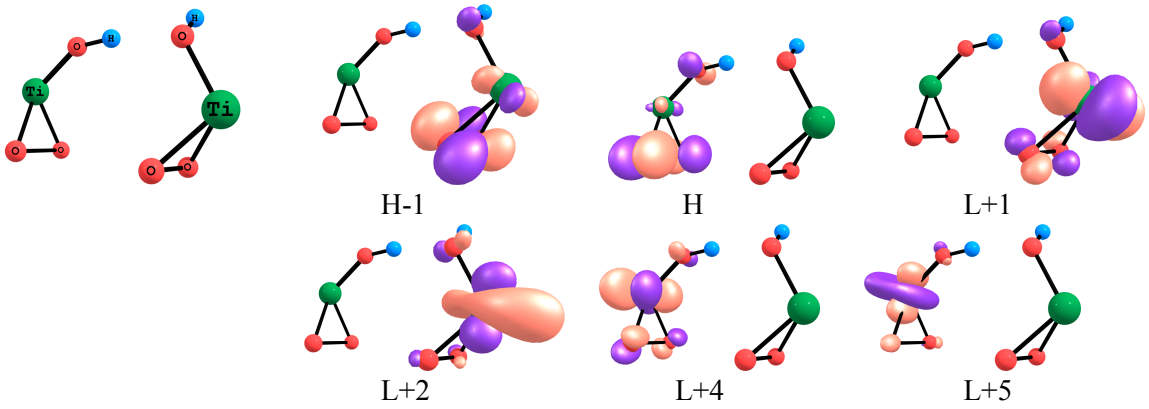

Fig. 7. Pictorial representation of MO for the complexes with two monomer units 2. Absorption bands and the corresponding electron transitions: 371 nm: H→L+5 (*–0.90*), H→L+2 (*0.36*); 356 nm: H–1→L+2 (*0.87*), H→L+2 (*–0.35*); 351 nm: H→L+4 (*0.92*); 341 nm: H–1→L+1 (*0.80*), H→L+2 (*–0.34*)

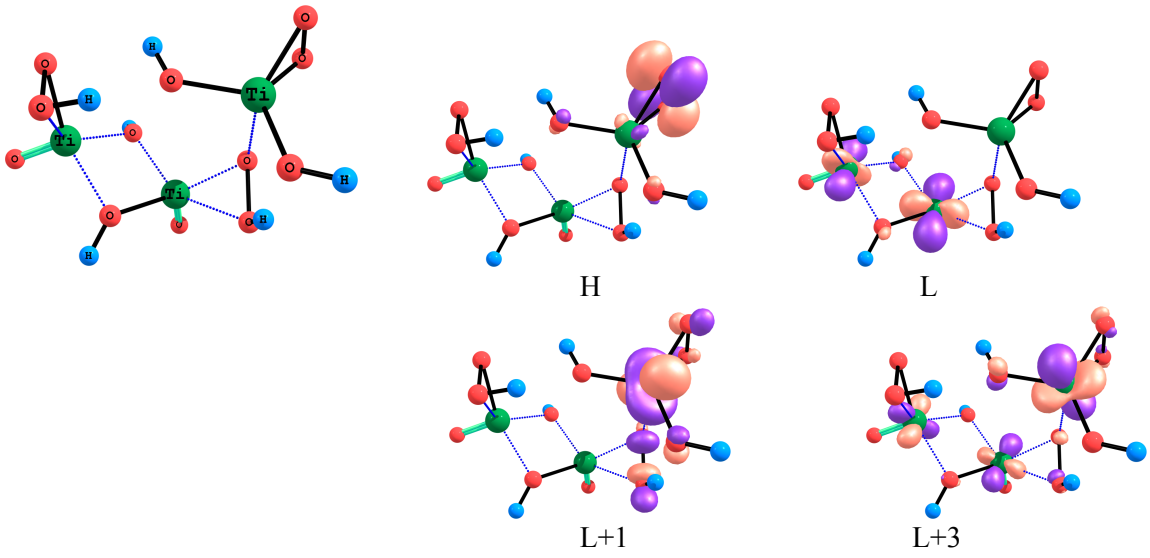

Fig. 8. Pictorial representation of MO for the complex with three monomer units 3. Absorption bands and the corresponding electron transitions:

Use of great excess of hydrogen peroxide during the synthesis of peroxotitanate complexes can lead to coordination of several peroxy groups on one titanium atom (excepting strongly acidic medium), therefore the spectra of neutral complexes of the series (**II**) have been calculated for purposes of comparison. For these spectra it has been shown (Fig. 4) that the range of wavelengths lower than 320 nm is also of low information value because of the great number of intensive closely-spaced absorption bands. As opposed to neutral complexes of the series (**I**), the spectra include intensive bands at 392, 359, 348 nm for one, two, and three monomer units in the complex, respectively. Probably, the yellow color of the peroxotitanate complexes synthesized in [26] up to basic pH values is due to occurrence of the series (**II**) complexes. Analysis of electron transitions (Fig. 9–10) has shown that the presence of these bands is mostly determined by the transitions from the upper occupied MO (combination of AO of the peroxy group oxygen atoms) to the lower vacant MO with its peculiarities. It has been shown that for the series (**II**) such a MO is formed from the combination of not only vacant D-type AO of titanium atoms, but also of p-type AO of the bridging peroxy group oxygen atoms that are specific for the series (**II**). This suggests that the cause of appearance of the abovementioned bands for complexes of the series (**II**) is similar to the cause of coloring for the neutral complexes of the series (**I**). That is, the absorption band near 360 nm can serve as an indicator of existence of bridging hydroperoxy groups in the complex at neutral pH of the solution.

The factor that determines titania precipitation from peroxotitanate complexes is the stability of the hydrogen peroxide excess existing in the solution. Therefore the greatest rate of precipitation should be observed in weakly acidic medium, where peroxide is less stable compared to strongly acidic medium.

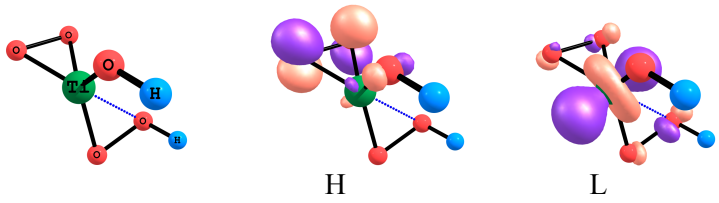

Fig. 9. Pictorial representation of MO for monomer unit 5. Absorption bands and the corresponding electron transitions: 392 nm: H→L (*0.96*)

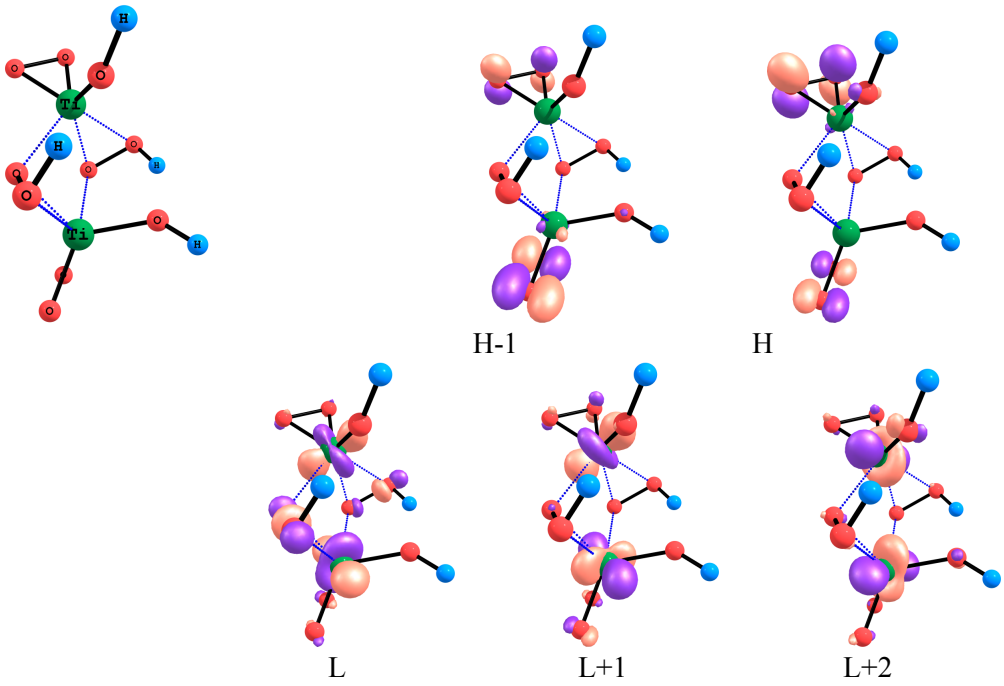

Fig. 10. Pictorial representation of MO for the complex with two monomer units 5. Absorption bands and the corresponding electron transitions: 359 nm: H-1→L (*0.81*); 310 nm: H→L+1 (*0.74*), H–1→L+2 (*–0.43*)

In these conditions the state of peroxotitanate complexes is nearer to the isoelectric point, that is, the probability of occurrence for the complexes formed from monomer units **3** and **5** (at great excess of hydrogen peroxide) is significantly higher. Such complexes are the most capable of oligomerization and, possibly, of hydrolysis that leads to further formation of hydrated titania precipitate. On the other hand, for neutral monomer units the value of the energy of complex formation from three units decreases compared to the complexes of two units (Table 1), which enables the former to occur in solution with less probability than the latter. For the series (**II**) the decrease is much steeper; relative stability of such a complex of two monomer units can determine the stability in time of peroxotitanate complex solutions in wide range of pH values, verified experimentally for the initial ratio "hydrogen peroxide – titanium" more than 10:1 [26].

Understanding how the bonds between monomer units in peroxotitanate complexes are formed and tracking of this process by means of UV-visible spectra analysis makes it possible to estimate probable directions of further oligomerization and hydrolysis reactions, as well as the probability of formation for this or that crystal or amorphous phase, in which the precipitate is formed (anatase, rutile, etc.). Attempts of the estimation with the use only of calculated data were made previously in [17], where polyperoxide complexes were studied. Oligomeric chains in such complexes are formed in two ways: a) two oxygen bridges between titanium atoms, which leads to subsequent formation of the structure of anatase type (octahedrons with common edges) – in the case of minimal and maximal concentration of added hydrogen peroxide; b) one oxygen bridge between titanium atoms, which helps subsequent formation of the structure of rutile type (octahedrons with common tips) – in the case of medium concentration of added hydrogen peroxide. Our research in the spectral characteristics of the solutions of peroxotitanate complexes at various synthesis conditions coupled with calculated data has shown that the use of UV-visible spectra can provide information about occurrence of monomer units of this of that kind in the complexes, as well as about the bonding pattern. We consider the possibility of further application of this information to prognosticate priority ways of the new phase formation in specified environment.

Conclusion

In the present paper the electronic spectra of peroxotitanate complexes formed from five types of monomer units have been investigated. Non-empirical calculations of the optimized complex structures have been carried out by Kohn-Sham method with the use of functional B3LYP and all-electron basis set 6-31G**, with allowance made for influence of water as a solvent in PCM. The calculation of the excited states has been carried out by TD-DFT method. It has been found that the spectra of complexes in the series (**I**) ($[Ti(O_2)(OH)_x]^{(2-x)+}$) have characteristic absorption bands, they are specific for wavelength range higher than 300 nm, namely: 413 nm for x = 0 and several bands in the ranges 335...360 nm and 370...380 nm for x = 1. It has been shown that the position of the absorption bands in the spectrum of the solution of peroxotitanate complexes at pH < 1 corresponds to the calculated spectrum of monomer unit **1**, while the spectrum of the solution at pH 2.0...2.5 corresponds to the calculated spectrum of the complexes with monomer unit **2**. At that the difference between the absorption band maxima and the intensive calculated lines does not exceed 10 nm. In the spectra of neutral complexes of the series (**I**) and (**II**) $[Ti(O_2)(OOH)(OH)]$ the absorption bands in the range 345...400 nm, that determine yellow color of the complexes in neutral medium, can appear subject to bonding between titanium atoms through the hydroperoxy group oxygen. The complex composition is related to the solution pH values and the excess of hydrogen peroxide relative to titanium, at that the tendency of solution spectrum change under varied conditions of complex existence correlates to the change of calculated spectra in accordance with the monomer unit predominating in the composition. Thus, comparison of the calculated electronic spectrum and the UV-visible spectrum of the peroxotitanate complex solution makes it possible to estimate the composition at specific conditions and prognosticate the possible reaction pathways.

Acknowledgments

We are grateful for financial support of the Ministry of Education and Science of the Russian Federation (grant No 16.2674.2014/K).

References

1. Sakka S. (Ed.) *Handbook of Sol-Gel Science and Technology, Volume 1 Sol-Gel Processing.* Kluwer academic publishers, 2005, pp. 108–112.

2. Muehlebach J., Mueller K., Schwarzenbach G. The Peroxo Complexes of Titanium. *Inorg. Chem.,* 1970, vol. 9, no. 11, pp. 2381–2390.

3. Kakihana M., Kobayashi M., Tomita K., Petrykin V. Application of Water-Soluble Titanium Complexes as Precursors for Synthesis of Titanium-Containing Oxides via Aqueous Solution Processes. *Bull. Chem. Soc. Japan,* 2010, vol. 83, no. 11, pp. 1285–1308.

4. Tengvall P., Wälivaara B., Westerling J., Lundström I. Stable Titanium Superoxide Radicals in Aqueous Ti-peroxy Gels and Ti-peroxide Solutions. *J. Colloid Interface Sci.,* 1991, vol. 143, no. 2, pp. 589–592.

5. Garifzyanova G.G., Chachkov D.V., Shamov A.G. Quantum Chemical Study of the Structure of Bimetal Platinum and Iridium Nanoclusters. Part 1. Cluster Pt_3Ir [Kvantovo-khimicheskoe issledovanie stroeniya bimetallicheskikh nanoklasterov platiny i iridiya. ch. 1. Klaster Pt_3Ir]. *Vestnik KGTU [Bulletin of KSTU]*, 2010, vol. 10, pp. 11–17. (in Russ.)

6. Runge E., Gross E. K. U. Density-Functional Theory for Time-Dependent Systems. *Phys. Rev. Lett.,* 1984, vol. 52, pp. 997–1000.

7. Dreuw A., Head-Gordon M. Single-Reference ab Initio Methods for the Calculation of Excited States of Large Molecules. *Chem. Rev.,* 2005, vol. 105, pp. 4009–4037.

8. Sever R.R., Root T.W. DFT Study of Solvent Coordination Effects on Titanium-Based Epoxidation Catalysts. Part One: Formation of the Titanium Hydroperoxo Intermediate. *J. Phys. Chem. B,* 2003, vol. 107, pp. 4080–4089.

9. Barker C.M., Gleeson D., Kaltsoyannis N., Catlow C.R.A., Sankar G., Thomas J.M. On the Structure and Coordination of the Oxygen-donating Species in Ti|MCM-41/TBHP Oxidation Catalysts: a Density Functional Theory and EXAFS Study. *Phys. Chem. Chem. Phys.,* 2002, vol. 4, pp. 1228–1240.

10. Munakata H., Oumi Y., Miyamoto A. A DFT Study on Peroxo-Complex in Titanosilicate Catalyst: Hydrogen Peroxide Activation on Titanosilicalite-1 Catalyst and Reaction Mechanisms for Catalytic Olefin Epoxidation and for Hydroxylamine Formation from Ammonia *J. Phys. Chem. B,* 2001, vol. 105, pp. 3493–3501.

11. Chin-Lung Kuo, Wei-Guang Chen, Tzu-Ying Chen The Electronic Structure Changes and the Origin of the Enhanced Optical Properties in N-doped Anatase TiO_2 – a Theoretical Revisit. *J. Appl. Phys.,* 2014, vol. 116, pp. 093709-1–7.

12. Govind N., Lopata K., Rousseau R., Andersen A., Kowalski K. Visible Light Absorption of N-Doped TiO_2 Rutile Using (LR/RT)-TDDFT and Active Space EOMCCSD Calculations. *J. Phys. Chem. Lett.,* 2011, vol. 2, pp. 2696–2701.

13. Welliaa D.V., Qing Chi Xua, Mahasin Alam Sk, Kok Hwa Lim, Tuti Mariana Lim, Timothy Thatt Yang Tan Experimental and Theoretical Studies of Fe-doped TiO_2 Flms Prepared by Peroxo Sol-gel Method. *Appl. Catalysis A: General,* 2011, vol. 401, pp. 98–105.

14. Kholdeeva O.A., Trubitsina T.A., Maksimovskaya R.I., Golovin A.V., Neiwert W.A., Kolesov B.A., Lopez H., Poblet J.M. First Isolated Active Titanium Peroxo Complex: Characterization and Theoretical Study. *Inorg. Chem.,* 2004, vol. 43, pp. 2284–2292.

15. Mennucci B., Tomasi J., Cammi R., Cheeseman J. R., Frisch M. J., Devlin F. J., Gabriel S., Stephens P. J. Polarizable Continuum Model (PCM) Calculations of Solvent Effects on Optical Rotations of Chiral Molecules. *J. Phys. Chem. A,* 2002, vol. 106, pp. 6102–6113.

16. Tomasi J., Mennucci B., Cammi R. Quantum Mechanical Continuum Solvation Models. *Chem. Rev.,* 2005, vol. 105, pp. 2999–3094.

17. Manaswita Nag, Sutapa Ghosh, Rohit Kumar Rana, Sunkara V. Manorama Controlling Phase, Crystallinity, and Morphology of Titania Nanoparticles with Peroxotitanium Complex: Experimental and Theoretical Insights. *J. Phys. Chem. Lett.,* 2010, vol. 1, pp. 2881–2885.

18. Adamo C., Barone V. Toward Reliable Density Functional Methods without Adjustable Parameters: The PBE0 Model. *J. Chem. Phys.,* 1999, vol. 110, pp. 6158–6170.

19. Becke A.D. Density-functional Thermochemistry. 3. The Role of Exact Exchange. *J. Chem. Phys.,* 1993, vol. 98, pp. 5648–5652.

20. Chengteh Lee, Weitao Yang, Parr R.G. Development of the Colle-Salvetti Correlation-Energy

Formula into a Functional of the Electron Density. *Phys. Rev. B,* 1988, vol. 37, pp. 785–789.

21. Hariharan P. C., Pople J. A. The Influence of Polarization Functions on Molecular Orbital Hydrogenation Energies. *Theor. Chim. Acta,* 1973, vol. 28, no. 3, pp. 213–222.

22. Rassolov V.A., Pople J.A., Ratner M.A., Windus T.L. 6-31G* Basis Set for Atoms K through Zn. *J. Chem. Phys.,* 1998, vol. 109, pp. 1223–1229.

23. Wadt W.R., Jeffrey Hay P. Ab initio Effective Core Potentials for Molecular Calculations. Potentials for Main Group Elements Na to Bi. *J. Chem. Phys.,* 1985, vol. 82, pp. 284–298.

24. Emsley J. *The Elements (3rd Ed.).* Oxford, Oxford University Press, 1998. 300 p.

25. Granovsky A.A. *Firefly version 8.* Available at: http://classic.chem.msu.su/gran/firefly/index.html (accessed 28 February 2015).

26. Ruxiong Cai, Kiminori Itoh and Changqing Sun pH Effect on the Optical Properties of Peroxo-Titanium Complex. *Mater. Res. Soc. Symp. Proc.,* 2006, vol. 900, pp. 0900-O13-05.1–0900-O13-05.8.

Received 23 May 2015

УДК 544.164, 546.82

УФ-ВИД СПЕКТРЫ ПЕРОКСОТИТАНАТНЫХ КОМПЛЕКСОВ

Ю.В. Матвейчук, И.В. Кривцов, М.В. Илькаева, В.В. Авдин
Южно-Уральский государственный университет, г. Челябинск

Выполнен сравнительный анализ расчётных (с учётом влияния растворителя в модели PCM) и экспериментальных УФ-вид спектров растворов пероксотитанатных комплексов при варьировании условий их существования. Показано, что изменение состава комплексов, зависящего от величины pH раствора, приводит к изменению характерных полос поглощения УФ-вид спектров в области длин волн более 320 нм. Тенденция сдвига полос поглощения в спектрах растворов соответствует изменению расчётных спектров в зависимости от мономерной единицы комплекса. Предположено, что окраска раствора комплексов в слабокислой и нейтральной среде связана с возникновением гидропероксосвязей между атомами титана.

Ключевые слова: пероксотитанатные комплексы, электронные спектры поглощения, PCM, TD-DFT.

Литература

1. Handbook of Sol-Gel Science and Technology. Vol. 1. Sol-Gel Processing / Sakka, S. (Ed.). – KLUWER ACADEMIC PUBLISHERS, 2005. – P. 108–112.

2. Muehlebach, J. The Peroxo Complexes of Titanium / J. Muehlebach, K. Mueller, G. Schwarzenbach // Inorganic Chemistry. – 1970. – Vol. 9. – No. 11. – P. 2381–2390.

3. Application of Water-Soluble Titanium Complexes as Precursors for Synthesis of Titanium-Containing Oxides via Aqueous Solution Processes / M. Kakihana, M. Kobayashi, K. Tomita, V. Petrykin // Bulletin of the Chemical Society of Japan. – 2010. – Vol. 83. – No. 11. – P. 1285–1308.

4. Stable Titanium Superoxide Radicals in Aqueous Ti-peroxy Gels and Ti-peroxide Solutions / P. Tengvall, B. Wälivaara, J. Westerling, I. Lundström // Journal of Colloid and Interface Science. – 1991. – Vol. 143. – No. 2. – P. 589–592.

5. Гарифзянова, Г.Г. Квантово-химическое исследование строения биметаллических нанокластеров платины и иридия. ч. 1. Кластер Pt_3Ir. / Г.Г. Гарифзянова, Д. В. Чачков, А. Г. Шамов // Вестник КГТУ. – 2010. – Т. 10. – С. 11–17.

6. Runge, E. Density-Functional Theory for Time-Dependent Systems / E. Runge, E. K. Gross // Physical Review Letters. – 1984. – Vol. 52. – P. 997–1000.

7. Dreuw, A. Single-Reference ab Initio Methods for the Calculation of Excited States of Large Molecules / A. Dreuw, M. Head-Gordon // Chemical Reviews. – 2005. – Vol. 105. – P. 4009–4037.

8. Sever, R.R. DFT Study of Solvent Coordination Effects on Titanium-Based Epoxidation Catalysts. Part One: Formation of the Titanium Hydroperoxo Intermediate / R.R. Sever, T.W. Root // The Journal of Physical Chemistry B. – 2003. – Vol. 107. – P. 4080–4089.

9. On the Structure and Coordination of the Oxygen-donating Species in Ti|MCM-41/TBHP Oxidation Catalysts: a Density Functional Theory and EXAFS Study / Barker C.M., Gleeson D., Kaltsoyannis N. et al. // Physical Chemistry Chemical Physics. – 2002. – Vol. 4. – P. 1228–1240.

10. Munakata, H. DFT Study on Peroxo-Complex in Titanosilicate Catalyst: Hydrogen Peroxide Activation on Titanosilicalite-1 Catalyst and Reaction Mechanisms for Catalytic Olefin Epoxidation and for Hydroxylamine Formation from Ammonia / H. Munakata, Y. Oumi, A. Miyamoto // The Journal of Physical Chemistry B. – 2001. – Vol. 105. – P. 3493–3501.

11. Chin-Lung Kuo The Electronic Structure Changes and the Origin of the Enhanced Optical Properties in N-doped Anatase TiO_2 – a Theoretical Revisit / Chin-Lung Kuo, Wei-Guang Chen, Tzu-Ying Chen // Journal of Applied Physics. – 2014. – Vol. 116. – P. 093709-1–7.

12. Visible Light Absorption of N-Doped TiO_2 Rutile Using (LR/RT)-TDDFT and Active Space EOMCCSD Calculations / N. Govind, K. Lopata, R. Rousseau et al. // The Journal of Physical Chemistry Letters. – 2011. – Vol. 2. – P. 2696–2701.

13. Experimental and Theoretical Studies of Fe-doped TiO_2 Flms Prepared by Peroxo Sol-gel Method / D.V. Welliaa, Qing Chi Xua, Mahasin Alam Sk et al. // Applied Catalysis A: General. – 2011. – Vol. 401. – P. 98–105.

14. First Isolated Active Titanium Peroxo Complex: Characterization and Theoretical Study / O.A. Kholdeeva, T.A. Trubitsina, R.I. Maksimovskaya et al. // Inorganic Chemistry. – 2004. – Vol. 43. – P. 2284–2292.

15. Polarizable Continuum Model (PCM) Calculations of Solvent Effects on Optical Rotations of Chiral Molecules / B. Mennucci, J. Tomasi, R. Cammi et al. // The Journal of Physical Chemistry A. – 2002. – Vol. 106. – P. 6102–6113.

16. Tomasi, J. Quantum Mechanical Continuum Solvation Models / J. Tomasi, B. Mennucci, R. Cammi // Chemical Reviews. – 2005. – Vol. 105. – P. 2999–3094.

17. Controlling Phase, Crystallinity, and Morphology of Titania Nanoparticles with Peroxotitanium Complex: Experimental and Theoretical Insights / Manaswita Nag, Sutapa Ghosh, Rohit Kumar Rana et al. // The Journal of Physical Chemistry Letters. – 2010. – Vol. 1. – P. 2881–2885.

18. Adamo, C. Toward Reliable Density Functional Methods without Adjustable Parameters: The PBE0 Model / C. Adamo, V. Barone // The Journal of Chemical Physics. – 1999. – Vol. 110. – P. 6158–6170.

19. Becke, A.D. Density-functional Thermochemistry. 3. The Role of Exact Exchange / A.D. Becke // The Journal of Chemical Physics. – 1993. – Vol. 98. – P. 5648–5652.

20. Chengteh Lee Development of the Colle-Salvetti Correlation-Energy Formula into a Functional of the Electron Density / Chengteh Lee, Weitao Yang, R.G. Parr // Physical Review B: Condensed Matter and Materials Physics. – 1988. – Vol. 37. – P. 785–789.

21. Hariharan, P. C. The Influence of Polarization Functions on Molecular Orbital Hydrogenation Energies / P. C. Hariharan, J. A. Pople // Theoretica Chimica Acta. – 1973. – Vol. 28. – No. 3. – P. 213–222.

22. 6-31G* Basis Set for Atoms K through Zn / V.A. Rassolov, J.A. Pople, M.A. Ratner, T.L. Windus // The Journal of Chemical Physics. – 1998. – Vol. 109. – P. 1223–1229.

23. Wadt, W.R. Ab initio Effective Core Potentials for Molecular Calculations. Potentials for Main Group Elements Na to Bi / W.R. Wadt, P. Jeffrey Hay // The Journal of Chemical Physics. – 1985. – Vol. 82. – P. 284–298.

24. Emsley, J. The Elements (3rd Ed.) / Emsley J. – Oxford: Oxford University Press, 1998. – 300 p.

25. Granovsky, A.A. Firefly version 8 / A.A. Granovsky. – http://classic.chem.msu.su/gran/firefly/index.html (дата обращения 01.06.2015).

26. Ruxiong Cai pH Effect on the Optical Properties of Peroxo-Titanium Complex / Ruxiong Cai, Kiminori Itoh, Changqing Sun // Materials Research Society Proceedings. – 2006. – Vol. 900. – P. 0900-O13-05.1–0900-O13-05.8.

Матвейчук Юрий Васильевич – кандидат химических наук, ведущий инженер кафедры экологии и природопользования, Химический факультет, Южно-Уральский государственный университет. 454080, г. Челябинск, пр. им. В.И. Ленина, 76. E-mail: diff@inbox.ru

Кривцов Игорь Владимирович – кандидат химических наук, инженер НОЦ «Нанотехнологии», Южно-Уральский государственный университет. 454080, г. Челябинск, пр. им. В.И. Ленина, 76. E-mail: zapasoul@gmail.com

Илькаева Марина Викторовна – аспирант, Химический факультет, Южно-Уральский государственный университет. 454080, г. Челябинск, пр. им. В.И. Ленина, 76. E-mail: mylegenda@gmail.com

Авдин Вячеслав Викторович – доктор химических наук, декан химического факультета, Южно-Уральский государственный университет. 454080, г. Челябинск, пр. им. В.И. Ленина, 76. E-mail: avdin@susu.ru

Поступила в редакцию 23 мая 2015 г.

ОБРАЗЕЦ ЦИТИРОВАНИЯ

UV-visible spectra of peroxotitanate complexes / Yu.V. Matveychuk, I.V. Krivtsov, M.V. Ilkaeva, V.V. Avdin // Вестник ЮУрГУ. Серия «Химия». – 2015. – Т. 7, № 3. – С. 33–45.

FOR CITATION

Matveychuk Yu.V., Krivtsov I.V., Ilkaeva M.V., Avdin V.V. UV-visible Spectra of Peroxotitanate Complexes. *Bulletin of the South Ural State University. Ser. Chemistry.* 2015, vol. 7, no. 3, pp. 33–45.

SPECTROSCOPIC INVESTIGATION OF THE INFLUENCE OF ALUMINUM ADDITION ON CHARACTERISTIC FEATURES OF ALKALI BOROSILICATE GLASSES

V.E. Eremyashev, *Zlatoust Branch of South Ural State University, Zlatoust, Russian Federation, vee-zlat@mail.ru*
G.G. Korinevskaya, *Institute of Mineralogy UB RAS, Miass, Russian Federation, galkor@mineralogy.ru*
R.R. Aysin, *A.N. Nesmeyanov Institute of Organoelement Compounds of RAS (INEOS RAS), Moscow, Russian Federation, aysin.rinat@gmail.com*

The influence of aluminum on the structure of alkali borosilicate glasses with various ratios of network former cations and modifier cations has been studied with the use of vibrational spectroscopy. It has been found that addition of modest amounts of aluminum to borosilicate glasses decreases the difference of sodium and potassium distribution between silicon- and boron-containing structural units of the glasses. This fact allows consideration of aluminum as an additive contributory to homogeneity of borosilicate glasses containing both sodium and potassium, as well as increase in thermal and chemical stability of matrix materials based on such glasses.

Keywords: borosilicate glass, spectroscopy, structure, aluminum.

Introduction

During investigation of structural peculiarities of alkali borosilicate glasses with the use of vibrational spectroscopy and NMR spectroscopy the significant difference of sodium and potassium distribution between silicate and borate structural units has been established [1, 2], which determines greater depolymerization of anion structure of sodium-containing borosilicate glasses compared to potassium glasses of similar composition. This explains appearance of structural heterogeneity in the structure of borosilicate glasses containing both sodium and potassium ions [3], besides, it negatively affects physicochemical characteristics of matrix materials based on them [4].

With the aim of looking for additives increasing homogeneity of alkali borosilicate glasses, the influence of aluminum addition on structural features of sodium and potassium borosilicate glasses has been studied by vibrational spectroscopy at various ratios of network former cations and modifier cations. The choice of aluminum as an additive has been caused by the assignment of aluminum to network former cations, highly active in distribution of sodium and potassium ions, which manifest themselves as modifier cations in the glass structure [5–8]. Addition of aluminum to glass composition suggests redistribution of modifier cations between structural units due to their participation in compensation of electrical charge for the AlO_4 tetrahedrons.

Experimental

Aluminum-free and aluminum-containing sodium and potassium borosilicate glasses of the chosen composition were synthesized with the use of following reactants: analytical grade SiO_2, high purity grade B_2O_3, chemical purity grade Al_2O_3, chemical purity grade Na_2CO_3 and K_2CO_3, according to the procedure described in [2, 9]. Table 1 contains the composition of the synthesized glasses and their reference designations. The investigation of the characteristic structural features was carried out by infrared spectroscopy (IR) and Raman spectroscopy. IR transmission spectra were registered on the single-beam Fourier-transform IR spectrometer Nicolet 6700 Thermo Scientific with the use of KBr pellet pressing technique. The iHR 320 Labram spectrometer with Olimpus BX41 microscope was used for registration of Raman spectra. The obtained spectra are shown in Fig. 1–4.

Table 1

Chemical composition of the synthesized glasses

Sample	Composition, mole fractions
15N35B	$0.15Na_2O{\cdot}0.35B_2O_3{\cdot}0.5SiO_2$
35N15B	$0.35Na_2O{\cdot}0.15B_2O_3{\cdot}0.5SiO_2$
15K35B	$0.15K_2O{\cdot}0.35B_2O_3{\cdot}0.5SiO_2$
35K15B	$0.35K_2O{\cdot}0.15B_2O_3{\cdot}0.5SiO_2$
A15N35B	$0.9(0.15Na_2O{\cdot}0.35B_2O_3{\cdot}0.5SiO_2)+0.1Al_2O_3$
A35N15B	$0.9(0.35Na_2O{\cdot}0.15B_2O_3{\cdot}0.5SiO_2)+0.1Al_2O_3$
A15K35B	$0.9(0.15K_2O{\cdot}0.35B_2O_3{\cdot}0.5SiO_2)+0.1Al_2O_3$
A35K15B	$0.9(0.35K_2O{\cdot}0.15B_2O_3{\cdot}0.5SiO_2)+0.1Al_2O_3$

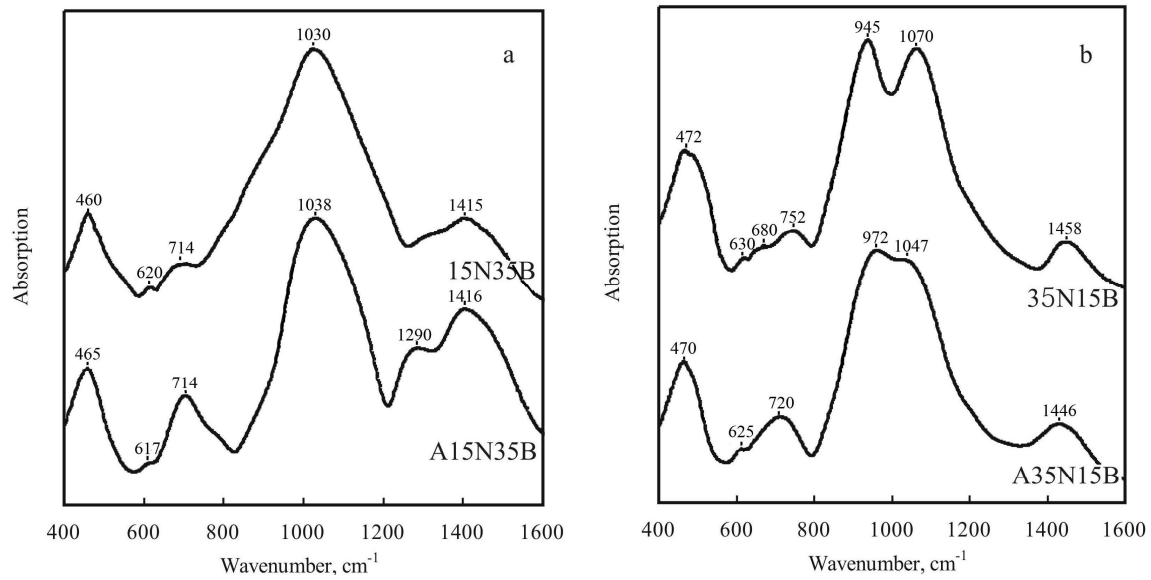

Fig. 1. IR spectra of the sodium glasses:
a – glasses with low content of sodium and high content of boron, b – glasses with high content of sodium and low content of boron (designations of the samples correspond to Table 1)

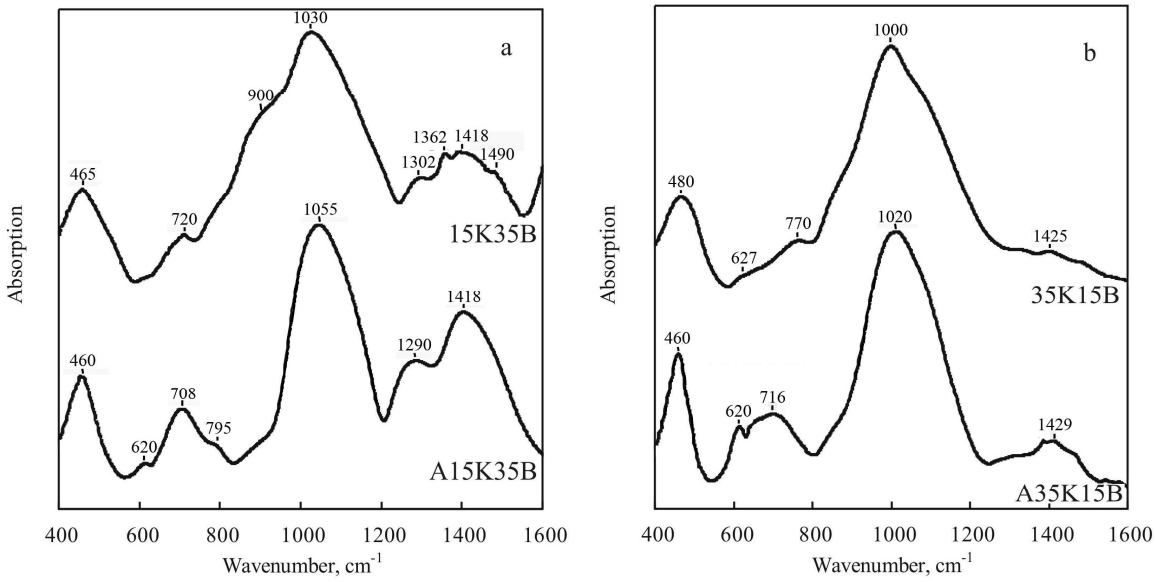

Fig. 2. IR spectra of the potassium glasses:
a – glasses with low content of potassium and high content of boron, b – glasses with high content of potassium and low content of boron (designations of the samples correspond to Table 1)

Results and Discussion

All IR spectra of the synthesized glasses (Fig. 1 and 2) contain bands with maxima near 460–480, 610–800, 800–1200 and 1350–1490 cm^{-1}. In the IR spectra of aluminum-free sodium glasses (Fig. 1) the increase of alkali metal content and the decrease of boron content leads to the increase of band intensity for the maximum near 460–480 cm^{-1}, the change of band shape for the maximum near 610–800 cm^{-1}, and the decrease of band intensity for the maximum near 1350–1490 cm^{-1}. In the spectrum of 35N15B glass the following features are observed: the band with the maximum near 1030 cm^{-1}, which dominates in the spectrum of 35N15B glass, separates into two components with maxima near 945 cm^{-1} and 1070 cm^{-1}.

Changes in the IR spectra of aluminum-free potassium glasses with similar changes in composition are also related to the change in band shape in the range 800–1200 cm^{-1} and the decrease of band intensity for the maximum near 1350–1490 cm^{-1} (Fig. 2). At low content of potassium and high content of boron in the glass composition (15K35B) the band with maximum near 1030 cm^{-1} and the plateau near 900 cm^{-1} are observed in the range 800–1200 cm^{-1}. At the increase of potassium content and the decrease of boron content in the glass composition (35K15B) the maximum of this band shifts to 1000 cm^{-1} with significant change in the position and intensity of its branches.

The IR spectra of all synthesized aluminum-containing sodium and potassium glasses (A15N35B, A35N15B, A15K35B, A35K15B) are characterized by higher intensity of bands with the maxima near 610–800 cm^{-1}, significant changes in band shape in the range 800–1200 cm^{-1}, and the increase of band intensity for the maximum near 1350–1490 cm^{-1}. It is especially noticeable in the spectra of glasses with low content of alkali metal and high content of boron (Fig. 1 and 2).

IR absorption near 460-480 and 1050–1090 cm^{-1} is related to deformation and asymmetric stretching vibrations of Si–O–Si(Al) bonds in complex silicate anions [10–12], its intensity in spectra is determined by the content of SiO_2 in the glass composition. The band near 610–800 cm^{-1} makes itself evident as the superimposed on one another bands due to symmetric vibrations of Si(Al)–O–Si bonds, asymmetric stretching vibrations of B–O–B bonds, deformation vibrations of B–O bond in the BO_3 triangles, and vibrations of the bonds in the AlO_4 tetrahedrons. This complicates the use of absorption in this range for discussion of changes in the glass structure. Absorption in the range 940–980 cm^{-1} is related to deformation and asymmetric stretching vibrations of B–O bond in the BO_4 tetrahedra, which allows estimating the change of boron ions content in the tetrahedral coordination [10, 12]. The band in the range 1350–1490 cm^{-1} is related to deformation and stretching vibrations of B–O bonds of the BO_3 triangles. Decrease of its intensity reflects the decrease of the tri-coordinated boron content in the glass structure [10, 11]. Changes in IR spectra of glasses observed at aluminum addition correlate with the increase of the fraction of BO_3 triangles, the decrease of BO_4 tetrahedra, and the changes in the nearest environment of silicon atoms through the development of AlO_4 tetrahedra in the glass structure, as well as the formation of bridging intertetrahedral Si–O–Al bonds.

The Raman spectra of all synthesized aluminum-free sodium and potassium glasses strongly differ from each other. In the Raman spectrum of 15N35B glass (Fig. 3a) there are intensive bands with maxima at 510 and 1150 cm^{-1}, as well as the set of closely spaced bands of lower intensity with the maxima near 630, 700, 760 and 800 cm^{-1}. In the Raman spectrum of 35N15B glass (Fig. 3b) intensive bands with the maxima near 600, 955 and 1090 cm^{-1} are observed. In the Raman spectrum of 15K35B glass (Fig. 4a) we have registered the intensive band with the maximum at 510 cm^{-1}, the set of closely spaced bands of lower intensity with the maxima near 630, 700, 770 and 800 cm^{-1}, as well as three weak broad bands with the maxima near 940, 1150 and 1450 cm^{-1}. The Raman spectrum of 35K15B glass (Fig. 4b) is characterized by the band with the maximum near 600 cm^{-1} and the plateau near 530 cm^{-1}, as well as the narrower intensive band 1095 cm^{-1} and weak bands with the maxima near 940 and 1450 cm^{-1}.

Addition of aluminum to glass composition significantly influences the position and intensity of the Raman bands. In the Raman spectrum of aluminum-containing sodium glass A15N35B (Fig. 3a) the significant decrease of the band intensity with the maxima near 630, 700 and 1150 cm^{-1} is observed. In spite of obvious differences in the spectra of parent glasses 15N35B and 15K35B, taking into account slight differences in intensity ratios and extra plateaus, the spectrum of aluminum-containing potassium glass A15K35B (Fig. 4a), has the similar appearance to the Raman spectrum of A15N35B glass. In the low-frequency (300–800 cm^{-1}) part of the Raman spectrum of aluminum-containing sodium glass A35N15B (Fig. 3b) the band of complex shape with the maximum near 510 cm^{-1} and plateaus near 570,

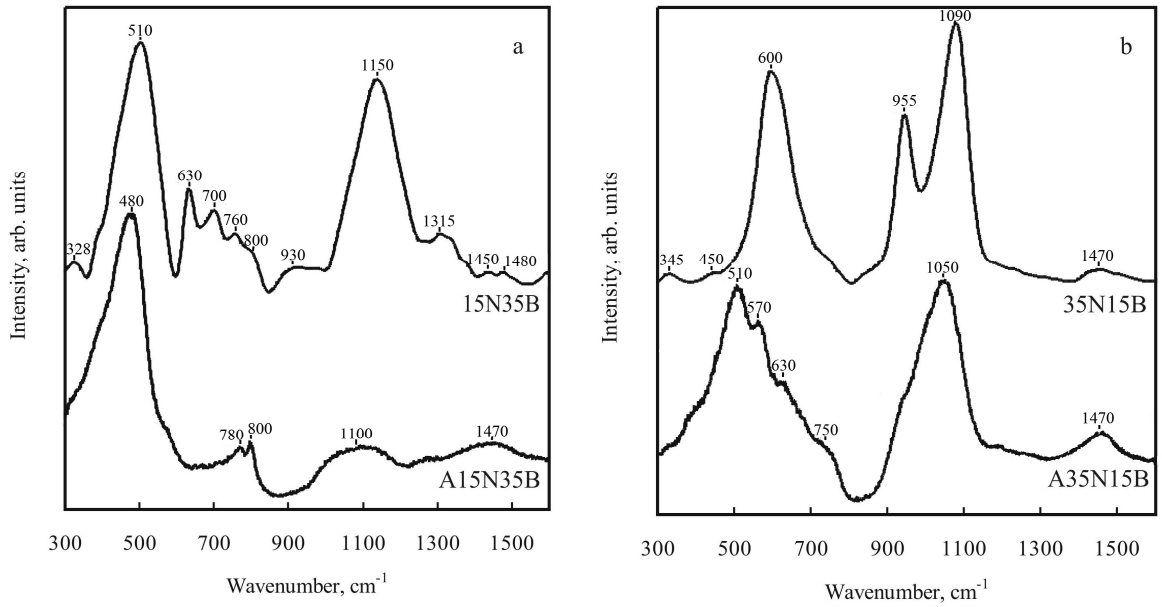

Fig. 3. Raman spectra of the sodium glasses:
a – glasses with low content of sodium and high content of boron, b – glasses with high content of sodium and low content of boron (designations of the samples correspond to Table 1)

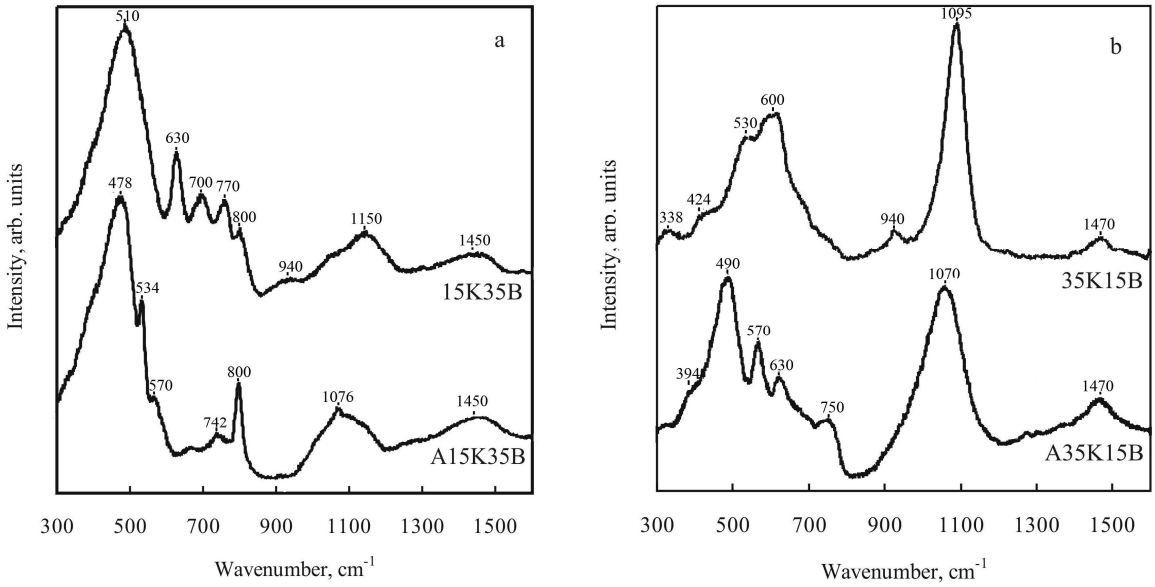

Fig. 4. Raman spectra of the potassium glasses:
a – glasses with low content of potassium and high content of boron, b – glasses with high content of potassium and low content of boron (designations of the samples correspond to Table 1)

630 and 750 cm^{-1} is registered. In the high-frequency part of the Raman spectrum of this glass the band with the maximum near 1050 cm^{-1} is observed, with strongly expressed asymmetry as viewed from low wavenumbers. Besides, the band of low intensity with the maximum 1470 cm^{-1} is clearly defined in the spectrum. The Raman spectrum of aluminum-containing potassium glass A35K15B (Fig. 4b) is distinguished from the spectrum of A35N15B glass only by the slight shift of the band maxima (510→490 cm^{-1} and 1050→1070 cm^{-1}) and better defined plateaus near 570, 630 and 750 cm^{-1}. Hence the aluminum addition increases resemblance of the Raman spectra of sodium and potassium glasses of similar composition, both with low and high content of alkali metal.

The bands with the maxima near 400–600 cm^{-1} in the low-frequency part of the Raman spectra of borosilicate glasses are related to symmetrical stretching and deformation vibrations of Si–O–Si(Al) and Si(Al)–O–B bridging bonds in anions with complex structure [13, 14]. High intensity of these bands,

observed in the Raman spectra of all investigated glasses indicate the relatively high polymerization degree of their anion structure. The band with the maximum near 630 cm^{-1} reflects the vibrations of mixed silicon-boron rings, and decrease of intensity for this band indicates decrease of boron content in the glass composition or at decrease of its participation in formation of the mixed borosilicate rings. The bands in the range 700–800 cm^{-1} are related to vibrations of B–O bonds included in the BO_4 tetrahedra, which helps us to use these bands for estimation of the boron state in the glass structure. The bands in the range 950–1150 cm^{-1} are related to the manifestation of stretching vibrations of the Si–O– nonbridging bonds in Q^2 and Q^3 structural units [15]. Their presence in the glass spectra indicates participation of sodium and potassium ions in coordination of the nonbridging bonds, while the observed change of symmetry in these bands at aluminum addition arises from the presence of the AlO_4 tetrahedrons in the nearest environment of those structural units. The band with the maximum near 1470 cm^{-1} reflects the vibrations of the BO_3 structural units. Low intensity of this band in the spectra of borosilicate glasses generally points at boron in tetrahedral coordination (BO_4) dominating in the structure of such glasses.

Conclusion

The characteristic features of obtained Raman spectra indicate the difference in distribution of modifier cations between various kinds of structural units in the structure of aluminum-free and aluminum-containing sodium and potassium borosilicate glasses. In aluminum-containing glasses the development of the AlO_4 structural units, participating in formation of the bridging Si–O–Al bonds, is observed in the studied composition range. The fraction of the BO_4 tetrahedra decreases, while the fraction of the BO_3 triangles, which form the isolated boron ring structures, increases. Mostly these changes appear in the glasses with low content of alkali metals and high content of boron. In the glasses with high content of alkali metals and low content of boron the changes touch upon the silicate part of the glass structure, too. The decrease of the fraction of silicate structural units with nonbridging oxygen atoms (Q^n) is under way, as well as the decrease of the fraction of nonbridging bonds in the composition of the borate structural units. It correlates with the decrease of participation of alkali metal cations in the coordination of the charge of boron-containing structural units BO_4, which decreases the difference in the distribution of sodium and potassium between silicate and borate structural units and enhances the structural semblance of sodium and potassium glasses with the similar composition. The significant fraction of sodium and potassium ions in the structure of aluminum-containing glasses participate in the coordination of the charge of aluminum in tetrahedral coordination, which corresponds to stronger binding of Na^+ and K^+ and promotes increase of thermal and chemical stability of matrix materials based on such glasses.

We are grateful for financial support of RFBR (grant No 14–08–00323–a).

References

1. Du L.-S., Stebbins J.F. J. Solid-state NMR Study of Metastable Immiscibility in Alkali Borosilicate Glasses. *Journal of Non-Crystalline Solids,* 2003, V. 315, pp. 239–255.

2. Eremyashev V.E., Shabunina L.A. [Influence of R and K Parameters on Anionic Sructure of Alkaline Borosilicate Glasses]. *Bulletin of South Ural State University. Ser. Chemistry*, 2011, vol. 6 (33), pp. 68–72. (in Russ.)

3. MacKenzie J.W., Bhatnagar A., Bain D., Bhowmik S., Parameswar C., Budhwani K., Feller S.A., Royle M.L., Martin S.W. ^{29}Si MAS-NMR Study of the Short Range Order in Alkali Borosilicate Glasses. *Journal of Non-Crystalline Solids*, 1994, vol. 177, no. 2, pp. 269–276.

4. Roderick J.M., Holland D., Howes A.P., and Scales C.R. Density–Structure Relations in Mixed-Alkali Borosilicate Glasses by ^{29}Si and ^{11}B MAS–NMR. *Journal of Non-Crystalline Solids*, 2001, vol. 293–295, pp. 746–751.

5. Mysen B. O. Structural Behavior of Al^{3+} in Silicate Melts: In Situ, High-Temperature Measurements as a Function of Bulk Chemical Composition. *Geochimica et Cosmochimica Acta*, 1995, vol. 59, no. 3, pp. 455–474.

6. Eremyashev V.E., Osipov A.A., Volkov A.U., Bykov V.N. [Structure of Aluminosilicate Glasses and Melts of $NaAlSi_3O_8$-$Na_2Si_2O_5$ according to RAMAN data]. *Rasplavy* [Melts], 2004, no. 3, pp. 92–96. (in Russ.)

7. Eremyashev V.E., Osipov A.A., Bykov V.N. [Structure of Aluminosilicate Glasses and Melts of $KAlSi_3O_8$-$K_2Si_2O_5$ according to RAMAN data]. *Rasplavy* [Melts], 2005, no. 4, pp. 93–95. (in Russ.)

8. Stebbins J., Wu J., Thompson L. Interaction between Network Cation Coordination and Non-Bridging Oxygen Abundance in Oxide Glasses and Melts: Insights from NMR Spectroscopy. *Chemical Geology*, 2013, vol. 346, pp. 34–46.

9. Eremyashev V.E., Osipov A.A., Osipova L.M. Borosilicate Glass Structure with Rate-Earth-Metal Cations Substituted for Sodium Cations. *Glass and ceramics*, 2011, vol. 68, iss. 7–8, pp. 205–208.

10. El-Egili K. Infrared Studies of Na_2O–B_2O_3–SiO_2 and Al_2O_3–Na_2O–B_2O_3–SiO_2 Glasses. Physica B, 2003, vol. 325, pp. 340–348.

11. Wan J., Cheng J., Lu P. The Coordination State of B and Al of Borosilicate Glass by IR Spectra. *Journal of Wuhan University of Technology Mater*, 2008, vol. 23, no 3, pp. 419–421.

12. Xiu T., Liu Q., Wang J. Alkali–Free Borosilicate Glasses with Wormhole–Like Mesopores. *J. Mater. Chem*., 2006, no. 16, pp. 4022–4024.

13. Furukawa T., White W. Raman Spectroscopic Investigation of Sodium Borosilicate Glass Structure. *Journal of Materials Science*, 1981, vol. 16, no. 10, pp. 2689–2700.

14. Manara D., Grandjean A., Neuville D. R. Advances in Understanding the Structure of Borosilicate Glasses: A Raman Spectroscopy Study. *American Mineralogist*, 2009, vol. 94, no. 5–6, pp. 777–784.

15. McMillan P. Structural Studies of Silicate Glasses and Melts-Applications and Limitations of Raman Spectroscopy. *American Mineralogist*, 1984, vol. 69, pp. 622–644.

Received 1 February 2015

УДК 544.23+666.11

СПЕКТРОСКОПИЧЕСКОЕ ИССЛЕДОВАНИЕ ВЛИЯНИЯ ДОБАВОК АЛЮМИНИЯ НА СТРУКТУРНЫЕ ОСОБЕННОСТИ ЩЕЛОЧНЫХ БОРОСИЛИКАТНЫХ СТЕКОЛ

В.Е. Еремяшев[1], Г.Г. Кориневская[2], Р.Р. Айсин [3]

[1] Южно-Уральский государственный университет, филиал в г. Златоусте,

[2] Институт минералогии УрО РАН, г. Миасс,

[3] Институт элементоорганических соединений им. А.Н. Несмеянова РАН (ИНЭОС РАН), г. Москва

Методами колебательной спектроскопии изучено влияние алюминия на структуру щелочных боросиликатных стекол с разным соотношением катионов-сеткообразователей и катионов-модификаторов. Установлено, что при добавлении небольшого количества алюминия в состав стекол происходит уменьшение различия в распределении натрия и калия между боратными и силикатными составляющими структуры боросиликатных стекол. Это позволяет рассматривать алюминий в качестве добавки, способствующей увеличению однородности боросиликатных стекол, одновременно содержащих натрий и калий, и повышению термической и химической устойчивости матричных материалов, создаваемых на основе этих стекол.

Keywords: боросиликатные стекла, спектроскопия, структура, алюминий

Литература

1. Du, L.-S. Solid-state NMR study of metastable immiscibility in alkali borosilicate glasses / L.-S. Du, J.F. J. Stebbins // Journal of Non-Crystalline Solids. – 2003. – V. 315. – P. 239–255.

2. Еремяшев, В.Е. Влияние параметров R и K на особенности анионной структуры щелочных боросиликатных стекол / В.Е. Еремяшев, Л.А. Шабунина // Вестник ЮУрГУ. Серия «Химия». – 2011. – №6 (33). – С. 68–72.

3. ^{29}Si MAS-NMR study of the short range order in alkali borosilicate glasses / J.W. MacKenzie, A. Bhatnagar, D. Bain, S. Bhowmik, C. Parameswar, K. Budhwani, S.A. Feller, M.L Royle, S.W. Martin // Journal of Non-Crystalline Solids. – 1994. – V. 177. – № 2. – P. 269–276.

4. Density–structure relations in mixed-alkali borosilicate glasses by ^{29}Si and ^{11}B MAS–NMR / J.M. Roderick, D. Holland, A.P. Howes, C.R. Scales // Journal Non-Crystalline Solids. – 2001. – V. 293–295. – P. 746–751.

5. Mysen, B.O. Structural behavior of Al^{3+} in silicate melts: In situ, high-temperature measurements as a function of bulk chemical composition / B.O. Mysen // Geochimica et Cosmochica Acta. – 1995. – V. 59. – № 3. – P. 455–474.

6. Структура алюмосиликатных стекол и расплавов разреза $NaAlSi_3O_8$-$Na_2Si_2O_5$ по данным спектроскопии комбинационного рассеяния / В.Е. Еремяшев, А.А. Осипов, А.Ю. Волков, В.Н. Быков // Расплавы. – 2004. – № 3. – С. 92–96.

7. Еремяшев, В.Е. Структура алюмосиликатных стекол и расплавов разреза $KAlSi_3O_8$-$K_2Si_2O_5$ по данным спектроскопии комбинационного рассеяния / В.Е. Еремяшев, А.А. Осипов, В.Н. Быков // Расплавы. – 2005. – № 4. – С. 93–95.

8. Еремяшев, В.Е. Изучение влияния замещения катиона натрия катионами щелочноземельных металлов на структуру боросиликатных стекол / В.Е. Еремяшев, А.А. Осипов, Л.М. Осипова // Стекло и керамика. – 2011. – № 7. – С. 3–6.

9. Stebbins, J. Interaction between network cation coordination and non-bridging oxygen abundance in oxide glasses and melts: Insights from NMR spectroscopy / J. Stebbins, J. Wu, L. Thompson // Chemical Geology. – 2013. – V. 346. – P. 34–46.

10. El-Egili, K. Infrared studies of Na_2O–B_2O_3–SiO_2 and Al_2O_3–Na_2O–B_2O_3–SiO_2 glasses / K. El-Egili // Physica B. – 2003. – V. 325. – P. 340–348.

11. Wan, J. The Coordination State of B and Al of Borosilicate Glass by IR Spectra / J. Wan, J. Cheng, P. Lu // Journal of Wuhan University of Technology Mater. – 2008. – V. 23. – № 3. – P. 419–421.

12. Xiu, T. Alkali–free borosilicate glasses with wormhole–like mesopores / T. Xiu, Q. Liu, J. Wang // J. Mater. Chem. – 2006. – № 16. – P. 4022–4024.

13. Furukawa, T. Raman spectroscopic investigation of sodium borosilicate glass structure / T. Furukawa, W. White // Journal of materials science. – 1981. – V. 16. – № 10. – P. 2689–2700.

14. Manara, D. Advances in understanding the structure of borosilicate glasses: A Raman spectroscopy study / D. Manara, A. Grandjean, D.R. Neuville // American Mineralogist. – 2009. – V. 94. – № 5–6. – P. 777–784.

15. McMillan, P. Structural studies of silicate glasses and melts-applications and limitations of Raman spectroscopy / P. McMillan // American Mineralogist. – 1984. – V. 69. – P. 622–644.

Еремяшев Вячеслав Евгеньевич – доктор химических наук, доцент, заведующий кафедрой физики, Южно-Уральский государственный университет, филиал в г. Златоусте. 456209, г. Златоуст, ул. Тургенева, 16. E-mail: vee-zlat@mail.ru

Кориневская Галина Геннадьевна – младший научный сотрудник, Институт минералогии УрО РАН. 456317, г. Миасс, Институт минералогии. E-mail: galkor@mineralogy.ru

Айсин Ринат Равильевич – кандидат химических наук, научный сотрудник, Институт элементоорганических соединений им. А.Н. Несмеянова РАН (ИНЭОС РАН). 119991, ГСП-1, Москва, В-334, ул. Вавилова, 28. E-mail: aysin.rinat@gmail.com.

Поступила в редакцию 1 февраля 2015 г.

ОБРАЗЕЦ ЦИТИРОВАНИЯ

Eremyashev, V.E. Spectroscopic investigation of the influence of aluminum addition on characteristic features of alkali borosilicate glasses / V.E. Eremyashev, G.G. Korinevskaya, R.R. Aysin // Вестник ЮУрГУ. Серия «Химия». – 2015. – Т. 7, № 3. – С. 46–52.

FOR CITATION

Eremyashev V.E., Korinevskaya G.G., Aysin R.R. Spectroscopic Investigation of the Influence of Aluminum Addition on Characteristic Features of Alkali Borosilicate Glasses. *Bulletin of the South Ural State University. Ser. Chemistry.* 2015, vol. 7, no. 3, pp. 46–52.

THEORETICAL STUDY OF THE THERMODYNAMIC AND KINETIC FACTORS INFLUENCE ON NANOSIZED TITANIUM DIOXIDE PARTICLES GROWTH FEATURES

M.A. Grishina, *South Ural State Medical University, Chelyabinsk, Russian Federation, pvapva2006@yandex.ru*
A.V. Potemkin, *Saint Petersburg National Research University of Information Technologies, Mechanics and Optics, Saint Petersburg, Russian Federation,appanpotemkin@gmail.com*
O.I. Bolshakov, *South Ural State University, Chelyabinsk, Russian Federation, bolshakovoi@susu.ru*
V.A. Potemkin, *South Ural State Medical University, Chelyabinsk, Russian Federation, pva@csu.ru*

A theoretical study of the crystal lattice of titanium dioxide (anatase), its spatial and thermodynamic characteristics, face growth characteristics and ways of formation of its macromolecular structures is performed. It is shown that the growth along c axis of the crystal is more favorable thermodynamically. The variants for controlling of the growth of various faces by introducing of the acidic and basic components, as well as by temperature changes are proposed.

Keywords: titanium dioxide, anatase, nanostructure, thermodynamic calculations, kinetic features.

Introduction

Nanocrystalline titanium dioxide is widespread photocatalyst for destruction of organic pollutants [1], a semiconductor in solar cells [2], a component of ceramic, composite, catalytic [3] and sorption materials [4], because of its efficiency, low cost, non-toxicity, photo- and thermal stability. Frequently nanocrystalline titanium oxide used as the photocatalyst, because of its ability to form part of a pair of "electron – hole" under the UV and visible light radiation. The effectiveness of photocatalysts based on nanocrystalline titanium dioxide is determined by many factors, such as phase content, the morphology features, the specific surface area, the pore volume, the presence of dopant additives [5]. All of the above mentioned characteristics of the material are formed by the processes of hydrolytic or non-hydrolytic decomposition of TiO_2 precursors and templating agents used in the synthetic processes. Currently, a lot of technique allows to obtain photocatalysts with specified properties using a sol-gel or hydrothermal synthesis. However, most of the known methods for producing crystalline titanium oxides require high temperatures or pressures for crystallization of the amorphous precursor into the desired crystalline modification. Preparation of nanocrystalline titanium dioxide under mild conditions at a temperature close to room temperature is an important problem, the solution of which will significantly reduce the cost of production of functional materials. A way for the achievement this goal is the usage of biomineralizing agents in the synthesis of titanium dioxide that allow both to obtain crystalline titanium dioxide under mild conditions, and to control its crystalline structure, and particles sizes. An important advantage of biomineralization, along with the "ecology and economy", is unequivalent or "quasi-catalytic" nature of the process, i.e. the process does not require the equivalent amounts of template. In addition to the importance of the applied research of the crystalline phase of the titanium oxide formation, the problem of the general features determining the formation of metal oxide materials is fundamentally important. A lot of quantum DFT and *ab initio* calculations of the titanium dioxide, ranging from small particles of TiO_2, to large enough nanoclusters such as $Ti_{428}O_{856}$, for example, [6–8], was performed. But so far, a little is known on the specific ways of macromolecular structures (phases) of the titanium oxide formation, on the hydrolysis of oligomeric intermediates, as well as the on the mechanism of formation of oligomeric intermediates themselves [9, 10]. Determination of the mechanism, identification of intermediates of structure formation processes, definition of the dependence between the structure of the template and the parameters of nanocrystalline TiO_2 will create new ways for the effective control of the formation of titanium oxide nanostructures, which will allow to increase the characteristics of existing materials and yield in principally new functional materials. Therefore, the aim of this work is a

theoretical study of the crystal lattice of titanium dioxide (anatase), its spatial and thermodynamic characteristics, face growth characteristics and pathways of formation of its macromolecular structures.

Research Methodology

The crystal structure of anatase was used for the study. X-ray diffraction data for the anatase lattice was taken from [11] and Crystallography Open Database (http://www.crystallography.net/ ID 9015929). The crystal system of anatase is tetragonal, the space group is I41/amd, unit cell parameters are $a = b = 3.7845$ Å; $c = 9.5143$ Å; $\alpha = \beta = \gamma = 90°$. The cell volume is 136.268 Å^3, ideal crystal density is 3.894 g/cm3. The cell contains two formula units of titanium dioxide.

The investigation of the titanium dioxide was performed within MERA force field [12–22] beginning from one unit cell (cluster formula $Ti_{29}O_{58}$) to 30 unit cells, propagated along the *a* and *c* axes of the crystal (cluster formula $Ti_{870}O_{1740}$). In the framework of this approach the potential energy of interactions in the system is the sum of intra- and intermolecular Coulomb and Van der Waals interactions. Energy of intra- and intermolecular electrostatic interactions are calculated by the usual formula of Coulomb's law. The energy of intermolecular van der Waals interactions is calculated using the Lennard-Jones equation

$$E_V = \sum_{i=1}^{N} \sum_{j=i+1}^{N} \left(-2U_{ij} \left(\frac{R_{ij}^e}{R_{ij}} \right)^6 + U_{ij} \left(\frac{R_{ij}^e}{R_{ij}} \right)^{12} \right).$$

R_{ij}^e is the equilibrium distance of the van der Waals contact of the *i* and *j* atoms, equal to the sum of their van der Waals radii calculated within the MERA model;
R_{ij} is the actual distance between the *i* and *j* atoms.
U_{ij} value corresponds to the minimum of potential energy of interaction between atoms *i* and *j* and can be calculated within the MERA model in accordance with the following formula

$$U_{ij} = \frac{7kR_{ij}^e}{48\alpha},$$

α – a constant equal to $6.662 \cdot 10^{-14}$ м/К;
k – the Boltzmann constant.

The energy of the intermolecular van der Waals interactions and hydrogen bonds is calculated as follows

$$E_{VI} = \sum_{i=1}^{M} \sum_{j=1}^{M} p_{ij} \left(-2U_{ij} R_{ij}^{e^6} \left(\frac{1}{(R_{ij}+ka)^6} + \frac{1}{(R_{ij}+kb)^6} + \frac{1}{(R_{ij}+kc)^6} \right) + U_{ij} R_{ij}^{e^{12}} \left(\frac{1}{(R_{ij}+ka)^{12}} + \frac{1}{(R_{ij}+kb)^{12}} + \frac{1}{(R_{ij}+kc)^{12}} \right) \right),$$

a, *b*, *c* – the unit cell parameters;
k – integers 0, 1, 2, 3, …

The calculation of the thermodynamic characteristics of the anatase crystal lattice was fulfilled using the MERA model by the scheme shown in [14, 20, 21]. The calculation of atomic charges, as well as the value of the charged surface was carried out within the framework of the full equalization of the orbital electronegativity formalism [23] in the modification of the model MERA [13]. The calculation of the electronegativity of crystals was performed the J. Gasteiger scheme within the formalism of full equalization of the orbital electronegativity [23].

Discussion

Calculation which was fulfilled for the anatase unit cell showed the following: the portion of a charged cell surface, responsible for soption of polar molecules (e.g., amino acids or oligopeptides that can be used for hydrolytic decomposition method of TiO_2 precursors), is low enough. Its value is only 2.19 % of the unit cell total surface (the square is 3.78 Å^2). About 80 % of the surface belongs to the side faces of the cell and just over 20 % belongs to base faces. Thus, each side face possesses about 20% of the charged surface, whereas each base face possesses just over 10 %.

Modelling of the crystal lattice growth along the *a* axis showed the following: the thermal effect of the unit translation along the *a* axis is quite significant, the standard enthalpy is –2743 kJ/mole, the entropy increment is 584 kJ/mole·K, lowering of the standard Gibbs free energy is 2917 kJ/mole. Electro-

negativity of the crystal increases with the crystal growth along *a* axis by 0.41 eV per cell unit. Thus the strength of sorption sites with respect to the positively charged hydrogens of carboxylic and ammonium groups of oligopeptides (which may be used in the synthesis of titanium dioxide nanosized particles). It should be noted that the electronegativity growth is nonlinear. The dependency represents a saturation curve (Fig. 1) and can be approximated by the following equation

$$\chi = 6.52 + \frac{3.025n}{1.671 + n},$$

χ – electronegativity of crystal eV;
n – the number of cells along the *a* axis.

Analyzing the equation, it is obvious, that the electronegativity can achieve the value 9.54 eV at the saturation. A 50 % degree of completion of the saturation process will be achieved when the number of cells will achieve n = 3. A 90 % degree of completion of the saturation process will be achieved when the number of cells will achieve n = 17. Since the length of the *a* axis is 3.7845 Å, the linear length of 17 unit cells equals 64.34 Å, or 6,434 nm, which will be the minimum size of the crystals at the equilibrium sorption of polar components.

Modelling of the crystal lattice growth along the *c* axis showed the following: the thermal effect when the unit translation along the *c* axis even greater than for the growth along *a* axis and – the standard enthalpy is –3482 kJ/mole, the increase of entropy is also significantly higher it equals 869 kJ/mole·K, lowering of the standard Gibbs free energy also greater and amounts to 3741 kJ/mole. Thus, the crystal growth along the *c* axis is more favorable than along the *a* or *b* axes under thermodynamic conditions. However, the number of side faces is twice greater than the base faces perpendicular to *c* axis.

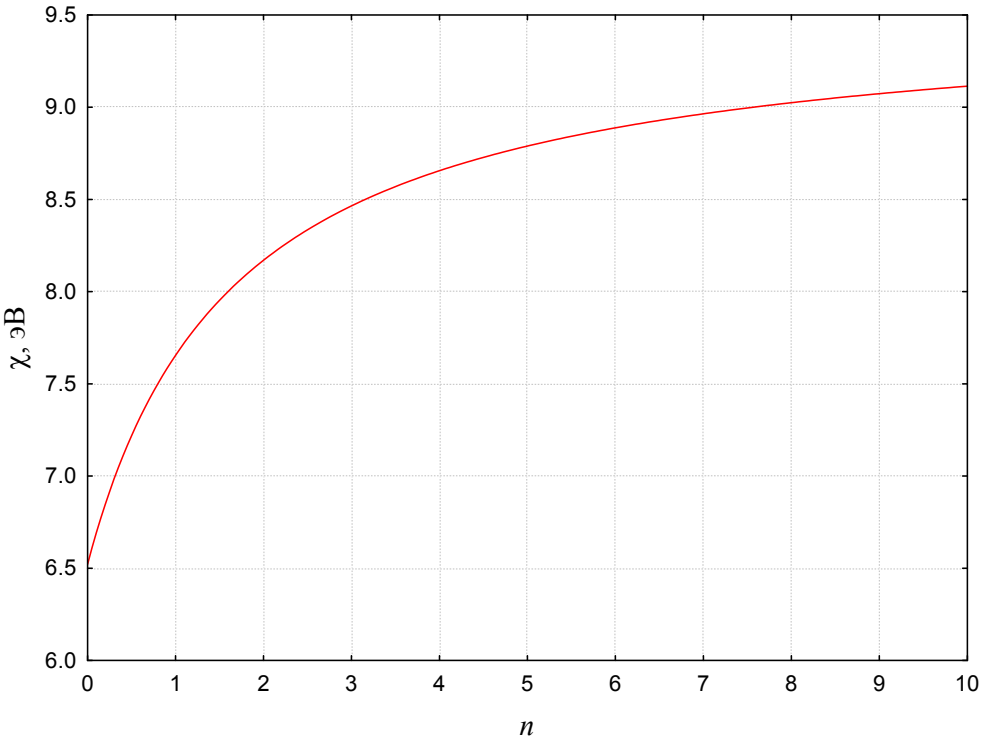

Fig. 1. The dependency of the crystal electronegativity on the number of unit cells along the *a* axis

Electronegativity of the crystal increases with growth along the *c* axis but its increment is almost twice less than for the growth along *a* axis: the increment is 0.22 eV per unit. The further electronegativity growth is nonlinear and dependency also represents a saturation curve (Fig. 2). It can be approximated using the following formula

$$\chi = 6.86 + \frac{1.6925n}{1.134 + n},$$

n – the number of unit cells along the *c* axis.

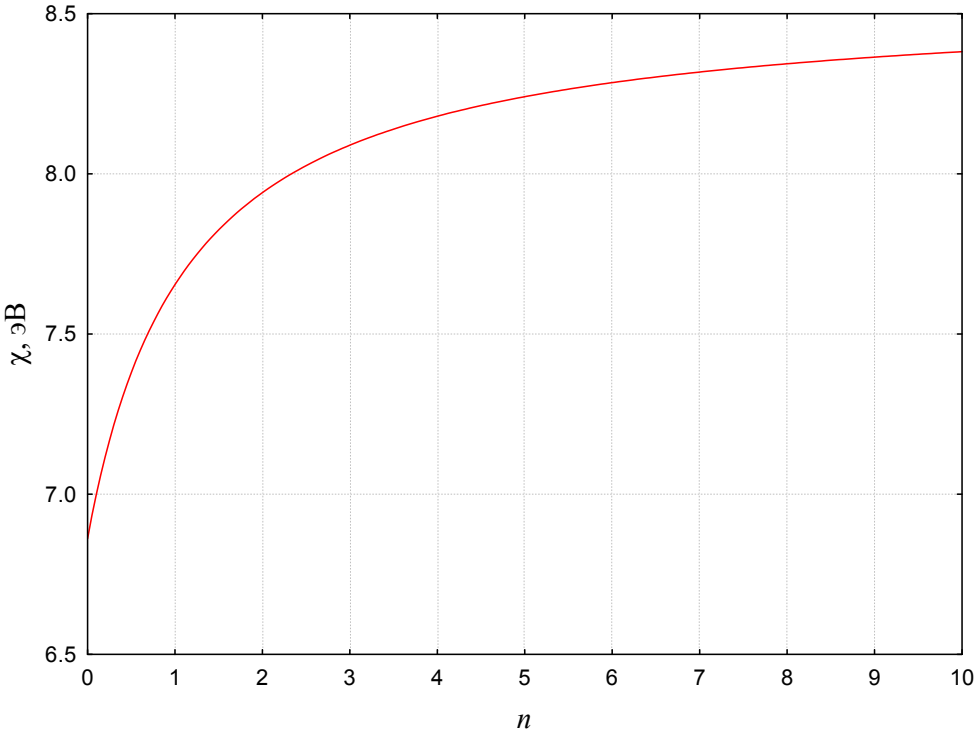

Fig. 2. The dependency of the crystal electronegativity on the number of unit cells along the *c* axis

Analyzing the equation, it is obvious, that the electronegativity can achieve the value 8.55 eV, which is less than the growth along the *a* axis by almost one. A 50 % degree of completion of the saturation process will be achieved when the number of cells will achieve $n = 4$. A 90 % degree of completion of the saturation process will be achieved when the number of cells will achieve $n = 12$. Since the length of the *c* axis is 9.5143 Å, the linear length of the 12 unit cells equals 114.17 Å, or 11.417 nm, which will be the minimum size of the crystals at the equilibrium sorption of polar components.

A comparison of anatase crystal growth along the *a* and *c* axes shows that the more thermodynamically favorable is a growth along *c* axis, which must provide a crystal habit elongated along *c* axis. However, when a doubling of unit cell along *c* axis leads to a doubling of the free energy of the growth along *a* axis. So, the next step provides adding a layer of unit cells along *a* direction. Thus, the ratio of the size of the crystal during the growth under ideal thermodynamic conditions should be the ratio of the free energies of growth, i.e.

$$a : c = b : c = 2917 : 3741.$$

It is possible to make changes into this ratio in any direction under kinetic conditions. Since the electronegativity of the crystal during the growth along the *a* axis increases much stronger than during the growth along the *c* axis, the insertion components with the positively charged fragments, such as acids or conjugated acids (for example, consisting of ammonia or carboxylic group) should accelerate the growth along the *a* axis and yielding smaller particles (from 6.434 nm); the insertion of the conjugate bases or bases should accelerate growth along the *c* axis and yielding larger particles (from 11.417 nm). It is well confirmed by the data of [24], where the sorption of neutral, acidic and basic amino acids on titanium dioxide is elucidated. Since the entropy factor favors the growth along the *c*, the growth in this direction will increase with the temperature increase; a reducing of the temperature will be favorable to growth in the direction *a*. In both cases possible to obtain nanosized titanium dioxide particles.

Conclusion

Some thermodynamic and kinetic factors on the growth characteristics of nanoscale titanium dioxide particles are studied in the work. The conditions providing larger and smaller particles with higher

and lower sorption capacity for acidic and basic peptides within hydrolytic decomposition method of titanium dioxide precursors are offered.

Acknowledgements
The reported study was funded by RFBR according to the research project № 15-03-07834-a.

References

1. Macwan D.P., Dave P.N., Chaturvedi S. A Review on Nano-TiO_2 Sol–Gel Type Syntheses and its Applications. *Journal of Materials Science*, 2011, vol. 46, no. 11, pp. 3669–3686.

2. Yum J.H., Lee J.W., Kim Y., Humphry-Baker R., Park N.G., Graetzel M. Panchromatic Light Harvesting by Dye- and Quantum Dot-Sensitized Solar Cells. *Solar Energy*, 2014, vol. 109, pp. 183–188.

3. Tachikawa T., Yamashita S., Majima T. Evidence for Crystal-Face-Dependent TiO_2 Photocatalysis from Single-Molecule Imaging and Kinetic Analysis. *J. Am. Chem. Soc.*, 2011, vol. 133, pp. 7197–7204.

4. Thomas A.G., Syres K.L. Adsorption of Organic Molecules on Rutile TiO_2 and Anatase TiO_2 Single Crystal Surfaces. *Chem. Soc. Rev.*, 2012, vol. 41, pp. 4207–4217.

5. Henderson M.A., Lyubinetsky I. Molecular-Level Insights into Photocatalysis from Scanning Probe Microscopy Studies on TiO_2(110). *Chem. Rev.*, 2013, vol. 113, no. 6. pp. 4428–4455.

6. Lundqvist M.J., Nilsing M., Persson P., Lunell S. DFT Study of Bare and Dye-Sensitized TiO_2 Clusters and Nanocrystals. *Int. J. Quant. Chem*., 2006, vol. 106, no. 15, pp. 3214–3234.

7. Vittadini A., Casarin M., Selloni A. Chemistry of and on TiO_2-Anatase Surfaces by DFT Calculations: a Partial Review. *Theor. Chem. Acc.*, 2007, vol. 117, no. 5–6, pp. 663–671.

8. Andreev A.S., Kuznetsov V.N., Chizhov Yu.V. Atomic Hydrogen Activated TiO_2 Nanocluster: DFT Calculations. *J. Phys. Chem. C*, 2012, vol. 116, no. 34, pp. 18139–18145.

9. Benedict J.B., Freindorf R., Trzop E., Cogswell J., Coppens P. Large Polyoxotitanate Clusters: Well-Defined Models for Pure-Phase TiO_2 Structures and Surfaces. *J. Am. Chem. Soc.*, 2010, vol. 132, pp. 13669–13671.

10. Seisenbaeva G.A., Daniel G., Nedelec J.M., Kessler V.G. Solution Equilibrium behind the Room-Temperature Synthesis of Nanocrystalline Titanium Dioxide. *Nanoscale*, 2013, vol. 5, pp. 3330–3336.

11. Howard C.J., Sabine T.M., Dickson, F. Structural and Thermal Parameters for Rutile and Anatase. *Acta Crystallographica. Section B*, 1991, vol. 47, pp. 462–468.

12. Potemkin V.A., Bartashevich E.V., Belik A.V. [New Representation of Spatial Shape of Molecules]. *Zhurnal Obshei Khimii* [Russian Journal of General Chemistry], 1995, vol. 65, no. 2, pp. 205–208. (in Russ.)

13. Potemkin V.A., Bartashevich E.V., Belik A.V. [Calculation of Atomic Radii Adjusted for Electrostatic Interactions]. *Zhurnal Physicheskoi Khimii* [Russian Journal of Physical Chemistry], 1995, vol. 69, no. 1, pp. 106–109. (in Russ.)

14. Potemkin V.A., Bartashevich E.V., Belik A.V. [A New Approach to Predicting the Thermodynamic Parameters of Substances from Molecular Characteristics]. *Zhurnal Physicheskoi Khimii* [Russian Journal of Physical Chemistry], 1996, vol. 70, no. 3, pp. 411–416. (in Russ.)

15. Potemkin V.A., Bartashevich E.V., Belik A.V. [A Model for Calculation of Atomic Volume Characteristics in Molecular Systems]. *Russkii Zhurnal Physicheskoi Khimii* [Russian Journal of Physical Chemistry], 1998, vol. 72, no. 4, pp. 650–656. (in Russ.)

16. Bartashevich E.V., Potemkin V.A., Grishina M.A., Belik A.V. A Method for Multiconformational Modeling of the Three-Dimensional Shape of a Molecule. *J. Struct. Chem.*, vol. 43, no. 6, pp. 1033–1039.

17. Grishina M.A., Bartashevich E.V., Potemkin V.A., Belik A.V. Genetic Algorithm for Predicting Structures and Properties of Molecular Aggregates in Organic Substances. *J. Struct. Chem.*, vol. 43, no. 6, pp. 1040–1044.

18. Potemkin V.A., Sukharev Yu.I. Formation of Liotropic Features of Zirconium Oxyhydrate Gels. *Chem. Phys. Lett.*, 2003, vol. 371, pp. 626–633.

19. Potemkin V.A., Maksakov V.A., Kirin V.P. Conformational States of Triosmium Clusters with Aminoacid Ligands: A Theoretical Study. *J. Struct. Chem.*, vol. 44, no. 5, pp. 741–747.

20. Aladko E.Ya., Ancharov A.I., Goryainov S.V., et al. New Type of Phase Transformation in Gas Hydrate Forming System at High Pressures. Some Experimental and Computational Investigations of Clathrate Hydrates Formed in the SF_6-H_2O. *J. Phys. Chem. B*, 2006, vol. 110, no. 42, pp. 21371–21376.

21. Potemkin V.A., Ivshina N.N., Maksakov V.A. Theoretical study of the conformational features of triosmium clusters. *J. Struct. Chem.*, vol. 50, no. 1, pp. 143–151.

22. Manakov A.Yu., Likhacheva A.Yu., Potemkin V.A. et al Compressibility of Gas Hydrates// *Chem. Phys. Chem*, 2011, vol. 12, no. 13, pp. 2476–2484.

23. Mortier W.J., Van Genechten K., Gasteiger J. Electronegativity Equalization: Application and Parametrization. *J. Am. Chem. Soc.*, 1985, vol. 107, pp. 829–835.

24. Okazaki S., Aoki T., Tani K. The Adsorption of Basic Alpha-Amino-Acids in an Aqueous-Solution by Titanium (IV) Oxide. *Bull. Chem. Soc. Jpn.*, 1981, vol. 54, pp. 1595–1599.

Received 16 May 2015

УДК 541.64:541.66:548.523

ТЕОРЕТИЧЕСКОЕ ИССЛЕДОВАНИЕ ВЛИЯНИЯ РЯДА ТЕРМОДИНАМИЧЕСКИХ И КИНЕТИЧЕСКИХ ФАКТОРОВ НА ОСОБЕННОСТИ РОСТА НАНОРАЗМЕРНЫХ ЧАСТИЦ ДВУОКИСИ ТИТАНА

М.А. Гришина[1], А.В. Потемкин[2], О.И. Большаков[3], В.А. Потемкин[1]

[1] Южно-Уральский государственный медицинский университет, г. Челябинск,

[2] Санкт-Петербургский национальный исследовательский университет информационных технологий, механики и оптики, г. Санкт-Петербург,

[3] Южно-Уральский государственный университет, г. Челябинск

Проведено теоретическое исследование кристаллической решетки диоксида титана (анатаза), его пространственных и термодинамических характеристик, особенностей роста граней и путей формирования его макромолекулярных структур. Показано, что термодинамически более благоприятным является рост вдоль направления с кристалла. Предложены варианты управления ростом тех или иных граней путем введения кислотных и основных компонентов, а также посредством изменения температуры.

Ключевые слова: диоксид титана, анатаз, наноструктура, термодинамические расчеты, кинетические особенности.

Литература

1. Macwan, D.P. Review on Nano-TiO_2 Sol–Gel Type Syntheses and its Applications / D.P. Macwan, P.N. Dave, S. Chaturvedi // Journal of Materials Science. – 2011. – Vol. 46. – No. 11. – P. 3669–3686.

2. Panchromatic Light Harvesting by Dye- and Quantum Dot-Sensitized Solar Cells / J.H. Yum, J.W. Lee, Y. Kim et al. // Solar Energy. – 2014. – Vol. 109. – P. 183–188.

3. Tachikawa, T. Evidence for Crystal-Face-Dependent TiO_2 Photocatalysis from Single-Molecule Imaging and Kinetic Analysis / T. Tachikawa, S. Yamashita, T. Majima // Journal of the American Chemical Society. – 2011. – Vol. 133. – P. 7197–7204.

4. Thomas, A.G. Adsorption of Organic Molecules on Rutile TiO_2 and Anatase TiO_2 Single Crystal Surfaces / A.G. Thomas, K.L. Syres // Chemical Society Reviews. – 2012. – Vol. 41. – P. 4207–4217.

5. Henderson, M.A. Molecular-Level Insights into Photocatalysis from Scanning Probe Microscopy Studies on TiO_2(110) / M.A. Henderson, I. Lyubinetsky // Chemical Reviews. – 2013. – Vol. 113. – No. 6. – P. 4428–4455.

6. DFT Study of Bare and Dye-Sensitized TiO_2 Clusters and Nanocrystals / M.J. Lundqvist, M. Nilsing, P. Persson et al. // International Journal of Quantum Chemistry. – 2013. – Vol. 106. – No. 15. – P. 3214–3234.

7. Vittadini, A. Chemistry of and on TiO_2-Anatase Surfaces by DFT Calculations: a Partial Review / A. Vittadini, M. Casarin, A. Selloni // Theoretical Chemistry Accounts. – 2007. – Vol. 117. – No. 5–6. – P. 663–671.

8. Andreev, A.S. Atomic Hydrogen Activated TiO_2Nanocluster: DFT Calculations /A.S. Andreev, V.N. Kuznetsov, Yu.V. Chizhov // The Journal of Physical Chemistry C. – 2012. – Vol. 116. – No. 34. – P. 18139–18145.

9. Large Polyoxotitanate Clusters: Well-Defined Models for Pure-Phase TiO_2 Structures and Surfaces / J.B. Benedict, R. Freindorf, E. Trzop et al. // Journal of the American Chemical Society. – 2010. – Vol. 132. – P. 13669–13671.

10. Seisenbaeva, G.A. Solution Equilibrium behind the Room-Temperature Synthesis of Nanocrystalline Titanium Dioxide / G.A. Seisenbaeva, G. Daniel, J.M. Nedelecet et al. // Nanoscale. – 2013. – Vol. 5. – P. 3330–3336.

11. Howard, C.J. Structural and Thermal Parameters for Rutile and Anatase/ C.J. Howard, T.M. Sabine, F. Dickson // Acta Crystallographica. Section B. – 1991. – Vol. 47. – P. 462–468.

12. Потемкин, В.А. Новые представления об объемной форме молекул / В.А. Потемкин, Е.В. Барташевич, А.В. Белик // Журн. общ. химии. – 1995. – Т. 65. – № 2. – С. 205–208.

13. Потемкин, В.А. Расчет атомных радиусов с поправкой на электростатические взаимодействия / В.А. Потемкин, Е.В. Барташевич, А.В. Белик // Журн. физ. химии. – 1995. – Т. 69. – № 1. – С. 106–109.

14. Потемкин, В.А., Новые подходы к прогнозу термодинамических параметров веществ по молекулярным данным / В.А. Потемкин, Е.В. Барташевич, А.В. Белик // Журн. физ. химии. – 1996. – Т. 70. – № 3. – С. 448–452.

15. Потемкин, В.А. Модель расчета атомных объемных характеристик в молекулярных системах./ В.А. Потемкин, Е.В. Барташевич, А.В. Белик // Журн. физ. химии. – 1998. – Т. 72. – № 4. – С. 650–656.

16. A Method for Multiconformational Modeling of the Three-Dimensional Shape of a Molecule / E.V. Bartashevich, V.A. Potemkin, M.A. Grishinaet al. // Journal of Structural Chemistry. – 2002. – Vol. 43. – No. 6. – P. 1033–1039.

17. Genetic Algorithm for Predicting Structures and Properties of Molecular Aggregates in Organic Substances / M.A. Grishina, E.V. Bartashevich, V.A. Potemkin et al. // Journal of Structural Chemistry. – 2002. – Vol. 43. – No. 6. – P. 1040–1044.

18. Potemkin, V.A. Formation of Liotropic Features of Zirconium Oxyhydrate Gels / V.A. Potemkin, Yu.I. Sukharev // Chemical Physics Letters. – 2003. – Vol. 371. – P. 626–633.

19. Potemkin, V.A. Conformational States of Triosmium Clusters with Aminoacid Ligands: A Theoretical Study / V.A. Potemkin, V.A. Maksakov, V.P. Kirin // Journal of Structural Chemistry. – 2003. – Vol. 44. – No. 5. – P. 741–747.

20. New Type of Phase Transformation in Gas Hydrate Forming System at High Pressures. Some Experimental and Computational Investigations of Clathrate Hydrates Formed in the SF_6-H_2O / E.Ya. Aladko, A.I. Ancharov, S.V. Goryainov et al. // The Journal of Physical Chemistry B. – 2006. – Vol. 110. – No. 42. – P. 21371–21376.

21. Potemkin, V.A. Theoretical study of the conformational features of triosmium clusters / V.A. Potemkin, N.N. Ivshina, V.A. Maksakov // Journal of Structural Chemistry. – Vol. 50. – No. 1. – P. 143–151.

22. Compressibility of Gas Hydrates / A.Yu. Manakov, A.Yu. Likhacheva, V.A. Potemkin et al. // ChemPhysChem. – 2011. – Vol. 12. – No. 13. – P. 2476–2484.

23. Mortier, W.J. Electronegativity Equalization: Application and Parametrization / W.J. Mortier, K.Van Genechten, J. Gasteiger // Journal of the American Chemical Society. – 1985. – Vol. 107. – P. 829–835.

24. Okazaki, S. The Adsorption of Basic Alpha-Amino-Acids in an Aqueous-Solution by Titanium (IV) Oxide / S. Okazaki, T. Aoki, K. Tani // Bulletin of the Chemical Society of Japan. – 1981. – Vol. 54. – P. 1595–1599.

Гришина Мария Александровна – доктор химических наук, доцент, Южно-Уральский государственный медицинский университет, г. Челябинск. E-mail: pvapva2006@yandex.ru

Потемкин Андрей Владимирович – студент, Санкт-Петербургский национальный исследовательский университет информационных технологий, механики и оптики, г. Санкт-Петербург. E-mail: appanpotemkin@gmail.com

Большаков Олег Игоревич – докторант, кандидат химических наук, Южно-Уральский государственный университет, г. Челябинск. E-mail: bolshakovoi@susu.ru

Потемкин Владимир Александрович – доцент, кандидат химических наук, Южно-Уральский государственный медицинский университет, г. Челябинск. E-mail: pva@csu.ru.

Поступила в редакцию 16 мая 2015 г.

ОБРАЗЕЦ ЦИТИРОВАНИЯ

Theoretical study of the thermodynamic and kinetic factors influence on nanosized titanium dioxide particles growth features / M.A. Grishina, A.V. Potemkin, O.I. Bolshakov, V.A. Potemkin // Вестник ЮУрГУ. Серия «Химия». – 2015. – Т. 7, № 3. – С. 53–60.

FOR CITATION

Grishina M.A., Potemkin A.V., Bolshakov O.I., Potemkin V.A. Theoretical Study of the Thermodynamic and Kinetic Factors Influence on Nanosized Titanium Dioxide Particles Growth Features. *Bulletin of the South Ural State University. Ser. Chemistry.* 2015, vol. 7, no. 3, pp. 53–60.

Химия элементоорганических соединений

SYNTHESIS OF TRIPHENYLBISMUTH *BIS*(2-METHYLPROPENOATE)

V.A. Verkhovykh, *Lobachevsky State University of Nizhny Novgorod, Russian Federation, gushchin@chem.unn.ru*
O.S. Kalistratova, *Lobachevsky State University of Nizhny Novgorod, Russian Federation, olga.kalistratova@yandex.ru*
A.I. Grishina, *Lobachevsky State University of Nizhny Novgorod, Russian Federation, gushchin@chem.unn.ru*
V.G. Artemova, *Lobachevsky State University of Nizhny Novgorod, Russian Federation, decanat2005@yandex.ru*
A.V. Gushchin, *Lobachevsky State University of Nizhny Novgorod, Russian Federation, gushchin@chem.unn.ru*

Triphenylbismuth bis(2-methylpropenoate) $Ph_3Bi(O_2CMe{=}CH_2)_2$ has been obtained by the interaction of triphenylbismuth with methacrylic acid and hydrogen peroxide in tetrahydrofuran. Its structure has been determined by IR and ^1H NMR spectroscopy.

Keywords: triphenylbismuth bis(2-methylpropenoate), synthesis, structure, IR spectroscopy, NMR spectroscopy.

Introduction

Organometallic compounds of bismuth are the unique reagents in the arylation reactions of amines, alcohols, phenols, and glycols in the presence of catalytic amounts of copper, as well as unsaturated compounds under the catalytic action of palladium salts. Recently, chemistry of the metal-filled polymers, including bismuth-containing ones, develops intensively. Some known copolymers of various unsaturated bismuth compounds with organic monomers are already used for the synthesis of metal-containing polymers (including organic glasses) exhibiting the fungicidal and biocidal activity, X-ray protection properties [1]. For this reason the synthesis of new organic bismuth-containing compounds and their application as methylmethacrylate comonomers are important.

Methods for obtaining organobismuth compounds $Ph_3Bi(O_2CR)_2$ by the reaction of triphenylbismuth dihalides with silver, sodium and ammonium salts of carboxylic acids [2–4], triphenylbismuth carbonate with carboxylic acids [5], triphenylbismuth with carboxylic acids in the presence of benzoyl peroxide, H_2O_2, *t*-BuOOH [6], triphenylbismuth with anhydrides of carboxylic acids in the presence of *t*-BuOOH [7–11], triphenylbismuth with *tert*-butylperacetate and carboxylic acid [1], and triphenylbismuth with peracid [3] are known.

The aim of this work has been the synthesis of triphenylbismuth *bis*(2-methylpropenoate) by the reaction of triphenylbismuth with methacrylic acid and hydrogen peroxide. The presence of two methacrylate groups in the molecule can provide the use of the compound as a comonomer in the synthesis of a bismuth-containing polymer.

Experimental

Purification of solvents and reagents

Benzene, diethyl ether, tetrahydrofuran (THF) were dried over $CaCl_2$, distilled and stored over sodium. Chloroform was distilled, petroleum ether and bromobenzene were used without primary purification. Methacrylic acid was purified by sublimation.

Synthesis of triphenylbismuth

Triphenylbismuth was prepared by a modernized technique [2]. Magnesium chips (12 g, 0.5 mol), 100 mL THF and 50 mL benzene were placed in a one-liter three-necked flask equipped with a stirrer, reflux condenser and dropping funnel. Bromobenzene (52.5 mL) was added, and then the mixture was heated for 1 h in an air bath. In the end the mixture was cooled, the flask was filled with argon and left overnight. Then the mixture was heated for dissolving of Grignard reagent, the residual magnesium was

filtered through a wire filter. Solution of $BiCl_3$ (40 g, 0.13 mol) using benzene with THF (1:2) as solvent was added to the heated Grignard reagent. Then the reaction mixture was heated for 1 h in an air bath, then it was decomposed by 25 mL H_2O and 100 mL saturated NH_4Cl solution while cooling in a water bath. The top organic layer was dried by Na_2SO_4, the solvents were removed in a rotary evaporator at reduced pressure. The resultant triphenylbismuth had MP 76 ºC after purification by recrystallization from hot isopropyl alcohol, the product yield was 77 %.

Synthesis of triphenylbismuth bis(2-methylpropenoate) (**1**)

Methacrylic acid (1.27 mL, 15 mmol) was added to Ph_3Bi solution (2.2 g, 5 mmol) in 20 mL ether, then 2.5 mL 2.03 M anhydrous H_2O_2 solution in diethyl ether was added dropwise at cooling with cold water. The mixture was left at 5 °C for 38 h. The solution attained weak yellowish color; large crystals of product **1** were formed at the bottom of the flask. The solution was decanted from the precipitate, and the crystals were washed with 4 mL of ether. The product yield was 79 %, MP: 149 °C (literature data for the product obtained by the reaction of triphenylbismuth, *tert*-butylperoxide and methacrylic acid were 165 °C [1]).

The product was dissolved in 10 mL of warm freshly distilled chloroform for purification by recrystallization. Hexane (40 mL) was added in portions of 5 mL to the transparent solution. Fine-crystalline white precipitate was formed. For complete precipitation the solution was left in a refrigerator for 1.5 h. The product was filtered off by means of Shott filter, washed 2 times with 4 mL hexane, and then dried in the air. The product yield of compound **1** was 60 % (1.83 g), MP: 164 °C.

After recrystallization the product did not contain impurities of methacrylic acid and triphenylbismuth, which was determined by thin-layer chromatography method (hexane:ethylacetate eluent, 4:1 by volume).

IR spectrum

The IR absorption spectra were recorded on the IR-spectrometer «IR Prestige-21» of the company Shimadzu (Japan) in a potassium bromide pellet containing 1 % of the investigated compound.

NMR spectrum

The ^1H, ^{13}C-NMR spectra were recorded on the NMR-spectrometer «Ajilent DD2 400» in deuterochloroform. Decoding and modeling of spectra were performed using the program MestReNova (demo version).

Elemental analysis

Elemental analysis was carried out using the manual express gravimetric method based on pyrolytic burning of a substance in a quartz tube in oxygen flow. This method allows determination of carbon and hydrogen contents, as well as bismuth by the remainder of bismuth (III) oxide. An automatic CH-analyzer was used in parallel. We developed a titrimetric method of analysis of product **1** given in the results and discussion section.

Results and Discussion

Compound **1** has been obtained by the method of oxidative addition from triphenylbismuth, hydrogen peroxide, and excess of methacrylic acid, mixed in the 1:1:3 ratio, respectively:

$$Ph_3Bi + 2\ CH_2{=}CMeCOOH + H_2O_2 \rightarrow Ph_3Bi(O_2CMeC{=}CH_2)_2 + 2\ H_2O \quad (1)$$

Diethyl ether was used as solvent. The reaction was carried out at room temperature. Yield of target product with m. p. 164 ºC equaled 60 % after recrystallization from the mixture of chloroform and hexane.

Compound **1** is white crystalline substance, air- and moisture-stable, well soluble in chloroform, THF, methyl methacrylate, styrene, benzene, sparingly soluble in hexane and isopropyl alcohol. Good solubility in styrene and methyl methacrylate makes the product promising in order to obtain bismuth-containing polymers.

For investigation of composition and structure of compound **1**, elemental analysis, ^1H, ^{13}C NMR, and IR spectroscopy were used.

The elemental analysis data are in good agreement with the calculated values. Found, %: C 51.00; H 4.12; Bi 35.00 (manual apparatus for combustion); C 51.25; H 4.18 (automatic analyzer); Bi 34.23 (titrimetric bismuth determination). Calculated for $C_{26}H_{25}O_4Bi$, %: C 51.13; H 4.13; Bi 34.25.

For titrimetric bismuth determination, which we had worked out for the first time, a sample of the analyzed compound (0.05–0.15 g) and 5 mL of concentrated H_2SO_4 were heated in 100 mL conical flask to appearance of white vapours. Then the solution was cooled, 5 mL of concentrated HNO_3 was added and the mixture was heated to its discoloration. After cooling of the mixture, 20 mL of water was added, followed by the concentrated solution of ammonia, until slightly acidic pH was reached. Xylenol orange indicator was added into the hot solution and it was titrated by 0.1 N solution of disodium EDTA, until the colour of the solution changed from pink to lemon yellow. Content of bismuth in the sample was determined according to the formula:

$$\omega(\mathrm{Bi}) = 1.045 V \cdot m^{-1},$$

V is the equivalent volume of 0.1 N solution of disodium EDTA, mL; m is the mass of the analyzed sample, g.

If addition of ammonia leads to precipitation of $Bi(OH)_3$, it is dissolved in concentrated HNO_3 and ammonia is again added, until slightly acidic pH is reached.

Triphenylbismuth dicarboxylate turns into triphenylbismuth sulfate Ph_3BiSO_4 at heating with concentrated H_2SO_4 according to equation (2); Ph_3BiSO_4 decomposes with decrease of Bi oxidation state according to equation (3). The phenyl derivative of Bi(III) is dephenylated to $Bi_2(SO_4)_3$ and benzene by sulfuric acid according to equation (4), benzene is sulfonated to benzenesulfonic acid according to equation (5):

$$Ph_3Bi(O_2CMeC{=}CH_2)_2 + H_2SO_4 \rightarrow Ph_3BiSO_4 + 2\ CH_2{=}CMeCOOH \quad (2)$$

$$2\ Ph_3BiSO_4 \rightarrow (Ph_2Bi)_2SO_4 + PhOSO_2OPh \quad (3)$$

$$(Ph_2Bi)_2SO_4 + 2\ H_2SO_4 \rightarrow Bi_2(SO_4)_3 + 4\ PhH \quad (4)$$

$$PhH + H_2SO_4 \rightarrow PhSO_3H + H_2O \quad (5)$$

$$CH_2{=}CMeCOOH + 22\ HNO_3 \rightarrow 4\ CO_2 + 22\ NO_2 + 13\ H_2O \quad (6)$$

$$PhOSO_2OPh + 56\ HNO_3 \rightarrow 12\ CO_2 + 32\ H_2O + 34\ NO_2 + H_2SO_4 \quad (7)$$

$$PhSO_3H + 30\ HNO_3 \rightarrow 6\ CO_2 + 17\ H_2O + 30\ NO_2 + H_2SO_4 \quad (8)$$

Concentrated HNO_3 oxidizes all organic products to CO_2, H_2SO_4 and H_2O with formation of brown NO_2 in the presence of sulfuric acid according to equations (6–8).

During the titration, colour change is caused by the interaction of pink xylenol orange complex of triphenylbismuth sulfate with colourless disodium EDTA, that leads to formation of disodium xylenol orange complex with lemon yellow colour.

As the result of the chemical analysis, described above, reproducible results have been obtained. Percent of bismuth has been found to be 34.23 %; this is in good agreement with the combustion results, described above. The suggested volumetric method of bismuth content analysis of compound **1** is faster and more convenient than the known gravimetric method for bismuth determination in the BiOCl form [2].

In IR spectrum of the product, the medium absorption band, due to the stretching vibrations of Bi–C bonds, is at 679 cm^{-1}. The band at 449 cm^{-1} belongs to the stretching vibration frequency of Bi–O bonds. The strong bands with maxima at 1362 cm^{-1} and 1559 cm^{-1} are related to the asymmetric and symmetric absorption vibration frequencies of COO groups, respectively. The band with maximum at 3045 cm^{-1} belongs to the stretching vibration frequency of C–H bonds of phenyl groups. The wavenumbers of the noted vibrations are close to similar values for triphenylantimony dimethacrylate [12].

In ^1H NMR spectrum of compound **1** the multiplet of protons of Ph groups is observed in a weak field (δ 7.4–8.2 ppm); two singlets of CH_2 protons are observed in a stronger field (5.9 and 5.3 ppm); the singlet of CH_3 protons is observed in a strong field (1.8 ppm). The chemical shift values of these proton groups are close to similar values for triphenylantimony dimethacrylate [12]. In ^{13}C NMR spectrum of

compound **1** the signals of carbon atoms of phenyl groups (130.5; 130.9; 133.8; 160.4 ppm) and methacrylate groups (19.0; 122.9; 139.1; 173.5 ppm) are present.

Conclusions

1. Triphenylbismuth *bis*(2-methylpropenoate) has been synthesized by the reaction of triphenylbismuth with hydrogen peroxide and methacrylic acid.

2. The compound is air- and moisture-stable, well soluble in chloroform, THF, methyl methacrylate, styrene, benzene, sparingly soluble in hexane and isopropyl alcohol.

3. Composition and structure of the product have been confirmed by means of IR, ^{1}H, ^{13}C NMR spectroscopy, and elemental analysis.

4. New technique for titrimetric bismuth content analysis of triphenylbismuth bis(2-methylpropenoate) has been suggested.

Acknowledgements

The work has been carried out with financial support of the Russian Foundation for Basic Research (assignment N 14-03-31625) and the Ministry of Education and Science of the Russian Federation (project N 2033, basic part of government contract).

References

1. Gushchin A.V. *Poluchenie organicheskikh proizvodnykh sur'my(V), vismuta(V) i primenenie ikh v organicheskom sinteze: dis. …d-ra khim. nauk* [Obtaining organic derivative compounds of antimony(V), bismuth(V) and their use in organic synthesis: thesis… D.Sc (Chemistry)]. Nizhny Novgorod, State University of Nizhny Novgorod Publ., 1998. 283 p.

2. Kocheshkov K.A., Skoldinov A.P., Zemlyanskii N.N. *Metody elementoorganicheskoi khimii. Sur'ma, vismut* [Methods of Organometallic Chemistry. Antimony, Bismuth]. Moscow, Nauka Publ., 1976. 483 p.

3. Suzuki H. *Organobismuth Chemistry.* Amsterdam-London-New York-Oxford-Paris-Shannon-Tokyo, Elsevier, 2001. 619 p.

4. Finet J.-P. *Ligand Coupling Reactions with Heteroatomic Compounds*. New York, Pergamon, 1998, pp. 159–204.

5. Challenger F., Goddard A. E. L XXXII. Organo-derivatives of Bismuth. Part III. The Preparation of Derivatives of Quinquevalent Bismuth. *J. Chem. Soc.*, 1920, vol. 117, no. 692, pp. 762–773.

6. Dodonov V.A., Gushchin A.V., Brilkina T.G. [Synthesis and Some Reactions of Triphenylbismuth Diacylates]. *Zhurn. Obshch. Khmii* [*Journal of General Chemistry*], 1985, vol. 55, no. 1, pp. 73–80. (in Russ.)

7. Dodonov V.A., Gushchin A.V., Ezhova M.B. [Synthesis of Triphenylbismuth Diacylates]. *Zhurn. Obshch. Khmii* [*Journal of General Chemistry*], 1988, vol. 58, no. 9, pp. 2170–2171. (in Russ.)

8. Sharutin V.V., Sharutina O.K. Synthesis and Structure of Triphenylbismuth *Bis*(pentachlorobenzoate). *Russian Journal of Inorganic Chemistry*, 2014, vol. 59, no. 6, pp. 558–560. DOI: 10.1134/S0036023614060199.

9. Sharutin V.V., Senchurin V.S., Sharutina O.K. Synthesis and Structure of Triphenylbismuth *Bis*(1-adamantanecarboxylate). *Russian Journal of Inorganic Chemistry*, 2011, vol. 56, no. 10, pp. 1565–1567. DOI:10.1134/S0036023611100202

10. Sharutin V.V., Senchurin V.S., Sharutina O.K., Bregadze V.I., Zhigareva G.G. Synthesis and Structure of Triphenylbismuth *Bis*(phenylcarboranylcarboxylate). *Russian Journal of General Chemistry*, 2010, vol. 80, no. 10, pp. 1941–1944. DOI: 10.1134/S1070363210100117

11. Sharutin V.V., Egorova I.V., Kazakov M.A., Sharutina O.K. Synthesis and Structure of Triphenylbismuth *Bis*(2-Phenylaminobenzoate). *Russian Journal of Inorganic Chemistry*, 2009, vol. 54, no. 7, pp. 1095–1098. DOI: 10.1134/S0036023609070171

12. Gushchin A.V., Shashkin D.V., Prytkova L.K., Somov N.V., Baranov E.V., Shavyrin A.S., Rykalin V.I. Synthesis and Structure of Triphenylantinony Dimethacrylate. *Russian Journal of General Chemistry*, 2011, vol. 81, no. 3, pp. 493–496. DOI: 10.1134/S107036321103008X

Received 3 May 2015

УДК 547.1'13

СИНТЕЗ *БИС*(2-МЕТИЛПРОПЕНОАТА) ТРИФЕНИЛВИСМУТА

В.А. Верховых, О.С. Калистратова, А.И. Гришина, В.Г. Артемова, А.В. Гущин

Нижегородский государственный университет имени Н.И. Лобачевского, г. Нижний Новгород

Взаимодействием трифенилвисмута с метакриловой кислотой и пероксидом водорода в тетрагидрофуране получен бис(2-метилпропеноат) трифенилвисмута $Ph_3Bi(O_2CMe{=}CH_2)_2$, строение которого подтверждено данными ИК- и ^1H ЯМР-спектроскопии.

Ключевые слова: бис(2-метилпропеноат) трифенилвисмута, синтез, строение, ИК-спектроскопия, ЯМР-спектроскопия.

Верховых Вадим Алексеевич – студент химического факультета, Нижегородский государственный университет им. Н.И. Лобачевского. 603950, г. Нижний Новгород, пр. им. Ю.А. Гагарина, 23. E-mail: gushchin@chem.unn.ru.

Калистратова Ольга Сергеевна – аспирант химического факультета, Нижегородский государственный университет им. Н.И. Лобачевского. 603950, г. Нижний Новгород, пр. им. Ю.А. Гагарина, 23. E-mail: olga.kalistratova@yandex.ru.

Гришина Арина Ильинична – студент химического факультета, Нижегородский государственный университет им. Н.И. Лобачевского. 603950, г. Нижний Новгород, пр. им. Ю.А. Гагарина, 23. E-mail: gushchin@chem.unn.ru.

Артемова Валентина Гавриловна – кандидат философских наук, доцент факультета социальных наук, Нижегородский государственный университет им. Н.И. Лобачевского. 603950, г. Нижний Новгород, пр. им. Ю.А. Гагарина, 23. E-mail: decanat2005@yandex.ru.

Гущин Алексей Владимирович – доктор химических наук, профессор, декан химического факультета, Нижегородский государственный университет им. Н.И. Лобачевского. 603950, г. Нижний Новгород, пр. им. Ю.А. Гагарина, 23. E-mail: gushchin@chem.unn.ru.

Поступила в редакцию 3 мая 2015 г.

ОБРАЗЕЦ ЦИТИРОВАНИЯ

Synthesis of triphenylbismuth *bis*(2-methylpropenoate) / V.A. Verkhovykh, O.S. Kalistratova, A.I. Grishina et al. // Вестник ЮУрГУ. Серия «Химия». – 2015. – Т. 7, № 3. – С. 61–65.

FOR CITATION

Verkhovykh V.A., Kalistratova O.S., Grishina A.I., Artemova V.G., Gushchin A.V. Synthesis of Triphenylbismuth *Bis*(2-methylpropenoate). *Bulletin of the South Ural State University. Ser. Chemistry.* 2015, vol. 7, no. 3, pp. 61–65.

Краткие сообщения

4-NITROBENZALDOXIME AND CYNNAMALDOXIME STRUCTURES

V.V. Sharutin, *South Ural State University, Chelyabinsk, Russian Federation, vvsharutin@rambler.ru*
O.K. Sharutina, *South Ural State University, Chelyabinsk, Russian Federation, sharutinao@mail.ru*

The structures of 4-nitrobenzaldoxime (1) and cynnamaldoxime (2) have been determined by X-ray diffraction analysis. In the oxime molecules the distances C=N, N–O have the usual values for oximes (1.267(3), 1.403(2) Å for 1 and 1.278(4), 1.395(3) Å for 2a, 1.284(4), 1.384(3) Å for 2b). In crystals the oximes are observed as dimers: two oxime 1 molecules are interconnected by two hydrogen bonds N(1A)···H(1B) (2.12 Å), two oxime 2 molecules are interconnected by the single hydrogen bond N(1A)···H(1B) (1.66 Å).

Keywords: 4-nitrobenzaldoxime, cynnamaldoxime, molecular structures, X-ray analysis.

Introduction

Oximes are mono-, bi- and tridentate chelating ligands, which form numerous metal complexes that are well studied and find wide practical application. At the present time the crystalline and molecular structures of more than 3000 oximes are known, of which about 300 oximes are derivatives of benzaldehyde oxime [1].

Experimental

X-Ray diffraction analysis of crystals **1** and **2** was carried out on the Bruker D8 QUEST automatic four-circle diffractometer (Mo K_α- emission, $\lambda = 0.71073$ Å, graphite monochromator). Using *SMART* and *SAINT-Plus* programs, data were collected, edited; unit cell parameter and absorptivity were refined [2]. All calculations needed for determination and refinement of molecular structures were done using *SHELXL/PC* program [3]. The structures **1** and **2** were determined using the direct method and refined with the least squares method, all non-hydrogen atoms were refined anisotropically.

Selected crystallographic data and structure refinement results are listed in Table 1, selected bond lengths and bond angles are summarized in Table 2.

Table 1

Crystallographic data, experimental and structure refinement parameters for compounds 1–2

Parameter	Value	
	1	**2**
Formula	$C_7H_6O_3N_2$	$C_{18}H_{18}N_2O_2$
Formula weight	166.14	294.34
T, K	296(2)	296(2)
Crystal system	Monoclinic	Orthorhombic
Space group	$P2_1/c$	Pbca
a, Å	6.2548(3)	10.2935(11)
b, Å	4.8928(2)	7.7033(8)
c, Å	24.7226(11)	41.297(4)
α, deg	90.00	90.00
β, deg	94.536(2)	90.00
γ, deg	90.00	90.00
V, Å^3	754.23(6)	3274.6(6)
Z	4	8
$\rho_{(calcd)}$, g/cm^3	1.463	1.194
μ, mm^{-1}	0.117	0.079
F(000)	344.0	1248.0

Table 1 (end)

Crystal size, mm	0.78×0.55×0.22	0.25×0.22×0.16
2Θ range of data collection, deg	6.62 – 70.14°	6.68 – 39.18°
Range of refraction indices	$-10 \le h \le 9$, $-7 \le k \le 7$, $-29 \le l \le 39$	$-9 \le h \le 9$, $-7 \le k \le 7$, $-35 \le l \le 38$
Measured reflections	8109	6468
Independent reflections, R_{int}	3217 (R_{int} = 0.0274)	1428 (R_{int} = 0.0475)
Refinement variables	110	271
GOOF	1.140	1.078
R factors for $F^2 > 2\sigma(F^2)$	R_1 = 0.0855, wR_2 = 0.2119	R_1 = 0.0367, wR_2 = 0.0918
R factors for all reflections	R_1 = 0.1197, wR_2 = 0.2293	R_1 = 0.0565, wR_2 = 0.1003
Residual electron density (min/max), e/A^3	0.41/–0.34	0.11/–0.15

Table 2

Selected bond lengths and bond angles in the structures of compounds 1–2

Bond	*d*, Å	Angle	ω, deg	Bond	*d*, Å	Angle	ω, deg
1				**2**			
C(4)–N(2)	1.467(2)	C(3)C(4)N(2)	119.12(15)	O(1)–N(1)	1.395(3)	C(9)N(1)O(1)	111.8(3)
C(4)–C(5)	1.377(2)	C(5)C(4)N(2)	118.45(15)	C(1)–C(7)	1.452(4)	C(8)C(7)C(1)	128.3(3)
C(1)–C(6)	1.392(2)	C(2)C(1)C(7)	122.72(16)	C(1)–C(2)	1.390(4)	C(7)C(8)C(9)	123.1(4)
C(1)–C(2)	1.397(2)	O(2)N(2)C(4)	118.20(15)	C(1)–C(6)	1.382(4)	C(12)C(11)C(16)	119.6(3)
C(1)–C(7)	1.465(2)	O(2)N(2)O(3)	123.84(16)	N(1)–C(9)	1.278(4)	C(15)C(11)C(12)	118.2(3)
C(3)–C(2)	1.383(3)	O(3)N(2)C(4)	117.96(15)	C(7)–C(8)	1.324(4)	C(15)C(11)C(16)	122.2(3)
N(2)–O(2)	1.218(2)	C(5)C(6)C(1)	120.85(16)	O(2)–N(2)	1.384(3)	C(17)N(2)O(2)	111.5(3)
N(2)–O(3)	1.220(2)	C(3)C(2)C(1)	120.41(16)	C(8)–C(9)	1.441(4)	N(2)C(17)C(10)	128.3(4)
C(6)–C(5)	1.384(3)	N(1)C(7)C(1)	122.34(18)	N(2)–C(17)	1.284(4)	C(16)C(10)C(17)	123.1(4)
C(7)–N(1)	1.267(3)	C(4)C(5)C6	118.41(16)	C(17)–C(10)	1.427(4)	C(10)C(16)C(11)	128.5(4)
N(1)–O(1)	1.403(2)	C(7)N(1)O(1)	111.08(18)	C(10)–C(16)	1.331(4)	N(1)C(9)C(8)	129.2(4)

The full tables of atomic coordinates, bond lengths, and bond angles are deposited with the Cambridge Crystallographic Data Centre (CCDC 1045607, 1049482; deposit@ccdc.cam.ac.uk; http://www.ccdc.cam.ac.uk).

Results and Discussion

Oximes in the crystalline state exist as dimmers, in which oxime molecules are interconnected by two intermolecular hydrogen bonds N···H. For example, in the 4-dimethylaminobenzaldoxime dimer (Fig. 1) intermolecular hydrogen bonds N···H are equal to 2.09 Å [4] (the sum of Van der Waals radiuses of the said elements is equal to 2.70 Å [5]).

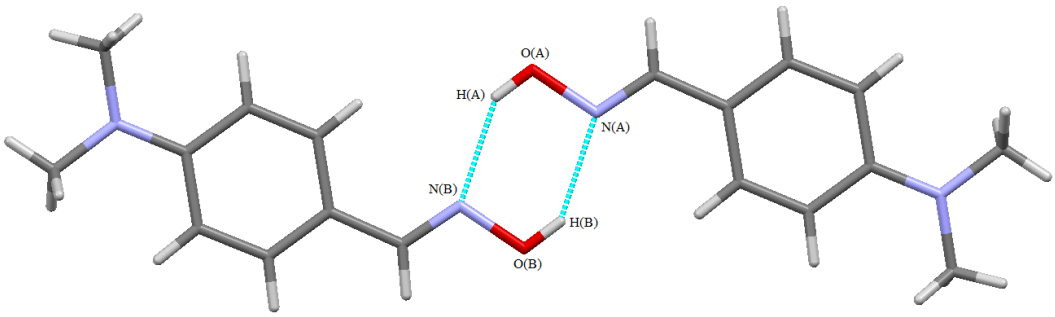

Fig. 1. Intermolecular hydrogen bonds in 4-dimethylaminobenzaldoxime crystal

We have found that such intermolecular hydrogen bonds exist in 4-nitrobezaldoxime crystal **(1)**, too (Fig. 2).

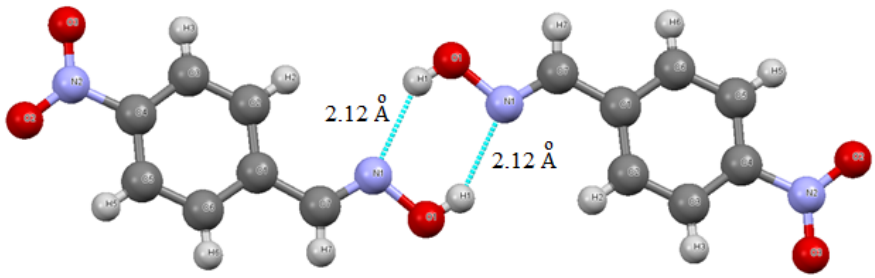

Fig. 2. Intermolecular hydrogen bonds N···H in 4-nitrobezaldoxime crystal (1)

We have also found that in the cynnamaldoxime crystal **(2)** two oxime molecules are connected in the dimer by only one abnormally short (1.66 Å) intermolecular hydrogen bond (Fig. 3).

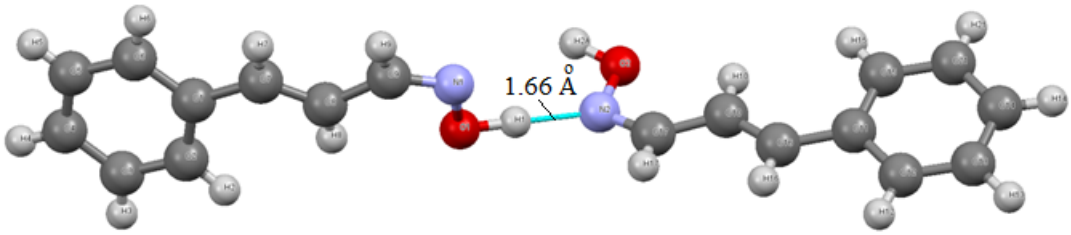

Fig. 3. Intermolecular hydrogen bond N(A)···H(B) in cynnamaldoxime dimer (2)

In oxime molecules the distances C=N, N–O have the usual values for oximes (1.267(3), 1.403(2) Å for **1** and 1.278(4), 1.395(3) Å for **2a**, 1.284(4), 1.384(3) Å for **2b**). Note the unusual linkage of two oxime molecules **2** into the dimer by only one intermolecular hydrogen bond, which is not typical for the most oximes [1].

Conclusion

Thus, 4-nitrobezaldoxime and cynnamaldoxime crystals exist as dimers interconnected by two or one intermolecular hydrogen bonds N···H, respectively.

References

1. Cambridge Crystallografic Database. Release 2015. Cambridge.

2. Bruker (2000) SMART. Bruker Molecular Analysis Research Tool, Versions 5.625 Bruker AXS, Madison, Wisconsin, USA.

3. Bruker (2000) SAINTPlus Data Reduction and Correction Program Versions 6.02a, Bruker AXS, Madison, Wisconsin, USA.

4. Sharutin V.V. [Crystal and molecular structure of 4-dimethylaminobezaldoxime]. *Butlerovskie soobshcheniya [Russian Journal Butlerov Communication]*, 2014, vol. 39, no. 7, pp. 163–164.

5. Batsanov S.S. [Atomic radiuses of the elements]. *Zhurn. Neorgan. Himii [Russian Journal of Inorganic Chemistry],* 1991, vol. 36, no. 12, pp. 3015–3037. (in Russ.)

Received 4 May 2015

УДК 547-304.6+547.53.024+548.312.5

СТРОЕНИЕ 4-НИТРОБЕНЗАЛЬДОКСИМА И ЦИННАМАЛЬДОКСИМА

В.В. Шарутин, О.К. Шарутина
Южно-Уральский государственный университет, г. Челябинск

Строение 4-нитробензальдоксима (1) и циннамальдоксима (2) определено методом рентгеноструктурного анализа. В молекулах оксимов расстояния C=N, N-O имеют обычные для оксимов значения (1,267(3), 1,403(2) Å для 1 и 1,278(4), 1,395(3) Å для 2а, 1,284(4), 1,384(3) Å для 2б). В кристаллах оксимы находится в виде димеров: две молекулы оксима 1 связываются между собой двумя водородными связями N(1A)···H(1B) (2,12 Å), две молекулы оксима 2 связаны между собой единственной водородной связью N(1A)···H(1B) (1,66 Å).

Ключевые слова: 4-нитробензальдоксим, циннамальдоксим, молекулярные структуры, рентгеноструктурный анализ.

Литература

1. Cambridge Crystallografic Database. Release 2015. Cambridge.
2. Bruker (2000) SMART. Bruker Molecular Analysis Research Tool, Versions 5.625 Bruker AXS, Madison, Wisconsin, USA.
3. Bruker (2000) SAINTPlus Data Reduction and Correction Program Versions 6.02a, Bruker AXS, Madison, Wisconsin, USA.
4. Шарутин, В.В. Кристаллическая и молекулярная структура 4-диметиламинобензальдоксима / В.В. Шарутин // Бутлеровские сообщения. – 2014. – Т. 39. – № 7. – С. 163–164.
5. Бацанов, С.С. Атомные радиусы элементов / С.С. Бацанов // Журн. неорган. химии. – 1991. – Т. 36. – № 12. – С. 3015–3037.

Шарутин Владимир Викторович – доктор химических наук, профессор, старший научный сотрудник УНИД, Южно-Уральский государственный университет. 454080, г. Челябинск, пр. им. В.И. Ленина, 76. E-mail: vvsharutin@rambler.ru.

Шарутина Ольга Константиновна – доктор химических наук, профессор, кафедра аналитической химии, Южно-Уральский государственный университет. 454080, г. Челябинск, пр. им. В.И. Ленина, 76. E-mail: sharutinao@mail.ru.

Поступила в редакцию 4 мая 2015 г.

ОБРАЗЕЦ ЦИТИРОВАНИЯ

Sharutin, V.V. 4-nitrobenzaldoxime and cynnamaldoxime structures / V.V. Sharutin, O.K. Sharutina // Вестник ЮУрГУ. Серия «Химия». – 2015. – Т. 7, № 3. – С. 66–69.

FOR CITATION

Sharutin,V.V., Sharutina O.K. 4-nitrobenzaldoxime and cynnamaldoxime structures . *Bulletin of the South Ural State University. Ser. Chemistry.* 2015, vol. 7, no. 3, pp. 66–69.

СВЕДЕНИЯ ОБ ИЗДАНИИ

Серия основана в 2009 году.

Свидетельство о регистрации ПИ № ФС 77-57404 выдано 24 марта 2014 г. Федеральной службой по надзору в сфере связи, информационных технологий и массовых коммуникаций.

Журнал включен в Реферативный журнал и Базы данных ВИНИТИ. Сведения о журнале ежегодно публикуются в международной справочной системе по периодическим и продолжающимся изданиям «Ulrich's Periodicals Directory».

Решением Президиума Высшей аттестационной комиссии Министерства образования и науки Российской Федерации от 19 февраля 2010 г. № 6/6 журнал включен в «Перечень ведущих рецензируемых научных журналов и изданий, в которых должны быть опубликованы основные научные результаты диссертаций на соискание ученых степеней доктора и кандидата наук».

Подписной индекс 29414 в объединенном каталоге «Пресса России».

Периодичность выхода – 4 номера в год.

ПРАВИЛА ДЛЯ АВТОРОВ

Статья предоставляется в электронной и печатной форме на русском или английском языках в формате редактора MS Word версии 2000 или 2003 (*.doc или *.rtf). В текст включают все рисунки и таблицы. Файл рукописи должен содержать: УДК, название, инициалы и фамилии авторов, аннотацию на русском и английском языках (не более 1000 символов на каждом языке) и ключевые слова/словосочетания на русском и английском языках (не более 10 на каждом языке), сведения об авторах: фамилию, имя, отчество полностью, место работы полностью, должность, учёная степень и учёное звание (если есть), электронную почту всех авторов, текст рукописи. Структура статьи: **введение, экспериментальная часть** или **методика исследования, обсуждение результатов, заключение, список литературы**. Список литературы оформляется в порядке цитирования в соответствии с ГОСТ 7.1–2003, названия статей в периодических изданиях указывать обязательно. Для электронного ресурса указывается полный адрес источника, достаточный для поиска в интернете. **Рисунки** должны быть вставлены в файл документа MS Word. Фотографии должны иметь разрешение не менее 300 dpi и быть присланы в виде отдельных файлов, имя которых содержит фамилию первого автора и номер рисунка в статье. Электронная версия может быть передана на компакт-диске или по электронной почте. Печатная версия (с подписями **всех** соавторов), а также акт экспертизы о возможности опубликования, лицензионный договор, акт приёмки-передачи произведения, и анкету о согласии на обработку персональных данных – обычной почтой или лично.

Параметры документа: **поля:** зеркальные, верхнее и нижнее – 23 мм, внутри – 22 мм, снаружи – 25 мм. **Межстрочный интервал** – одинарный. **Шрифты:** Times New Roman (для аннотации Arial), кегль 11 пт (для аннотации – 10 пт), абзацный отступ 0,7 см, без нумерации страниц. Рекомендуемый объём статьи (включая таблицы и рисунки) 5–10 страниц.

Адрес редакции: 454080, Челябинск, пр. им. В.И. Ленина, 76, Южно-Уральский государственный университет, Химический факультет, корпус 1а, Авдину В.В., e-mail: avdin@susu.ru; wik22@inbox.ru.

Полная версия правил подготовки рукописей находится на сайте журнала: http://vestnik.susu.ac.ru/chemistry.

Плата за публикацию не взимается.

Редактор *А.Н. Ивашкина*

Компьютерная верстка *В.Г. Харитоновой*

Издательский центр Южно-Уральского государственного университета

Подписано в печать 27.07.2015. Формат 60×84 1/8. Печать цифровая.
Усл. печ. л. 8,37. Тираж 500 экз. Заказ 301/388.

Отпечатано в типографии Издательского центра ЮУрГУ.
454080, г. Челябинск, пр. им. В.И. Ленина, 76.